Rute Marina Faria Mota

Licenciada em Ciências de Engenharia Química e Bioquímica

Leveraging cross-filtration membranes to extend the production of amorphous solid dispersions (ASDs) to non-volatile organic solvents

Dissertação para obtenção do
Grau de Mestre em Engenharia Química e Bioquímica

Orientador: Doutor Rui César Costa da Silva,
Senior Scientist, R&D, Hovione Farmaciência SA

Co-orientadora: Professora Doutora Ana Isabel Nobre Martins Aguiar de Oliveira Ricardo, Professora Catedrática, FCT UNL

Júri:

Presidente: Professor Doutor Mário Fernando José Eusébio,
Professor Auxiliar, FCT UNL

Arguente: Professora Doutora Isabel Maria Rôla Coelhoso,
Professora Associada com Agregação, FCT UNL

Vogal: Doutor Rui César Costa da Silva,
Senior Scientist, R&D, Hovione Farmaciência SA

Dezembro, 2020

FACULDADE DE CIÊNCIAS E TECNOLOGIA
UNIVERSIDADE NOVA DE LISBOA

Leveraging cross-filtration membranes to ex-tend the production of amorphous solid dispersions (ASDs) to non-volatile organic solvents

"Eles não sabem, nem sonham,

que o sonho comanda a vida.

Que sempre que um homem sonha

o mundo pula e avança

como bola colorida

entre as mãos de uma criança."

- António Gedeão

Acknowledgments/Agradecimentos

À Faculdade de Ciências e Tecnologia, por me proporcionar uma formação académica de excelente qualidade, num campus acolhedor e com um ótimo corpo docente.

À Hovione, pela oportunidade e privilégio que foi elaborar a minha tese de mestrado nos seus inovadores laboratórios de R&D, e pela possibilidade de manter parte do trabalho experimental, mesmo com as restrições associadas à situação pandémica.

Ao Rui César, pela orientação e por promover e estimular o meu espírito crítico durante toda esta etapa. Agradeço também a sua partilha de conhecimentos, conselhos, experiências e total disponibilidade.

À Professora Ana Aguiar Ricardo, pelo seu apoio nesta fase final do mestrado e pelos ensinamentos que me foi transmitindo durante o percurso académico.

Ao Paulo Lino, pelo grande apoio no *in silico screening*, pela ajuda e sugestões durante a fase de *screenings* e também no restante trabalho experimental. À Catarina Portugal, por agilizar toda a coordenação com as técnicas analíticas e pelo apoio nos resultados da caracterização. À Teresa Marta, por me ter ensinado as técnicas dos estudos de supersaturação, de dissolução e pelo auxílio no TGA. Ao Ricardo Gonçalves, pelos ensinamentos de HPLC que me transmitiu e por me ter ajudado a desenvolver o meu primeiro método. À Sara Sequeira, por me ter ensinado a trabalhar com o Sympatec. À Maria Paisana, por esclarecer as minhas dúvidas em relação aos DSCs. Aos lab tech do DPD, André, Calixto, Eloy, Miguel, Norberto, Pedro e Ricardo, por todo o apoio no laboratório, pelas piadas, músicas e boa disposição constante. Às estudantes de doutoramento, Patrícia Henriques, Patrícia Nunes e Susana por promoverem o sentimento de entre-ajuda entre os alunos, por partilharem as suas dicas (e até alguns equipamentos, como o HPLC32 e a hotte), sendo grandes ajudas, especialmente no turno da tarde. Às colegas trainees, e em particular à Filipa, pelo companheirismo durante esta experiência e pelo ótimo ambiente durante as nossas pausas e passeios. A todos colaboradores da Hovione que se disponibilizam para me ajudar.

Aos meus pais, pela forma como me educaram a mim e ao meu irmão, por sempre nos proporcionarem tudo aquilo que poderíamos precisar e por quererem sempre a nossa felicidade. Muito obrigada por apoiarem as minhas decisões, por me darem a liberdade de seguir o meu caminho e por se orgulharem de mim.

Ao meu irmão, pelo exemplo que é (e sempre foi) para mim e por partilhar comigo as melhores músicas e conselhos.

À minha grande família, que está sempre a torcer por mim.

Ao Artur, pela sua paciência e carinho, por ser um apoio fundamental e por me conseguir sempre motivar a ser uma melhor versão de mim.

Aos meus colegas de faculdade, Roomies, Iluminadíssimos&Má vizinhança, Niggas do Serrado, pelos convívios, jantares, estudos e partilha de bons e menos bons momentos, típicos do ensino superior.

Às minhas queridas amigas de longa data, Mariana P., Bárbara, Mariana A. e Soraia, pelas gargalhadas, pelos melhores jantarzinhos na Maison e pela viagem à Madeira pela qual ansiosamente aguardamos. À Mara, de quem guardo a sua amizade com muito carinho por todos os momentos que já passamos juntas. À Mariana S., pela boa companhia que é e por me ajudar a tornar os momentos mais felizes.

A todos os que de alguma forma contribuíram para a pessoa que sou hoje.

Muito obrigada!

Abstract

Currently, about 90% of drugs in development stages present poor-aqueous solubility, belonging to Biopharmaceutics Classification System (BCS) Classes II and IV. A leading technology to improve solubility is the production of amorphous solid dispersions (ASDs). ASDs are typically manufactured by spray drying (SD) and hot melt extrusion (HME), however these techniques are not suitable for “brick-dust” compounds.

Coprecipitation is an adequate technology to deal with “brick-dust” compounds, since high boiling point solvents, with higher solubilization power, can be employed. This technology is not without drawbacks: the high volume and low solids’ load of the resultant suspension and the challenging drying of non-volatile organic solvents.

With this work, these drawbacks are tackled through a proof-of-concept by incorporating crossflow filtration with hollow fiber membranes after coprecipitation to 1) concentrate the suspension, increasing solids’ load and 2) minimize the presence of the organic solvent, by diafiltration. Coprecipitation was carried out through two different techniques: high shear mixer and high--pressure homogenization (HPH). The suspensions were concentrated and washed in hollow fiber membranes unit and isolated through spray drying. Spray-dried ASDs were also produced to serve as benchmark against the coprecipitated prototypes. Coprecipitated prototypes and SD benchmarks were analytically characterized and the preliminary results seem to indicate a greater dissolution behavior of the HPH prototype.

In conclusion, this study demonstrated the advantages of including a cross-filtration with hollow fiber membranes, a straightforward and scalable technology that allows the circumvention of typical pitfalls of the production of “brick-dust” ASDs by coprecipitation. In 60 minutes, the concentration step reduced the mass of HPH suspension to a half, and the diafiltration operations lowered the DSMO initial content in approximately 50% within 112 minutes; although this last step should be optimized by the introduction of an online conductivity measurement.

Keywords: amorphous solid dispersions, coprecipitation, hollow fiber membranes, cross-flow filtration, spray drying, “brick-dust”

Resumo

Atualmente, aproximadamente 90% dos fármacos em fase de desenvolvimento apresentam baixa solubilidade aquosa, pertencendo às Classes II e IV do Sistema de Classificação Biofarmacêutica. Uma tecnologia líder para melhorar a solubilidade é a produção de dispersões sólidas amorfas (DSAs). DSAs são tradicionalmente produzidas por secagem por atomização (SA) ou extrusão por fusão a quente. Todavia, estas técnicas não são apropriadas para compostos "brick-dust".

A coprecipitação é uma tecnologia adequada para os "brick-dust", pois permite o uso de solventes com elevados pontos de ebulição e maior poder de solubilização. Porém, esta tecnologia tem as suas desvantagens: elevado volume e baixa concentração de sólidos na suspensão resultante e a desafiante secagem dos solventes orgânicos não voláteis.

Com o trabalho apresentado, estas limitações são abordadas em uma prova de conceito, onde se incorpora a filtração tangencial com membranas de fibras-ocas, para 1) concentrar a suspensão e 2) minimizar a quantidade de solvente orgânico, por diafiltração. A coprecipitação foi realizada por duas tecnologias: agitador de alta-rotação e homogeneização a alta-pressão (HAP). As suspensões resultantes foram concentradas e diafiltradas recorrendo às membranas e, por fim, isoladas através de SA. Também foram produzidas DSAs unicamente por SA, para servirem como referência em relação aos protótipos de coprecipitação. Todos os materiais produzidos foram caracterizados analiticamente. Os resultados preliminares parecem indicar uma maior dissolução do protótipo de coprecipitação por HAP.

Concluindo, este trabalho demonstrou as vantagens de incluir a filtração tangencial com membranas de fibras-ocas, como uma tecnologia simples e escalável, que permite contornar as desvantagens da produção de DSAs com "brick-dust" por coprecipitação. Durante 60 minutos, concentrou-se a suspensão de HPH para metade da sua massa, e em 112 minutos de diafiltração reduziu-se a quantidade inicial de DMSO em 50%; porém este último passo pode ser otimizado, através da introdução da medição de condutividade.

Palavras-chave: dispersões sólidas amorfas, coprecipitação, membranas de fibras-ocas, filtração tangencial, secagem por atomização, "brick-dust"

Table of Contents

Table of Figures

List of Tables

List of Abbreviations

ACN	Acetonitrile
AFM	Atomic force microscopy
API	Active pharmaceutical ingredient
ASD	Amorphous solid dispersion
APM	Auxiliary processing mode
BCS	Biopharmaceutics Classification System
CF	Concentration factor
CFF	Crossflow filtration
CMA	Critical material attribute
CPP	Critical process parameter
CQA	Critical quality attribute
DCM	Dichloromethane or methylene chloride
DMA	N,N-Dimethylacetamide
DMF	N,N-Dimethylformamide
DMSO	Dimethyl sulfoxide
DoE	Design of experiments
(m)DSC	(Modulated) Differential scanning calorimetry
EMA	European Medicines Agency
Eudragit L100	1:1 Methacrylic acid and methyl methacrylate co-polymer
FaSSFG	Fasted state simulated gastric fluid
FaSSIF	Fasted state simulated intestinal fluid
FDA	Food and Drug Administration
FTIR	Fourier transformed infrared spectroscopy
FUR	Furosemide
GC	Gas chromatography
GI	Gastrointestinal
HME	Hot melt extrusion
HMWC	High molecular weight compound
HPH	High-pressure homogenization
HPLC	High performance liquid chromatography
HPMCAS	Hydroxyl propyl methyl cellulose acetate succinate
HSP	Hansen solubility parameters
HSPiP	Hansen solubility parameters in practice

HTS	High throughput screening
ICH	International Council for Harmonisation
IMC	Isothermal microcalorimetry
ITZ	Itraconazole
IXC	Interaction chamber
LMWC	Low molecular weight compound
MAAC	Membrane-assisted antisolvent crystallization
MBP	Microprecipitated bulk powder
MeOH	Methanol
MF	Microfiltration
MiCoS	Miniaturized coprecipitation screening
NCE	New chemical entity
NF	Nanofiltration
NMP	N-Methyl-2-pyrrolidone
ODD	Oral drug delivery
OFAT	One factor at a time
ONF	Organophilic nanofiltration
OSN	Organic solvent nanofiltration
PHFAC	Porous hollow fiber antisolvent crystallization
PLM	Polarized light microscopy
PSD	Particle size distribution
QbD	Quality by design
RO	Reverse osmosis
SCF	Supercritical fluids
SCP	Solvent-controlled precipitation
SD	Spray drying
SEDDS	Self-emulsifying drug delivery systems
SEM	Scanning electron microscopy
SHFCC	Solid hollow fiber cooling crystallizer
SRNF	Solvent resistant nanofiltration
SS-NMR	Solid-state nuclear magnetic resonance
TEM	Transmission electronic microscopy
TFA	Trifluoroacetic acid
T_g	Glass transition temperature
TGA	Thermal gravimetric analysis
TMP	Transmembrane pressure
UF	Ultrafiltration
XRPD	X-ray powder diffraction

1

Introduction

In pharmaceutical industry, oral drug delivery (ODD) is typically the most preferred administration route, representing approximately 60% of the commercial products.[1–3] However, ODD faces some bioavailability challenges related with drug's aqueous solubility/dissolution and permeability through the gastrointestinal (GI) tract membrane.[4] Currently, about 40% of the market products and 90% of drugs in development stages present poor-aqueous solubility, belonging to Class II (low solubility; high permeability) and Class IV (low solubility; low permeability), according to the Biopharmaceutics Classification System (BCS).[5–9] These solubility constraints can, in turn, result in poor bioavailability.

To circumvent this solubility challenge, several techniques have been applied. Micelle formation, complexation with cyclodextrines are frequently used in APIs with high lipophilicity.[8–11] Formation of salts, co-crystals and production of amorphous solid dispersions are some examples of solid-state modifications for drug substances with strong intermolecular forces within the crystal lattice.[8–11] Additionally, lipid-based drug delivery systems, including self-emulsifying drug delivery systems (SEDDS) and liposomes, have also proved to be a viable alternative.[12,13]

Of all these alternatives, the one that stands out the most is amorphous solid dispersion (ASD). ASDs have been gaining ground in solubility enhancement technologies and are nowadays an established platform to solve solubility constraints and improve dissolution behavior and bioavailability of the new drug candidates.[5,14,15] The increasing number of references in literature (i.e. papers, patents…) and the significant quantity of commercialized products, with more than 20 FDA-approved therapies by 2019, corroborate the prevalence of ASDs.[14]

In ASDs, the API is kept in an amorphous state and stabilized by a polymer. With this platform, a supersaturated state is achieved and maintained, exceeding the drug's intrinsic solubility. Hence, higher and prolonged drug concentrations are attained, resulting in an increase in the absorbed dose and, consequently, in bioavailability.[5,16–19]

ASDs manufacturing technologies can be divided in: solved-based and fusion-based methods. Spray drying (SD), a solvent-based method, and Hot melt extrusion (HME), a fusion based-method, are well-established technologies in the pharmaceutical industry and the most frequently used for ASDs production.[19,20] Spray drying involves the atomization of the solution containing the drug and the polymer, followed by rapid evaporation of the solvent in a drying chamber. Volatile organic solvents are used and, since their boiling points are not too high, this is a suitable method for thermolabile compounds.[17] On the other hand, in HME, the API and the polymer are mixed under high temperatures inside an extruder.[21] As HME is a solvent-free method, there is no need to dry the product or to find a proper solvent system, which sometimes is not straightforward.[5,17,22]

Another solvent-based method for ASDs production has gained prominence due to its potential in formulating the so-called "brick-dust" compounds – drug substances that are not soluble in volatile organic solvents and that, at the same time, have melting points above 200°C, making them difficult to process through SD or HME, respectively.[1,19] Coprecipitation is a suitable alternative for "brick-dust" compounds, since it enables the use of non-volatile organic solvents with higher solubilization power, such as dimethylacetamide (DMA), dimethylformamide (DMF) and dimethyl sulfoxide (DMSO). In coprecipitation, the drug is dissolved in the organic solvent and the polymer may be dissolved either in the solvent or in the antisolvent.[19] Then, the organic solution is mixed with an antisolvent, in excess, which induces precipitation. Typically, solvent to antisolvent ratios of 1:5 – 1:10 are employed.[23] Coprecipitation commercial feasibility has been demonstrated by the FDA-approved product Zelboraf®.[1,6,24,25] Moreover, a recent strategy of co-precipitation has been reported, where rapid precipitation conditions are assured by microfluidization by high-pressure homogenization (HPH), allowing the production of nano or micro particles of API-polymer composite precipitate.[19]

Although coprecipitation circumvents the low solubility aspect of the "brick-dust" molecules it has the following drawbacks: the high volume and low solids' load of the resultant suspension, due to the use of excess antisolvent, and the challenging drying of non-volatile organic solvents. Therefore, coprecipitated suspensions require further processing: organic solvent removal/washing, numerous standard filtrations and secondary drying, resulting in an overall higher cycle time, with low throughput, which may not be financially appealing in early stage development.

To address these drawbacks and enable the production of ASDs of "brick-dust" compounds by coprecipitation, the work in this Thesis intends to conduct a proof of concept using hollow fiber membranes. After coprecipitation, crossflow filtration with hollow-fiber membranes will be accomplished to: firstly, concentrate the suspension from coprecipitation and increase solids' load, by reducing the excess volume of liquid; and secondly, reduce the organic solvent content, by replacing it with an aqueous-based (anti)solvent, through diafiltration. After this stage,

the process finishes with a spray drying step to dry the remaining aqueous antisolvent and isolate the particles – a final dried powder is obtained.

The aim of the work described in this Thesis is to produce ASDs via coprecipitation coupled with a crossflow filtration unit and demonstrate equivalent performance of the final powder(s) with typical spray-dried ASDs.

Two active pharmaceutical ingredients with solubility constrains will be selected to produce the ASDs: itraconazole, a BCS Class II, and furosemide, a BCS Class IV. Itraconazole (ITZ) is a broad-spectrum triazole antifungal agent and a BCS II Class drug.[26] ITZ is a weakly basic drug (pKa=3.7).[26] ITZ can easily permeate into intestinal membrane, as a result of its highly lipophilic nature (log P= 6.2).[26] But due to its poor aqueous solubility, oral administration may result in poor bioavailability. Furosemide (FUR) is a potent loop diuretic widely used for oral treatment of hypertension and edema.[27] FUR is a weakly acid with pKa of 3.5 and 9.9.[28] FUR exhibits a low aqueous solubility, that increases as a function of pH.[29] FUR often presents variable bioavailability, because in the acidic pH of the stomach, FUR absorption is incomplete and inconsistent and even with the pH increase in the intestine, the drug remains hardly adsorbed due to its low permeability (log P = 2.56).[27,28,30]

Primarily, an *in silico* screening study will be performed as a first indicator of polymer and drug load, followed by confirmatory *in vitro* screening experiments. This structured development approach helps to narrow down the selection of polymer and drug load to be selected for the final formulation/product. Based on these *in silico* and *in vitro* screening results, amorphous solid dispersions will be produced by typical spray drying – benchmarks – and by two distinct coprecipitation techniques. Coprecipitation prototypes will be produced with a High Shear Mixer (HSM) and with the microfluidization methodology using High-Pressure Homogenization (HPH).

The production of ASDs via coprecipitation can be divided into three major unit operations: ASDs production, concentration & diafiltration and isolation. The schematization is summarized in Figure 1.1, using HPH as example for ASDs production.

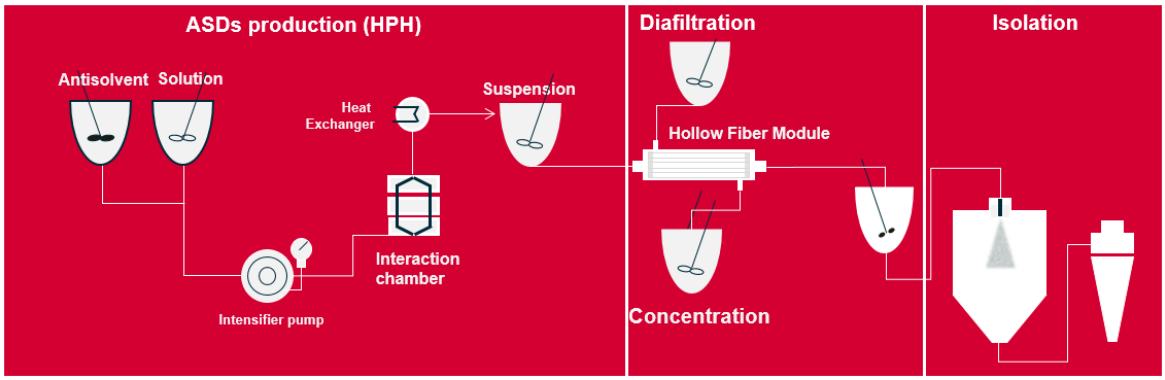

Figure 1.1 – Unit operations in ASDs production via coprecipitation. Exemplification with HPH technique.

Even though the membrane technology is not able to completely isolate the coprecipitated particles, it can overcome bottlenecks when processing high-volume suspensions and non-volatile organic solvents. With this membrane "pre-treatment", further isolation through SD is significantly facilitated, which can improve the process overall efficiency.[31] Hence, the suggested incorporation of a crossflow filtration unit will aim to extend the production of ASDs to include high boiling points organic solvents best suited for "brick-dust" compounds, while circumventing the need for secondary drying and reducing cycle time.

The coprecipitated prototypes powders produced will be compared with the SD benchmarks powders, through analytical characterization: DSC, XRPD, GC, TGA, HPLC, PSD, SEM, bulk density and *in vitro* biorelevant dissolution studies.

This Thesis is organized in 6 chapters:

- **Chapter 1** – Contains a brief contextualization of the focus of this study and the proposal of the objective for this Thesis;
- **Chapter 2** – Covers literature review on amorphous solid dispersions (with emphasis on their manufacturing technologies, screening methodologies and analytical characterization), membrane separation processes and an overview of design of experiments in pharmaceutical industry;
- **Chapter 3** – Describes the initially proposed experimental plan (with the corresponding DoEs) and the final reduced experimental plan; and the materials and methods employed;
- **Chapter 4** – Results presentation and their discussion.
- **Chapter 5** – Presents the conclusions of this Thesis and suggestions for future work.
- **Chapter 6** – References

2

State of the art

2.1. THE SOLUBILITY CHALLENGE IN PHARMA

Oral drug delivery (ODD) is usually the most preferred administration route, because it does not have many sterility restraints, it is allied with high patient compliance, flexible in the dosage form design (solution, suspension, emulsion, powder, granule, capsule, tablet and so forth) and usually the manufacturing costs are lower.[1–4] In 2019, 54% of the FDA's (Food and Drug Administration) new drug approvals corresponded to oral dosage forms.[32] Furthermore, the ODD route represents approximately 60% of the pharmaceutical commercial products.[1,2] However, oral delivery route presents some challenges, namely poor bioavailability. Bioavailability reflects formulation performance and it corresponds to the percentage of an administered dose that actually reaches the systemic circulation.[33] Hence, if the drug is administrated intravenously its bioavailability is 100%, which does not happen when it is administrated orally.[34]

The pharmaceutical pipelines have numerous new drug candidates presenting solubility limitations.[19] With the new high-throughput screening technologies and with the new chemical entities (NCEs) becoming structurally more complex with larger molecular weight and greater lipophilicity, the solubility challenge will not disappear in the future and research dedication will be given in order to continue solving this limitation.[1,5] Approximately 90% of drugs in development stages have solubility constraints, so it is expected that the percentage of the commercially available products suffering from poor aqueous solubility continues to grow.[5] Currently, about 40% of the commercially available products are poorly-water soluble drug substances and belong to Class II and Class IV according to Biopharmaceutics Classification System (BCS)[5–9]. The BCS (Figure 2.1) delineates active pharmaceutical ingredients (APIs) into four categories according to the key parameters controlling oral drug absorption: [3,9,35]

- drug's permeability through the gastrointestinal (GI) tract membrane and
- the aqueous solubility/dissolution of the drug dose in the GI milieu.

Figure 2.1 – Biopharmaceutics Classification System [Adapted from[35]].

When aqueous solubility is very low, it frequently results in poor oral bioavailability.[36] Bioavailability is influenced by dissolution, solubility and permeability.[4] Dissolution is a kinetic phenomenon that starts with the drug molecules' detachment from the solid surface followed by diffusion across the diffusion layer that surrounds that same solid surface.[3] Moreover, dissolution of the drug in the aqueous milieu of the GI is a requirement for oral absorption.[36] Dissolution rate is the amount of drug that goes in solution (dC) in a time interval (dt).[4] The relationship of dissolution rate and solubility is illustrated by the Nernst-Brunner equation (Noyes-Whitney equation modified with the diffusion layer concept of Fick's first law) (Equation 2.1), enlightening that "*the rate at which a solid substance dissolves in its own solution is proportional to the difference between the concentration of that solution and the concentration of the saturated solution*": [37,38]

$$\frac{dC}{dt} = \frac{D\,S}{V\,h}(C_s - C)$$

Equation 2.1 – Nernst-Brunner equation.

where $\frac{dC}{dt}$ is the concentration variation over time (i.e. dissolution rate) (mg.cm^{-3}.s^{-1}), D is the diffusion coefficient (cm^2.s^{-1}), S is the surface area (cm^2), V is the volume of the dissolution medium (cm^3), h is the thickness of the diffusion layer (cm), C_s is the saturation solubility (mg.cm^{-3}) and C the instantaneous concentration at time t (mg.cm^{-3}).[38] Under certain conditions, the equilibrium and saturation solubility may be surpassed to a metastable, supersaturated solution.[4]

2.2. OVERCOMING POOR SOLUBILITY: STRATEGIES FOR SOLUBILITY ENHANCEMENT

The low dissolution rate/poor solubility inherent to Class II and Class IV drugs are responsible for their low bioavailability, which translates into a lower percentage of the drug absorbed when compared to its initial dosage. Consequently, this leads to an unsuccessful treatment.[5–7,11] Hence, to circumvent this problem, scientists and engineers started developing innovative strategies and new drug delivery systems.

According to the Nernst-Brunner equation (Equation 2.1), the dissolution rate of drug particles, and, consequently, its bioavailability, can be improved by[23]:

- **particle-size reduction technologies** in a *top-down (*wet and jet milling, high-pressure homogenization) or *bottom-up* (crystallization/precipitation and solvent evaporation) approach, to produce micro/nanoparticles; it results in a higher surface area to volume ratio and a decrease in the diffusion layer thickness;[6]

and/or

- **solubility enhancement strategies** – if the drug has low solubility (low C_s) it will outcome in a small concentration gradient $(C_s - C)$.[3] The drug's aqueous solubility is a result of its lipophilicity and/or the intermolecular forces within the crystal lattice. Micelle formation, solubilization in co-solvents and complexation with cyclodextrines are frequently used techniques to cope with high lipophilic drugs.[8–11] Formation of salts, co-crystals and production of amorphous solid dispersions are some examples of solid state modifications when intermolecular forces are strong.[8–11] Additionally, lipid-based drug delivery systems, as liposomes or self-emulsifying drug delivery systems (SEDDs), have also proved to be viable alternatives.[12,13]

Generally, but not mandatorily, complexation, crystal modification and micronization are strategies applied to BCS Class II drugs, since they increase the dissolution rate or allow reaching sustained solubilization.[9] Conversely, as BCS Class IV drugs also have limited membrane permeability, it is more perceptive to modify drug's structures, using the aforementioned lipid-based delivery systems, amorphous solid dispersions, crystal engineering (nanocrystal and co-crystals technologies) and polymeric nanoparticulate systems.[9]

2.3. AMORPHOUS SOLID DISPERSIONS: A PLATFORM TO SOLVE SOLUBILITY CONSTRAINTS

Beyond all these possible approaches, according to reports in literature and approved products, the two leading strategies have been those based on nanocrystal technologies and amorphous solid dispersions (ASDs).[5] In nanocrystal technologies, particle size reduction provides an increase in dissolution rate and in solubility. On the other hand, ASDs overcome solubility constraints, improve dissolution behavior and bioavailability of poorly-water soluble drugs.[5,14,15]

A study performed by S.V. Jermain et al.[5] analyzed several research papers comparing nanocrystals and ASDs. Their findings were that drugs formulated as an amorphous solid dispersion seemed to perform more satisfactorily when compared to nanocrystal formulations. ASDs demonstrated effective dissolution release profiles *in vitro* or higher blood concentrations *in vivo* and overall better bioavailability, drug levels and absorption rates. Furthermore, when comparing FDA-approved products, a growth trend for ASD based products was found, while only a few nanocrystals products were approved before 2010 and none in the last years, as represented in

Figure 2.2.[5] Additionally, a list of FDA-approved products based on amorphous solid dispersions is presented in Table 2.1. From Table 2.1, it is possible to verify that most of the drug substances do indeed belong to BCS Classes II and IV and the administration route is oral.

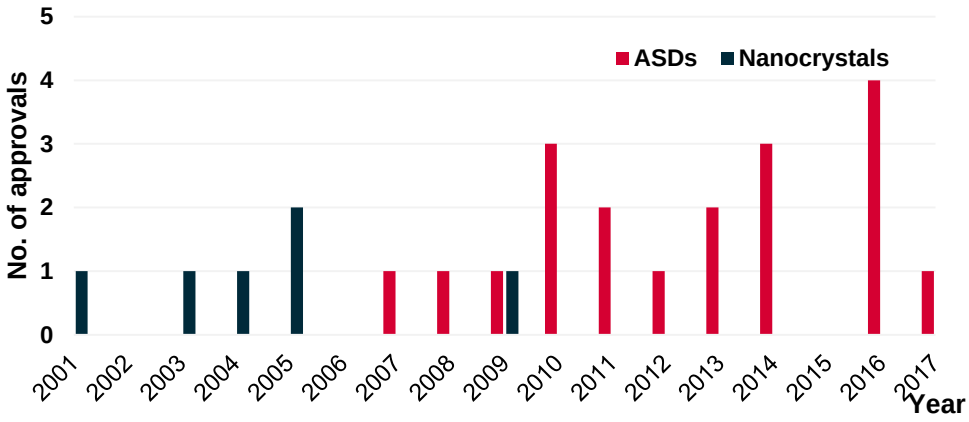

Figure 2.2 – Timeline of FDA-Approved ASDs and Nanocrystal Products. [Adapted from[5]]

An advanced search on Google Patents was also performed to comprehend the patent evolution over the last years on ASDs and nanocrystal technologies (Figure 2.3). Undoubtedly, ASDs patent publications have increased significantly, exceeding 35 last year.

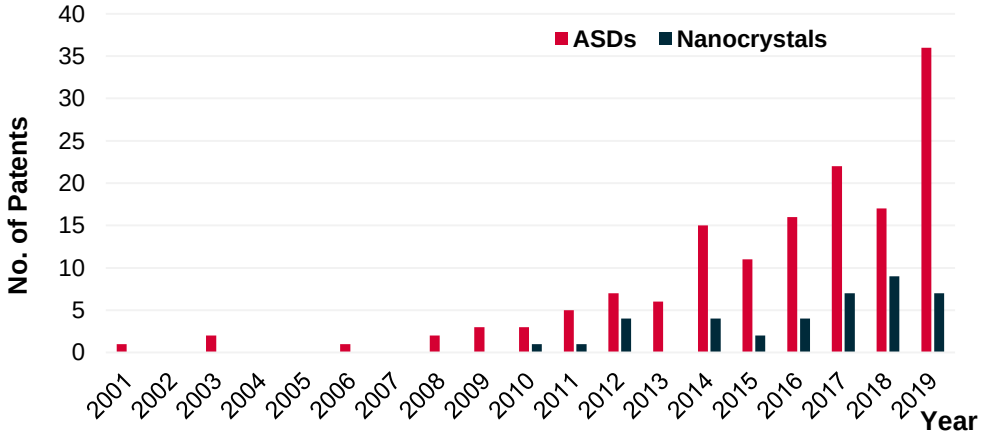

Figure 2.3 – Timeline of ASDs and Nanocrystal Patents.

Correlating the timelines of FDA-approved products and published patents, they suggest that amorphous solid dispersions are often an effective platform to solve solubility constraints for oral drug delivery and it is very likely that this trend continues in the next years.[5]

Table 2.1 – Examples of FDA-approved products that are based on amorphous solid dispersions.[5,11,22,24,39,40]

Trade Name	Drug (BCS Class)	Polymer	Dosage Form	Company/Manufacturer	Year
Cesamet ®	Nabilone (II)	PVP	Tablet	Meda Pharmaceuticals/Valeant	1985
ISOPTIN ® SR	Verapamil (II)	HPC/HMPC	Tablet	Ranbaxy Laboratories/Abbott	1987
Sporanox®	Itraconazole (II)	HPMC	Capsule	Janssen	1992
Prograf®	Tacrolimus (II)	HPMC	Capsule	Astellas Pharma/Fujisawa	1994
Kaletra®	Lopinavir (II) / Ritonavir (II)	PVP-VA64	Tablet	AbbVie/Abbott	2007
Intelence®	Etravirine (IV)	HPMC	Tablet	Janssen	2008
Modigraf®	Tacrolimus (II)	HPMC	Oral Suspension	Astellas Pharma	2009
Zortress®	Everolimus (IV)	HPMC	Tablet	Novartis	2010
Norvir® Tablet	Ritonavir (II)	PVP-VA64	Tablet	AbbVie/Abbott	2010
Onmel®	Itraconazole (II)	HPMC	Tablet	Merz Pharma/Stiefel	2010
INCIVEK®	Telaprevir (II)	HPMCAS	Tablet	Vertex	2011
Zelboraf®	Vemurafenib (IV)	HPMCAS	Tablet	Roche	2011
Kalydeco®	Ivacaftor (II/IV)	HPMCAS/SLS	Tablet	Vertex	2012
Noxafil®	Posaconazole (II)	HPMCAS	Tablet/Oral Suspension	Merck	2013
Astagraf XL®	Tacrolimus (II)	N/A	Capsule	Astellas Pharma	2013
Belsomra®	Suvorexant (II)	N/A	Tablet	Merck	2014
Harvoni®	Ledipasvir (II) / Sofosbuvir (III)	N/A	Tablet	Gilead Sciences	2014
Viekira®	Dasabuvir (II) / Ombitasvir (IV) / Paritaprevir (IV) / Ritonavir (IV)	PVP-VA/TPGS	Tablet	AbbVie	2014
Epclusa®	Sofosbuvir (III) / Velpatasvir (IV)	N/A	Tablet	Gilead Sciences	2016
Orkambi®	Lumacaftor (II) / Ivacaftor (II/IV)	HPMCAS/SLS	Tablet	Vertex	2016
Venclexta™	Venetoclax (IV)	N/A	Tablet	AbbVie	2016
Zepatier®	Elbasvir (IV) / Grazoprevir (II)	N/A	Tablet	Merck	2016
Mavyret™	Glecaprevir (IV) / Pibrentasvir (IV)	N/A	Tablet	AbbVie	2017

N/A – non-available

Amorphous solid dispersions combine an API and a stabilizer, usually a polymer. The API is converted into the amorphous state, meaning and that it lacks an organized structure, as opposed to the crystalline conformation. Moreover, drug molecules are randomly dispersed in a stabilizing (and also amorphous) polymer matrix as exemplified in Figure 2.4.[21,24] In solution, drug and polymer may form complexes via electrostatic bonds, van der Waals forces or hydrogen bonding.[41]

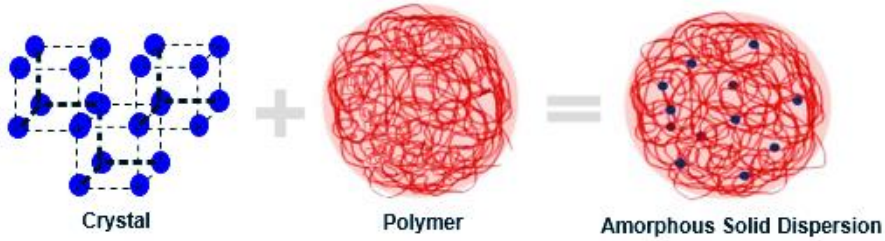

Figure 2.4 – Amorphous Solid Dispersion schematic illustration. [Adapted from[1]]

ASDs are in a metastable state and, due to the miscibility of drug-polymer, they are less prone to drug's crystallization when comparing to solely amorphous drug – with ASDs the chemical potential (μ) of the drug is reduced and the required activation energy (Ea) to crystallization increases as represented in Figure 2.5.[1]

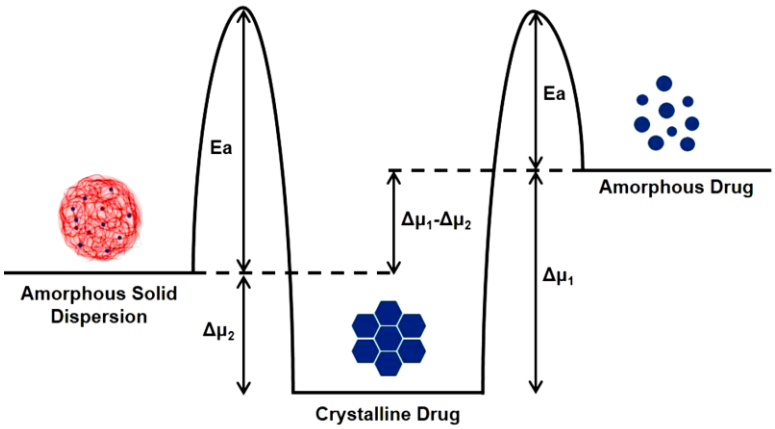

Figure 2.5 – Energy diagram representation of ASDs, crystalline and amorphous drug. [Taken from[1]]

The success of ASDs is mainly due to the so-called "spring and parachute effect" (Figure 2.6). Once the drug begins to dissolve in the GI tract, an instantaneous peak ("spring") occurs, due to the release of the stored potential energy. Drug's concentration in solution greatly increases exceeding its intrinsic solubility (C_{eq}) and a supersaturated state is reached. Bioavailability is improved since there is a higher amount of drug available to be absorbed. In addition, by maintaining and extending ("parachute") this supersaturated state, the maximum absorbable dose may be achieved and the rapid return to the drug's equilibrium solubility is avoided (preferred

"spring and parachute effect" represented by the blue line, over only "spring" represented by the red line in Figure 2.6).[5,16–19]

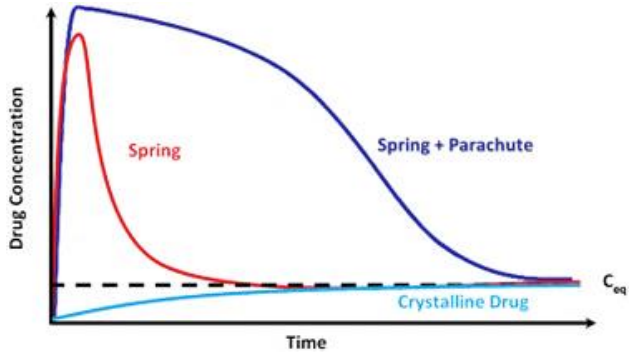

Figure 2.6 – "Spring and Parachute" Concept for supersaturation stability. [Taken from[5]]

Consequently, one of the major challenges of ASDs is the thermodynamic stability associated with supersaturation. If the amorphous API is not correctly stabilized by the polymer in a single-phase, phase separation may occur, originating drug-rich and polymer-rich regions. Ultimately, this may lead to drug's recrystallization, invalidating solubility advantages once gained. However, with the adequate formulation, it is possible to obtain and maintain a supersaturated state, that will improve dissolution and bioavailability of drugs with poor aqueous solubility, avoid drug's recrystallization, not only initially but also throughout product's shelf life, which is also an extremely relevant feature regarding pharmaceutical products.[21]

2.3.1. *ASDs Manufacturing Technologies*

Concerning existing manufacturing technologies to obtain ASDs, these can be categorized into two major distinct groups: solvent evaporation and fusion/melting processes[5,21,22]. Their selection will mainly depend on[21]:

- drug and polymer physicochemical properties (solubility, melting point and glass transition temperature);
- ASDs desirable properties in terms of further downstream processing (e.g. particle size and bulk density);
- finished drug product properties (e.g. stability and dissolution).

2.3.1.1. Fusion Methods and HME

Fusion methods were originally developed in the plastics industry over a century ago, but the first fusion-based method in pharma was only reported in 1961 by Sekiguchi and Obi. It consisted in heating the drug and polymer to produce a molten mixture and then cool and solidify it. The resultant would be crushed, pulverized and sieved to achieve a desirable particle size.[17,18]

Nowadays, hot melt extrusion (HME) is a well-established and a modern version of the traditional fusion methods. In HME, the physical mixture containing the drug and polymer is inserted into an extruder and heated above melting or glass temperature.[18] The rotating screw

inside the extruder's barrel along with heating induce disaggregation of drug particles and, consequently, these are incorporated in the molted amorphous polymer. Afterwards, this mixture is forced through a die, resulting in a uniformly shaped extrudate.[18,42] HME's schematic representation is presented in Figure 2.7.

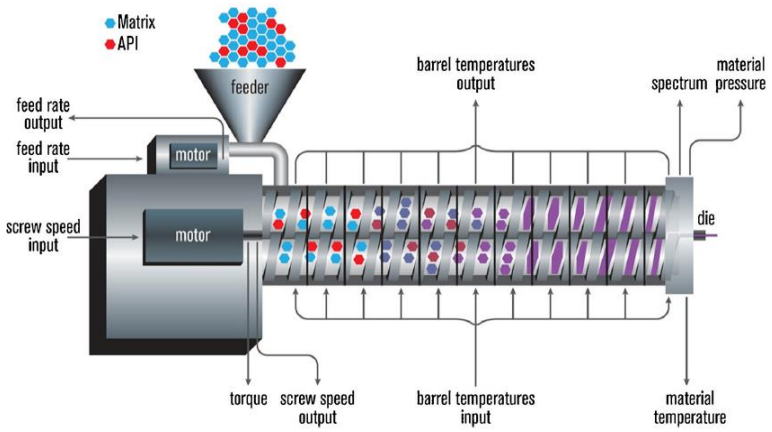

Figure 2.7 – Schematic representation of hot melt extrusion process. [Taken from[42]]

The quality of the final product will mainly be dictated by the following process parameters: feed rate, temperature, shear force, screw speed and die and barrel design.[11] The most competitive advantages of HME are related to the fact that this is a solvent-free process, so there is no need to dry the products, it can operate in continuous mode, it is scalable and it is a simple and few-stepped technique.[11,17] On the other hand, HME's biggest challenges are related to the fact that it is not a suitable process for heat and shear labile APIs, due to its high operating temperatures and intense mixing, and it requires complete miscibility of the API and polymer in the molten state.[11,17]

2.3.1.2. Solvent Methods

Solvent-based methods involve, as the name suggests, solubilization of the drug substance and carrier(s) in a solvent or solvent mixture, followed by evaporation of the latter.[17,22] It is possible to use a solvent mixture, by combining different solvents to enhance drug/polymer solubilization.[18] As drug substances are usually poorly-water soluble, (volatile) organic solvents are used.[15] Since the evaporation of these solvents can be accomplished at fairly low temperatures, degradation of thermolabile drugs/polymers can be avoided, which is the main advantage of solvent methods.[17]

Although there is a wide range organic solvents available, solvent selection may not be completely straightforward, especially if the drug and polymer have polarity divergences.[5,17,22] Furthermore, when API/polymer solubility is unavoidably low and large batches are required, the solvent volume will be necessarily high, consequently resulting in larger process times, higher costs and significant environmental issues.[17,18]

It is often necessary a secondary drying step in order to remove residual solvent.[5,17,20,43] This is typically done with vacuum in tray-dryers, but agitated conical/spherical dryers, drum dryers or fluid bed dryers can be used as well.[20,44] It is essential to assure solvent levels are bellow ICH limits.[45] Not only for safety reasons, but also because even small amounts of solvent can compromise product stability, as residual solvents may induce plasticization, increase molecular mobility and the chance for phase separation, consequently leading to (re)crystallization.[5,18]

Spray Drying

Spray drying (SD) was firstly used for the production of milk powder in the food industry.[46] However, it has reached other industries and is currently a well-established and a widely used solvent-based method to produce ASDs.[15,17,19] A typical spray drying process can be divided into four main stages[11,15,46,47]:

1. The liquid stream, containing the dissolved API and polymer, is pumped into an atomizer – spray nozzle – placed inside the drying chamber;
2. The nozzle atomizes the solution and small droplets are formed;
3. At the same time, concurrently, a hot drying gas stream (usually nitrogen to assure an inert atmosphere) contacts with the droplets and provides the necessary latent heat to a rapid solvent evaporation. Viscosity increases, leading to API's entrapment in the polymer matrix – solid dried particles are produced;
4. The dried particles exit the drying chamber and are separated from the wet gas, using a cyclone or filter bag. A solid dispersion powder is obtained.

Additionally, spray drying may also be employed to simply isolate already particle-formed suspensions or to encapsulate processing bulk APIs and excipients.[11]

Spray driers may operate in single-pass mode, where drying gas passes only once through the chamber. This is more common at laboratory-scale. Pilot and industrial production scales usually operate in closed-loop (or recycle mode), in which the wet drying gas exiting the drying chamber passes through a condenser and is reheated, before entering again in the atomizer, as illustrated in Figure 2.8.[15]

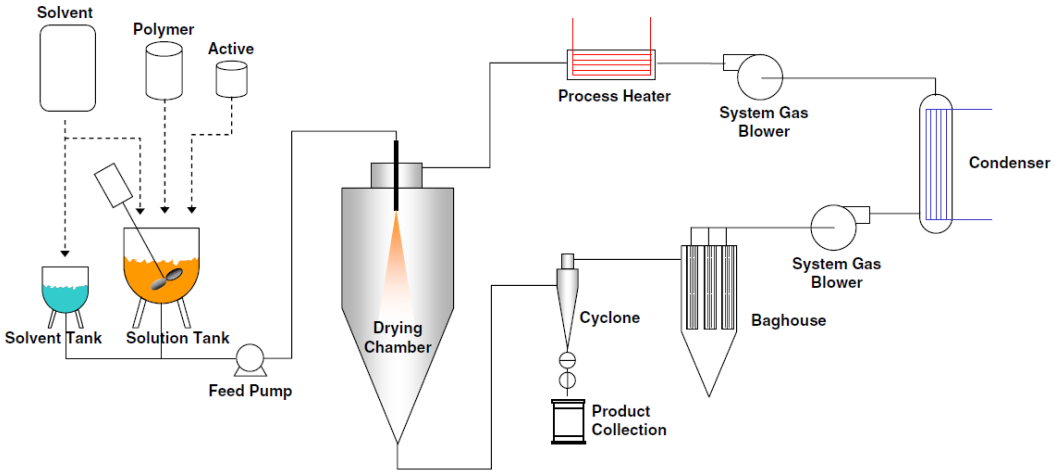

Figure 2.8 – Illustration of the spray drying process (in closed-loop). [Taken from[15]]

Desired attributes of the dried particles (e.g. morphology, density, particle size, …) can be achieved by controlling key process parameters: inlet and outlet temperature, drying gas flow rate and solution feed rate.[15,43,47] Formulation variables, such as composition (API, polymer, solvent), feed solids' concentration, solvent selection and viscosity and surface tension of the drying solution, also influence final product properties.[22] Additionally, spray nozzle's type and size have a significant impact in particle size, texture and smoothness of the resultant powder.[22] In particular, two-fluid nozzles and pressure nozzles are commonly preferred, since they are simple and scalable.[15,47] Two-fluid nozzles are more adequate to handle suspensions. Pressure nozzles enable a narrowed particle size distribution, but are not suited for suspensions, since clogging may occur.[47]

Spray drying main advantages are the simplicity of scaling-up, the ease of obtaining the desired product qualities through the fine-tuning of process parameters, it also avoids the decomposition of thermolabile molecules and can operate in continuous mode.[17,21] Disadvantages of this process are mainly related with the solvent: the struggle to remove residual organic solvents completely from the final product, especially when their classified as toxic, and the difficulty to find a proper volatile solvent-system for both polymer and API.[21,22]

Coprecipitation as an alternative to ASDs production

Beyond the referred advantages of the last two techniques to produce ASDs, there is a specific type of difficult-to-formulate drugs – "brick-dust" compounds – where neither of these processes are the best fit. The low solubility in aqueous and volatile organic solvents and the melting points above 200 °C are characteristic of "brick-dust" compounds and they preclude the use of SD or HME, respectively.[1,19] A strategic solution to address these compounds has come into play: coprecipitation, also known as Solvent-Controlled Precipitation (SCP). This is a relatively simple and scalable process, that can operate continuously and its commercial feasibility has already been demonstrated by the FDA-approved product Zelboraf®.[1,6,24,25] Approved in

2011 for the treatment of late stage melanoma, Zelboraf® is commercialized in tablet dosage.[1,5,11,22,24] Its API, vemurafenib, is a BCS Class IV drug, whose human bioavailability improved by using an amorphous polymer-stabilized solid dispersion.[25]

Coprecipitation is an antisolvent precipitation process, where the poorly water soluble drug is dissolved in an organic solvent, and is subsequently mixed with the antisolvent, typically water, under agitation.[23,24,39,48] The stabilizing polymer can be dissolved either in the solvent or in the antisolvent.[19] As the solvent effect is reduced, API solubility decreases.[23] Supersaturation occurs, which in turn induces precipitation.[19] It is crucial to assure rapid precipitation conditions (high degrees of supersaturation and particle stabilization), in order to avoid the arrangement of the molecules into a crystal structure and produce ASDs.[6,23] To prevent particle growth, a solvent-removal step can be included right after precipitation and lastly an isolation/drying step to obtain the final powder as represented in Figure 2.9.[23]

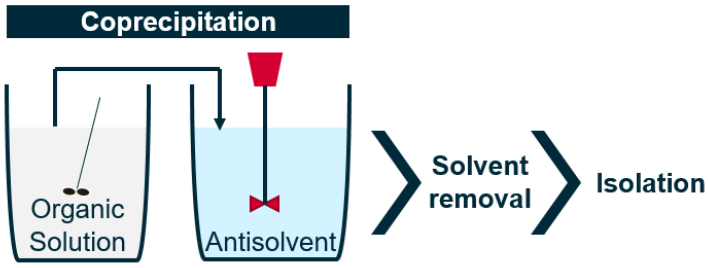

Figure 2.9 – Schematization of coprecipitation process. [Adapted from[23]]

Operational conditions (e.g. mixing time, temperature and shear rate), and formulation variables, including solvent/antisolvent ratio and their interactions, properties of the drug and polymer and their interactions and drug concentration in the solvent, will affect the outcome properties of the precipitate.[19,49] One major advantage of coprecipitation compared to SD is that this process enables the use of polar organic solvents with high boiling points and higher solubilization power, such as dimethylacetamide (DMA), dimethylformamide (DMF) and dimethyl sulfoxide (DMSO), to dissolve the drug substance.[19,23] In addition, coprecipitation is a suitable process for thermolabile compounds, unlike HME, since the antisolvent is generally cold to induce and improve precipitation and the final suspension may also be cooled in a heat exchanger.[19] On the other hand, coprecipitation bigger challenges include low solids load and the difficulty in solvent removal/drying when non-volatile polar solvents are used. Ultimately, this results in higher processing times and low throughputs, which may not be feasible, especially in early stage development.

There is a specific type of coprecipitation denominated Microprecipitated Bulk Powder (MBP) Technology where precipitation occurs in an acidified aqueous cooled media.[5,23,50] Due to the nature of this process, a polymer insoluble in the antisolvent is desired, thus ionic polymers

with pH dependent solubility, namely enteric polymers, are used.[50] This technology was implemented in the production of Zelboraf®.[25]

Recently, the new trend of flash precipitation has emerged to facilitate the production of ASDs and minimize mixing times.[23] A specific approach to rapidly produce nano or micro particles has been developed where coprecipitation is carried out using microfluidization.[19]

Microfluidization is a high-pressure homogenization (HPH) technique and is not recent – it has already been commercially used to accelerate the rate of chemical reactions (Microchannel Reaction Technology) and for particle size reduction of suspensions, in a *top-down* methodology.[51,52] Additionally, microfluidization has been applied to the production of nano-emulsions of vitamins, bioactive lipids, drugs, antioxidants and flavors.[53]

The microfluidization apparatus include[53]:

- Reservoirs for the inlet and outlet streams;
- A high-pressure/intensifier pneumatic pump;
- A pressure gauge or transducer;
- An interaction chamber (IXC), with micronized channels;
- An auxiliary processing mode (APM), which is another IXC, if needed;
- A heat exchanger.

This technology can be considered either a *top-down* process, if a pre-mixed stream is fed through a single inlet line and usually multiple passes through the system are performed; or a *bottom-up* process, if two different streams are separately fed and only a single pass through the system is performed.[54] To produce ASDs, the *bottom-up* methodology is applied: the antisolvent stream and the solvent stream with the API (and the polymer) will be fed at controlled rates, using pump(s), to maintain the solvent/antisolvent ratio. Then, both streams are pressurized through a high-pressure (intensifier) pump and delivered into the interaction chamber.[19,51] In the IXC, the pressurized stream is divided into microchannels, accelerated to a high velocity and recombined into an impingement zone, producing forces of shear, impaction and cavitation.[51,52,54] The outlet suspension passes through a heat exchanger to remove the heat generated in the IXC.[19,51,53] The process schematic representation is presented in Figure 2.10.

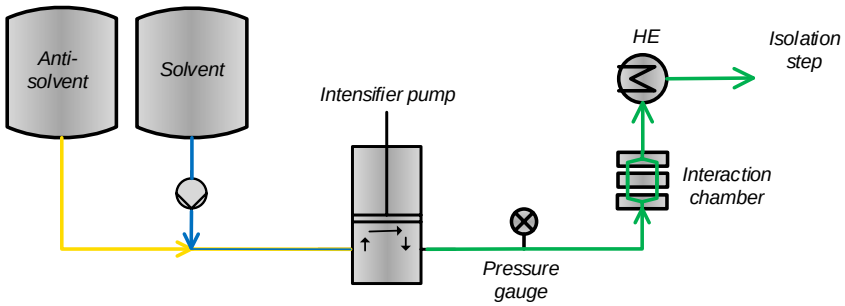

Figure 2.10 – Schematic representation of the microfluidization/HPH methodology to produce ASDs. [Taken from[19]]

The core of microfluidization will be the interaction chamber, where the impinging jet technology provides a micro-mixing environment inside a confined volume.[51] The interaction chamber has a fixed geometry and its channels depths and widths usually vary between 75µm and 300µm (see Table A.2 in Appendix), being several times smaller than other impinging jet designs.[51,53] The two main interaction chamber arrangements are Z-chamber and Y-chamber and they are illustrated in Figure 2.11. In a Z-chamber, improved turbulent mixing is generated when the high-velocity jet impacts the wall (jet-to-wall impingement), while in a Y-chamber the two jets impact each other (jet-to-jet impingement).[54] Y-chamber is generally preferred as it provides a more homogenous mixing and the jet-to-jet impingement minimizes wall shear, which lowers dissipated energy as heat and/or other losses.[53,54] Nevertheless, the Y-chamber is usually coupled with an APM, which is always a Z-type chamber. The APM can be positioned before or after the Y-chamber, to help the solids' pre-dispersion or to stabilize the flow rate and improve the homogenization efficiency, respectively.[53]

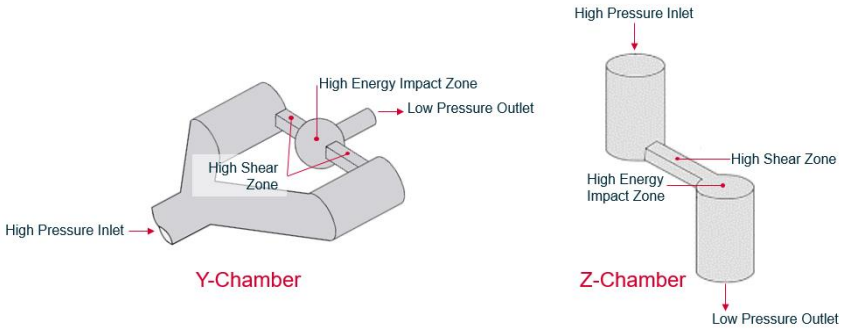

Figure 2.11 – Y-Type and Z-Type interaction chambers [Adapted from[54]].

Microfluidization has the advantage of enabling continuous fluid processing and the ease of scalability – interaction chambers can be single or multislotted, as represented in Figure 2.12, and the parallel arrays of the microchannels ensure linear scalability.[51,53,55]

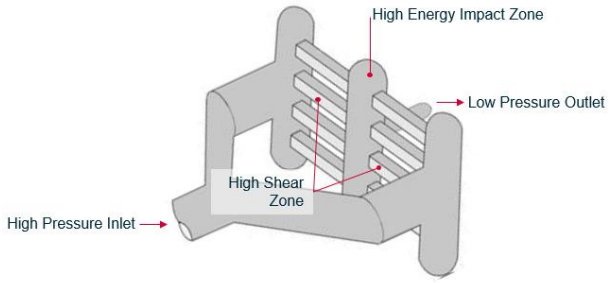

Figure 2.12 – Representation of multislotted Y-chamber. [Adapted from[56]]

In this novel coprecipitation process accomplished by microfluidization, a single passage through the interaction chamber provides a great control over the particle size distribution and a better solid-state stability of the nano or microparticles generated.[19] The IXC minimizes diffusion limitations between solvent and antisolvent streams, which decreases considerably mixing times,

and provides a great heat exchange, since it has a large surface-to-volume ratio.[19,57] This is advantageous because both mixing time and temperature are considered critical process parameters.[19,23]

Table 2.2 addresses principal manufacturing technologies, along with a brief description, advantages, drawbacks and the examples of FDA-approved products.

2.3.1.3. Other manufacturing technologies of ASDs

Besides coprecipitation, antisolvent precipitation can also be performed with compressed fluids or supercritical fluids (SCF), like supercritical carbon dioxide ($scCO_2$).[23] Moreover, spray granulation, fluid bed layering, co-grinding, ultra-rapid freezing, Kinetisol® and electrospinning are alternative technologies to produce amorphous solid dispersions.[5,11,22] However, all of them have limited applications, related to either slow evaporation rates, solvent solubility and/or incomplete conversion, consequently leading to challenges in commercial scalability and high production costs.[11,21]

Table 2.2 – Summary of the main ASDs manufacturing technologies.[5,11,21,40]

Process	Brief Description	Advantages	Drawbacks	Examples of FDA-approved products
HME	High temperatures and shear inside an extruder induce drug's incorporation in the polymer, resulting in a uniformly shaped extrudate.	Solvent-free process No drying step required Scalable Continuous operation is feasible Robust and well-established process	Not suitable for heat and shear labile compounds High melt viscosity may cause torque limitations	ISOPTIN ® SR Kaletra® Norvir® Tablet Onmel® Noxafil® Delayed-Release Tablet Belsomra® Viekira® Venclexta™ Mavyret™
SD	Atomization of a solution containing the drug and polymer in a spray nozzle inside the drying chamber. Hot nitrogen rapidly evaporates the volatile solvent in the droplets formed and the dried particles are collected using a cyclone and/or filter.	Suitable for thermolabile compounds Rapid solvent evaporation Easy scale-up Continuous operation is feasible	Difficulty in finding a solvent system for both API and polymer A secondary drying step may be necessary	Prograf® Intelence® Modigraf® Zortress® INCIVEK® Kalydeco® Harvoni® Epclusa® Orkambi® Zepatier®
Coprecipitation	Drug (and polymer) dissolved in the solvent are mixed with an antisolvent, which induces rapid precipitation. Solvent is then removed and a final step for drying/isolation is necessary to obtain the final powder.	Suitable for compounds that cannot be processed through SD and HME Provides high degree of supersaturation Continuous operation is feasible	Low solids load Downstream processing (Solvent removal and particles drying/isolation) Multiple washes to solvent removal may be needed if solvent and antisolvent are very miscible Processing times may be higher	Zelboraf®

2.3.2. *ASDs screening methodologies for ASDs formulations assessment and Analytical Characterization*

Key factors to develop a robust amorphous solid dispersion include: the design and preparation of a complete amorphous dispersion product, the maintenance of long-term physical stability over the product shelf-life and a preservation of a supersaturation state – spring and parachute effect – during *in vivo* dissolution and absorption.

A structured development approach to support and strengthen amorphous formulations is recommended and typically employed by scientists. Selection of the right polymer and drug load are determinant to achieve the aforementioned features.[21,58] Hence, preemptively, a wide--ranging assessment of both polymer and API physicochemical properties should be done. *In silico* screening based on solubility parameters, functional groups and thermal behavior (e.g. melting point and glass transition temperature) helps to narrow down the list of candidate polymers.[21] Appropriate drug loading is typically assessed by calculating of Flory-Huggins interaction parameters based on either solubility parameters or melting point depression methods. Other approaches reported in literature include solubility parameter (δ) calculation, drug-polymer thermodynamic phase diagrams prediction and crystallization inhibition with molecular dynamic calculation.[58] Even though the output of this *in silico* screening may seem promising, as any theoretical method, it should be tested experimentally.

Several experimental-based miniaturized high throughput ASD screening (HTS) systems have been available in the literature and help to further narrow down the appropriate polymer and drug load.[58] One of these miniaturized screenings is solvent casting, where drug/polymer solutions at the desired ratio are produced and placed in 96-well microplates, aluminum pans or other appropriate vessels. Then, organic solvent(s) is/are evaporated by a stream of inert gas or vacuum with heat and amorphous films are obtained. These amorphous films are further investigated for crystallinity, solubility, dissolution, supersaturation performance, and solid-state stability.[58] Another technique – Solvent-shift method – assesses the polymer ability to sustain drug's supersaturation state by dissolving the drug in a solvent (at a high concentration) and slowly add it to an aqueous/dissolution media containing the polymer being investigated.[58]

Screening methodologies contribute significantly to facilitate ASD formulation development, particularly during early stage drug development. The most favorable polymer and drug loading can be further employed in the scale-up production of ASDs prototypes.[58,59]

Figure 2.13 schematizes a summary of the steps in screening methodologies. Subsequently, analytical methods are needed to characterize the ASDs produced.

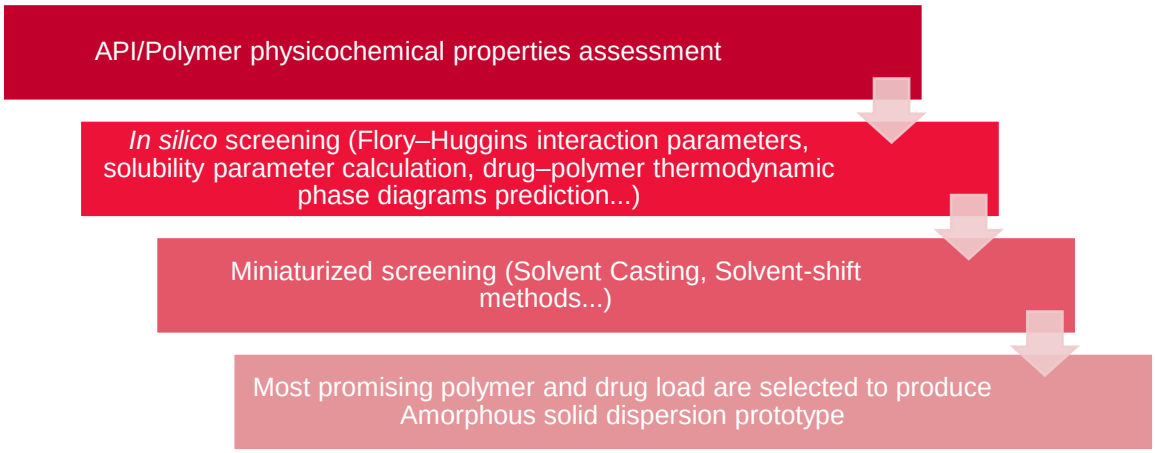

Figure 2.13 – Flow-chart of screening methodologies for ASDs formulation development.

Crystallinity presence/absence in ASDs is typically assessed with thermo-analytical approaches, including Differential Scaning Calorimetry (DSC) and modulated Differential Scaning Calorimetry (mDSC), isothermal microcalorimetry (IMC), and localized thermal analysis.[60] X-ray powder diffraction (XRPD) also detects and quantifies crystallinity.[60] To analyze the molecular interactions between ASDs components (carrier, API…) and structural changes during phase separation/crystallization and quantify crystallinity, characterization techniques, such as Thermal Gravimetric Analysis (TGA), solid-state nuclear magnetic resonance (SS-NMR), Fourier Transformed Infrared spectroscopy (FTIR) and Raman Spectroscopy are also employed.[60,61] Microscopy approaches, as optical microscopy, scanning electron microscopy (SEM), transmission electronic microscopy (TEM), atomic force microscopy (AFM) and polarized light microscopy (PLM), enable a qualitative characterization of crystallinity, molecular miscibility, phase separation and a perception of ASDs surface morphology.[61] Table 2.3 specifies the different characterization methods.

Table 2.3 – Amorphous solid dispersions characterization methods. [Adapted from[62]]

Examples of characterization methods		Description
Microscopic and surface analysis methods	SEM, TEM, AFM, PLM	Analysis of small samples for a wide range of physicochemical properties (e.g. particle size, particle morphology, crystallinity, surface properties…). Versatile, fast, and (sample) non-destructive technique.
Thermal analysis methods	TGA, DSC, mDSC, IMC, localized thermal analysis	Measurement of a material's response (e.g., variations in energy, temperature, mass) to a controlled heating/cooling. Typically used to monitor endothermic (e.g., glass transition, melting) and exothermic processes (e.g., crystallization, degradation).
Spectroscopic methods	SS-NMR, FTIR, Raman	Based on molecular and atomic-level changes (i.e. electronic transitions, vibrational transitions, and nuclear spin transitions) that occur when the sample is exposed to electromagnetic radiation. Spectroscopy offers molecular-level information about local structure in amorphous solids: drug-polymer interaction, phase separation and crystallization.

2.4. MEMBRANE SEPARATION PROCESSES

2.4.1. *Overview*

Membrane technology has been traditionally dominant in water treatment, including desalination.[63–65] Nevertheless, because of its advantages (e.g. smaller footprint, lower energy consumption, absence of phase transformation and fast processing) over common separation techniques, such as distillation and chromatography, membrane technology is becoming a promising alternative to the pharmaceutical industry.[6,63,66]

In membrane separation processes, the membrane is considered a semipermeable or selectively permeable barrier between two phases.[67] The membrane is capable of transporting the preferable(s) component(s) over others, due to differences in physical and/or chemical properties between the membrane itself and the permeating components.[67] The transport through the membrane is accomplished as a result of a driving force that is applied to the components in the feed stream.[68] Table 2.4 addresses different membrane processes according to their driving forces and examples of applications.

2.4.2. *Pressure-driven membrane processes*

Focusing on the pressure-driven membrane processes, they can be accomplished either in a dead-end flow mode or crossflow filtration (CFF) mode, also denominated tangential flow filtration. In dead-end filtration, the feed flows perpendicularly to the membrane surface.[68,69] As the feed stream is forced through the membrane, the retained particles accumulate at the membrane surface, forming a gel or cake layer.[31,68,70] As filtration proceeds and the thickness of this cake layer increases, a decline in the filtration rate is observed.[68,69,71,72] When the flow or the transmembrane pressure (as described below) reaches a limiting value, filtration must be interrupted to remove the accumulated solids – the membrane is cleaned, e.g. through backwashing, or replaced.[69] Alternatively, in CFF the feed flows parallel to the membrane surface, as represented in Figure 2.14.[71] A portion of the feed fluid passes through the membrane (permeate stream), while other components are rejected by the membrane and retained at the feed side (retentate or concentrate stream).[73] CFF is preferably chosen in comparison to dead-end filtration methods, because CFF has a very high separation efficiency, can be easily integrated within continuous processes and diminishes the probably of particle accumulation on the membrane, especially relevant at industrial applications.[70,71,74]

Table 2.4 – Classification of membrane processes according to their driving forces.[68,73]

Driving Force	Process	Phase 1	Phase 2	Examples of Applications
Pressure difference	Microfiltration (MF)	Liquid	Liquid	Analytical applications; Sterilization (food, pharmaceutics); Biotechnology (cells harvesting); Water treatment/purification.
	Ultrafiltration (UF)	Liquid	Liquid	Food processing (milk and cheese making; potato starch); Metallurgy (oil-water emulsions, electro paint recovery); Pharmaceutical (enzymes, antibiotics); Water treatment/purification.
	Nanofiltration (NF)	Liquid	Liquid	Waste water treatment; Water desalination; Textile industry (retention of dyes).
	Reverse osmosis (RO)	Liquid	Liquid	Desalination of water; Electronic industry (production of ultrapure water).
Concentration (activity) difference	Gas permeation	Gas	Gas	CO_2 & H_2S separation from CH_4; H_2 Recovery.
	Vapor permeation	Vapor	Vapor	Dehydration
	Pervaporation	Liquid	Vapor	Dehydration of organic solvents; Separation of isomers; Removal of organic components from water.
	Dialysis	Liquid	Liquid	Hemodialysis; Alcohol reduction in beer.
Electrical potential difference	Electrodialysis	Liquid	Liquid	Desalination, water treatment; Production of salt; Separation of aminoacids.
Temperature difference	Membrane distillation	Liquid	Liquid	Saline water and wastewater treatment

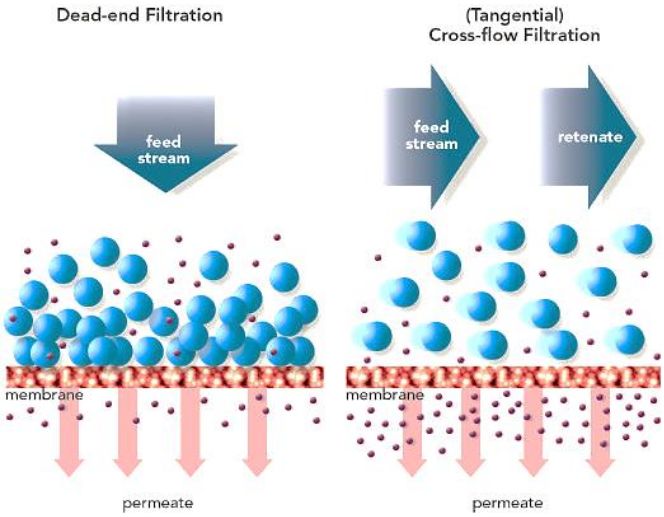

Figure 2.14 – Schematic representation of the two operation modes: dead-end filtration and CFF. [Taken from[75]]

It is the applied pressure that induces the passage of the solvent and sometimes some solutes through the membrane while other molecules or particles are rejected.[68] This pressure is called the transmembrane pressure (TMP or ΔP_{TM}) and controls the flow rate of the permeate.[69,76] TMP is given by:

$$TMP = \frac{P_{feed} + P_{retentate}}{2} - P_{permeate}$$

Equation 2.2 - Transmembrane pressure calculation.

where P_{feed} is the feed pressure (bar), $P_{permeate}$ the permeate pressure (bar) and $P_{retentate}$ the retentate pressure (bar).

Another important parameter is the permeate flux, J_v, that describes the quantity of permeate produced per unit of time (permeate flow rate) and per membrane surface area, with units of liters per square meter per hour ($Lm^{-2}h^{-1}$). The main challenge inherent to pressure-driven membranes processes is the flux decline over time, mostly due to fouling (deposition of particles/molecules in the surface or pores of the membrane that intensifies over time) and concentration polarization (build-up of the solute's concentration on the membrane wall that remains constant once established) (see Figure 2.15), which may limit process efficiency.[31,63,73] To avoid fouling, the correct adjustment of pH, temperature and the careful selection of the membrane properties (hydrophobicity, presence of charged or functional groups with specific interactions,…) should be considered.[31] Other strategies as the control of fluid dynamic conditions through the use of turbulence promoters and the increase of retentate flow rate (usually called crossflow rate) help minimizing concentration polarization.[31]

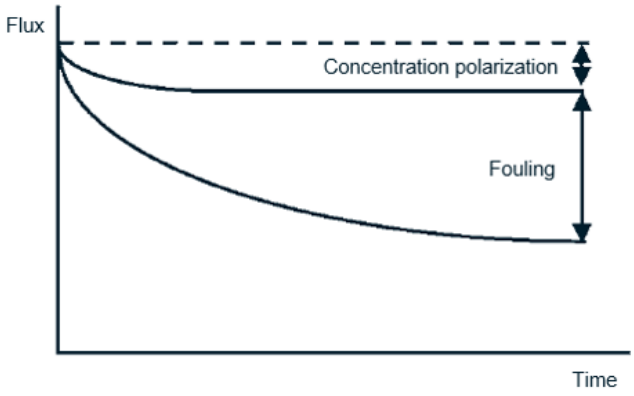

Figure 2.15 – Flux decline over time as a result of fouling or concentration polarization. [Taken from[31]]

In addition to the flux variation over time, the flux variation with TMP should also be taken into account. At first, TMP will control the permeate flux, for a given crossflow rate. However, if a gel layer is formed, an increase in TMP will not result in a flux increase and a higher crossflow rate should be considered to assure the intended flux. Therefore, the optimization of crossflow rate along with and TMP is of great relevance to achieve the highest flux possible, just before the gel layer accumulation, as represented in Figure 2.16.

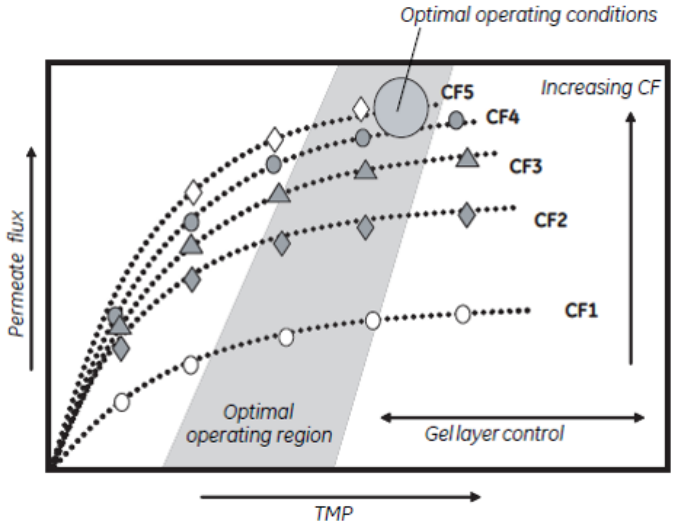

Figure 2.16 – Flux variation with TMP, at different crossflow (CF) rates. [Taken from[76]]

Addressing the range of the four pressure-driven membrane processes, the size (or molecular weight) of the particles/molecules separated will decrease from microfiltration to reverse osmosis (see Figure 2.17 and Table 2.5). Consequently, the membrane's pore size also decreases to ensure the intended rejection. This results in an increase in membrane resistance to mass transfer, which needs to be compensated with a higher applied pressure to guarantee the same flux through the membrane.[68]

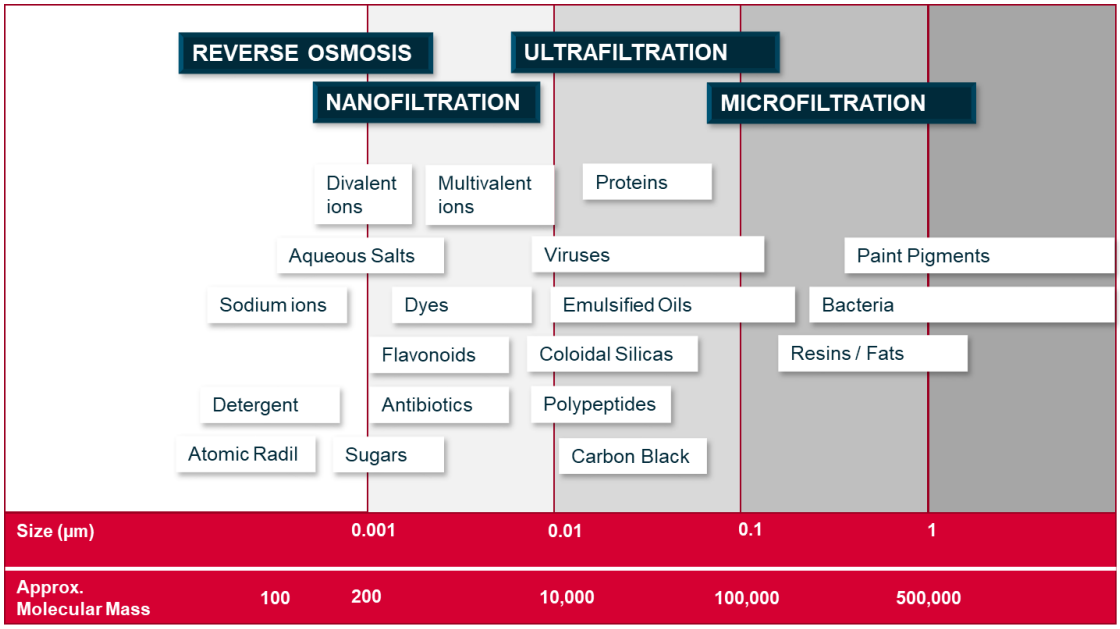

Figure 2.17 – Filtration Spectrum. [Adapted from[77]]

As presented in the Table 2.5, the applied pressure raises from MF to RO. Microfiltration is the most similar to the conventional coarse filtration and usually suitable for retaining suspensions and emulsions.[68] Ultrafiltration is typically employed in the retention of macromolecules and colloids from a solution. In both MF and UF the membrane can be considered as porous, where the rejection is predominantly based on the size and shape of the solute comparing to the membrane pore size. In opposition, in NF and RO the pores in membranes can be so small that the membrane is considered as being an intermediate between the open porous membranes (MF/UF) and the dense nonporous membranes (as in pervaporation and gas permeation). In NF and RO, the transport occurs through the membrane's free volume elements and in these processes the membrane material is critical: it should present a high affinity for the solvent and a low affinity to the solute(s).[31] Additionally, in NF and RO the osmotic pressure is no longer negligible and has to be overcome, contributing to the aforementioned higher applied pressure.[68]

Table 2.5 – Summary of the main properties of the pressure-driven separation processes.[31,68,73]

Properties	RO	NF	UF	MF
Main separation principle	Solution-diffusion + Convective flow	Solution-diffusion + Convective flow	Sieving/ Size exclusion	Sieving/ Size exclusion
Rejected components	HMWC, LMWC, Sodium Chloride, Glucose, Amino Acids	HMWC, mono-, di- and oli-gossaccharaides, multivalent ions	Macromolecules, Proteins, Vírus, Polysaccharides	Particles, yeasts, bacteria
Size of retained particles	< 1 nm	0.5 - 5 nm	1-100 nm	0.05-10 µm
Separating layer thickness	0.1-1.0 µm	0.1-1.0 µm	0.1-1.0 µm	10-150 µm
Membrane structure	Asymmetric	Asymmetric	Asymmetric	(mostly) Symmetric
Osmotic pressure	High (5-25 bar)	High (5-25 bar)	Negligible	Negligible
Applied pressure (bar)	10-100	5.0-20	1.0-5.0	0.1-2.0

Sometimes considered as another pressure-driven membrane process, diafiltration is a useful technique to perform solvent exchange, without the need of heating, as traditional batch distillation.[31,65,76] However, diafiltration it is nothing other than an enhanced design to achieve a better separation between high molecular and low molecular solutes and often ultrafiltration units are used.[31,71] Diafiltration can be executed in continuous or in discontinuous mode. The main difference is that in discontinuous mode, the feed is repetitively concentrated and re-diluted, while in continuous diafiltration, the new solvent is added constantly to the feed reservoir at the same rate the permeate is removed.[65,69,76,78] Continuous diafiltration (Figure 2.18) is the most preferred mode, due to its efficiency in terms of process time requirements to reach a given diafiltration factor ($diafiltration\ factor\ =\ new\ solvent\ volume/starting\ volume$).

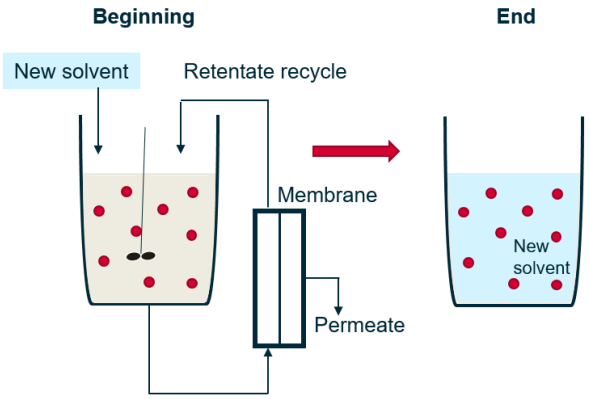

Figure 2.18 – Schematic drawing of continuous diafiltration. [Adapted from[79]]

In pressure-driven membrane processes, the concentration of the solute (particle or molecule) to be separated is relatively low and its size and chemical properties will dictate the necessary membrane structure (i.e. porous or dense, mean pore size, pore size distribution,…).[31,68] The proper membrane material will be co-determined by the solvent, the applied pressure, the operating temperature and the cleaning method.[31] For pressure-driven separations, membranes are either organic (polymeric) or inorganic (ceramic, metal or glass based).[31] Moreover, the configuration of the membrane module is process-dependent and the commercially available modules are the plate-and-frame, spiral-wound, tubular and hollow-fiber (Figure 2.19).[73] Some relevant aspects that should be taken into account when selecting a module include: scale of operation, type of separation, ease of cleaning and maintenance, possibility of membrane replacement and, of course, equipment costs.[71] Nevertheless, the most commonly used membrane modules are the hollow-fiber, along with spiral-wound, due to their higher area-to-volume ratio.[73]

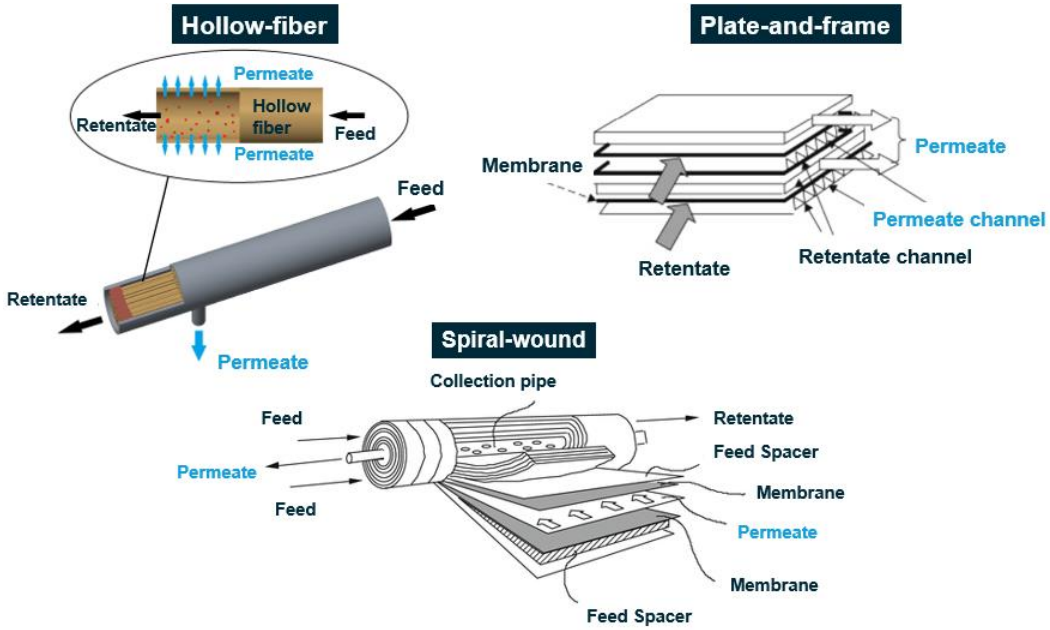

Figure 2.19 – Different membrane modules configuration. [Adapted from[80–82]]

As any process, membrane technology has its benefits and drawbacks and they are summarized in Table 2.6.

Table 2.6 – Membrane Separation Processes – Summary of benefits and drawbacks.

Benefits	Drawbacks
▪ Flexibility – Separation, concentration and purification processes of different products may be performed across a wide range of industries; ▪ Generally low energy requirements; ▪ Processes can be carried out under relatively low temperatures; ▪ Clean and environmentally friendly technology; ▪ Separation can be carried out continuously and coupled with other processes and operations; ▪ Scale-up is relatively straightforward.	▪ Concentration polarization; ▪ Membrane fouling; ▪ Necessary cleaning and maintenance; ▪ Short membrane lifetime; ▪ Equipment costs can be high.

2.4.3. *Membranes in pharmaceutical industry*

In the biopharmaceutical field, microfiltration, ultrafiltration and diafiltration are well-established techniques used in downstream processing, for broth clarification, desalting, buffer exchange and protein concentration.[65,74] However, membrane applications for the organic-solvent based processes of the pharmaceutical industry are emerging: solvent recovery/exchange, catalyst recovery, drug intermediate separation and crystallization are some examples.[65] Organic solvent nanofiltration (OSN), also known as organophilic nanofiltration (ONF) or solvent resistant nanofiltration (SRNF), has been used for solvent exchange/recovery, pharmaceutical concentration and catalyst recovery, although mostly at laboratory scale.[31,64,66,83–85] Organic solvent forward osmosis (OSFO) has also received attention as an alternative to pressure-driven OSN.[66] Moreover, continuous crystallization techniques using hollow-fiber membrane modules, namely porous hollow fiber antisolvent crystallization (PHFAC), solid hollow fiber cooling crystallizer (SHFCC) and membrane-assisted antisolvent crystallization (MAAC), to yield polymer-coated drug crystals have been reported in the literature.[86–89] To the best of this author knowledge, at this time, no major contributions to the incorporation of membrane filtration in ASDs production were found.

2.5. DESIGN OF EXPERIMENTS (DOE) IN PHARMACEUTICAL DEVELOPMENT

Traditionally, the development and optimization of pharmaceutical products was performed by analyzing one factor at a time (OFAT approach): one factor (e.g. temperature) is changed, while other factors (e.g. stirring speed) are kept constants.[90] A high number of experiments would be necessary, which makes this a very time-consuming and resource-demanding technique. Besides, as the OFAT approach is incapable of studying simultaneously several factor changes, it also lacks the ability of identifying the existence of possible interactions between different factors.[91]

Regulatory entities (FDA, EMA) suggest and encourage the implementation of Quality by Design (QbD) in pharmaceutical industry, a concept that was already implemented in other sectors.[91] QbD was introduced in 1992 by Juran[92] and, in pharmaceutical field, QbD is considered as a "*systematic approach to pharmaceutical development that begins with predefined objectives and emphasizes product and process understanding and process control, based on sound science and quality risk management*".[90,93] Since QbD was recommended, Design of Experiments (DoE) has been widely used as a statistical tool to identify, through mathematical models, the relationships between input factors (independent variables, e.g. temperature, stirring speed, solids' concentration) and one or more output responses (dependent variables, e.g. particle size, dissolution rate, crystallinity).[90] In DoE, experiments are planned and executed, the data are analyzed and the resulting model is evaluated and converted into information.[94] DoE may be applied throughout different stages of a product/process: [91,94]

- **Screening designs**: employed in the beginning of the experimental procedure, with the objective of exploring several factors, find out if they have an effect on the responses and find their approximate ranges. Hence, the critical process parameters (CPPs) and critical material attributes (CMAs), affecting the critical quality attributes (CQAs) are identified;
- **Optimization designs**: once screening is concluded, the significant factors are further studied. The goal is to be able to predict the response values for all possible factors' combinations within the design space region and identify the optimal experimental point – where the most influential factors are set at levels that improve product's CQAs.
- **Robustness testing**: performed as the last test before a product's release, to demonstrate its robustness, even to small fluctuations in the factor levels.

Factorial designs are extensively used in screening stages, but they are also applied in robustness testing.[94] In factorial designs, process parameters are intentionally and simultaneously varied according to a matrix of factor levels defined *a priori*.[94] Usually, 2-3 factors are studied with two investigation levels for each factor. Additionally, an optional number of center-point

experiments is carried out to investigate the experimental error. According to the number of experiments, factorial designs can be categorized either as full factorial or fractional factorial. In full factorials, all possible factor levels combinations are investigated. For example, if three factors with two levels are studied, $2^3 = 8$ experiments are performed (excluding center points). The major drawback of full factorials is related with the accentuated increase in the number of experiments with the number of factors. Contrariwise, in a fractional factorial design, only a half or a quarter of the total experiments are executed. Fractional factorials are especially helpful when more than four factors are studied. Nevertheless, their main limitation is associated with confounding or alias of main effects and interactions between factors.[91] For optimization stages, composite designs are employed to study more than two levels of each factor.[94] Figure 2.20 illustrates these different types of designs (circles represent experiments and asterisks center points).

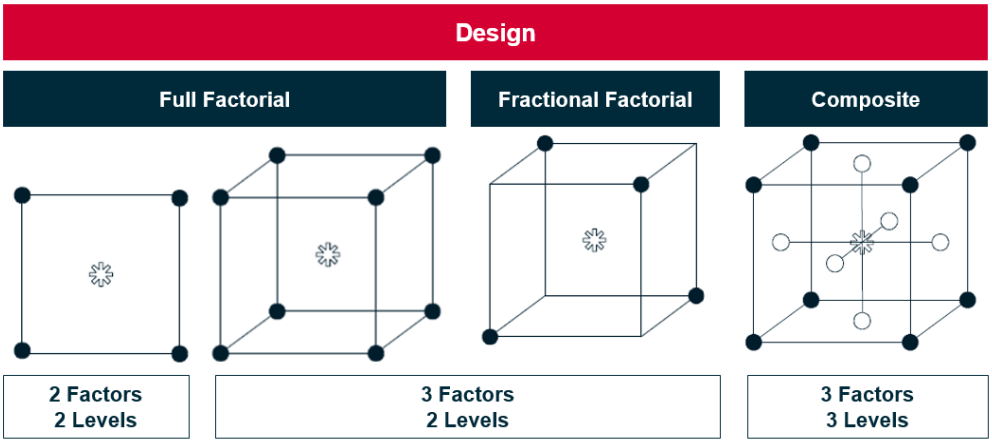

Figure 2.20 – Schematic representation of different designs. [Adapted from [94]]

3

Experimental Plan

A preliminary assessment was carried to identify the factors that should be studied in the DoEs, in order to identify the critical process parameters and their impact on the critical quality attributes. CQAs include:

- Crystallinity absence;
- Particle size distribution;
- Particle morphology;
- Bulk density;
- Residual solvents;
- Assay;
- *In vitro* dissolution profile.

The rationale supporting the different factors analyzed throughout the entire process – from coprecipitation to CFF and isolation by SD – and respective DoEs schematization is presented in DoEs and Rationale section. The followed experimental plan is presented at the end of this subchapter.

3.1. INITIAL EXPERIMENTAL PLAN

3.1.1. In Silico *Screening,* In Vitro *Screening and initial studies*

The *in silico* screening study is aligned with the QbD initiative, as it provides information of the most promising solvent system and formulation (API/polymer ratio and drug load), without experimental trials. Then, the most promising outcomes of this study will be experimentally tested through *in vitro* screening: solvent screening, solvent casting and supersaturation studies. As a result, the appropriate solvent (or solvent system) for the process is identified, the polymer with the greatest performance in ASDs stabilization is chosen and the drug load selected.

Other initial studies of this Thesis include: solvent/antisolvent ratio and pH effect study. The solvent/antisolvent (S/AS) ratio study will be conducted at different feed solids' concentration (5, 10 and 15 wt.%) and different S/AS ratios (1:3, 1:7, 1:12 wt.%). The focus is to identify the foremost S/AS ratio that maximizes precipitation of materials in solution. The pH effect study intends to examine the influence of acidic and neutral pH in crystallinity presence in coprecipitation. As a guideline, it is recommended that the pH of the antisolvent is controlled at a level not exceeding API's pKa, in order to minimize API solubility.[44]

3.1.2. *DoEs and Rationale*

As part of the main focus of this work, a DoE should be performed in the crossflow filtration – concentration and diafiltration step. Nevertheless, the production of the ASDs by coprecipitation, either with the HSM or by HPH, is also of great importance, since it is the stage where the particles are actually formed. Process variables in HSM/HPH may have a severe impact the final product attributes, namely particle size and morphology. Therefore, it was thought to carry out a total of three DoEs: two DoEs in both ASDs production strategies (HSM and HPH) and one DoE in the crossflow filtration step. Half factorials designs were considered to have a smaller number of experiments, with the downside of its inherent limitation of possible confounding or alias of main effects and interactions between factors.[91]

3.1.2.1. Production of ASDs by Coprecipitation with a High shear mixer (HSM)

- **Stirring speed**

The stirring speed influences the mixing conditions between the solvent and the antisolvent. Hence, stirring speed can affect particle size.[7] More intense mixing tends to yield smaller particles, but high-speed mixing during coprecipitation can be detrimental to amorphous particles formation.[7,23,44]

- **Addition rate ($Q_{solvent}$) and feed location**

The addition rate may have a significant impact on coprecipitate formation. The evaluation of the feed location, either at surface level or sub-surface (bellow impeller and at its level), is also considered relevant. This variable should be studied in a few experiments around this DoE's center point.

- **Temperature**

Operating temperature impacts particle formation process, especially in particle size distribuition.[7,23] As API solubility tends to increase at higher temperatures, this reduces supersaturation, often larger particle sizes and an increase in crystallinity can occur.[44] Moreover, if a significant amount of the API remains solubilized, the drug load will be negatively impacted as well as yield. Temperature impact will be studied by manipulating antisolvent temperature.

- **Solvent/Antisolvent (S/AS) ratio**

The antisolvent addition reduces API solubility. Consequently, this leads to supersaturation, inducing precipitation and particles formation. So, the quantity of antisolvent added is crucial to maximize precipitation. Furthermore, the S/AS ratio needs to be correctly adjusted to ensure the rapid quenching of the amorphous particles. Otherwise, crystalline particles may be yielded. Rapid precipitation rates are usually achievable at S/AS ratios of 1:5 – 1:10.[23] Moreover, increasing this ratio tends to decrease particle size.[7]

Even though S/AS ratio can have a significant impact on the nature of the particles produced (crystalline or amorphous), it was chosen not to study its impact in the DoE. Instead, preliminary tests will be conducted during initial studies to find the best S/AS ratio, as previously mentioned.

- **Feed solids' concentration**

Particle size may depend on the feed solids' concentration.[19] This variable may possibly impact particle morphology and density. The strategy will be to replicate the same DoE and change feed solids' concentration in other two different percentages (10 and 15 wt.%.).

The addressed variables for HSM DoE are summarized in Table 3.1 and DoE schematization is presented in Figure 3.1.

Table 3.1 – Summary of variables for HSM DoE along with their possible impact on process/product attributes. Selected factors are highlighted in bold.

Variables	Rationale
Stirring speed	RPMs may impact morphology and crystallinity
Antisolvent temperature	May impact solubility and yield
Addition rate ($Q_{solvent}$) and feed location	May impact morphology and assay
Solvent/Antisolvent ratio*	May impact assay and yield
Feed solids' concentration**	May impact morphology, PS and density

* Initial studies; ** Repeat DoE with different concentrations.

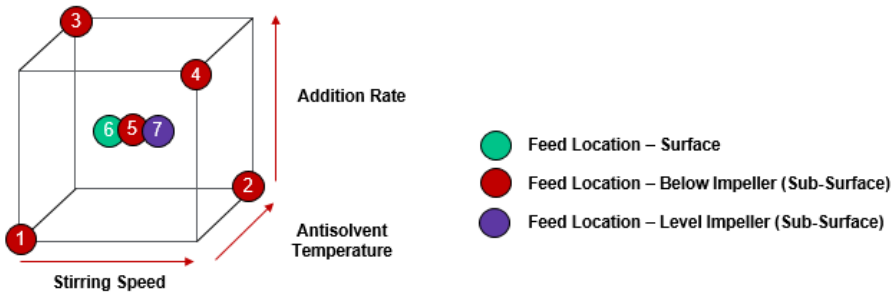

Figure 3.1 – HSM DoE Schematization (Initial Experimental Plan).

3.1.2.2. Production of ASDs by Coprecipitation with High-pressure homogenization (HPH)

- **Interaction chamber type and size**

As address in the State of the art section, the type of interaction chamber, Y or Z, differs in how the impinging jet(s) will impact, either on each other or against the chamber wall, respectively.[51,53,54] Chamber type and channel size may affect the particles generated in their PSD and morphology.

- **Pressure in HPH – Intensifier pump**

Due to the nature of this process, the effect of the pressure applied in the pump should be studied. Tendencies show that smaller particles are achieved at higher pressures.[95] Additionally, high operating pressures cause a temperature rise, which in turn may affect the stream viscosity and, if not controlled, can ultimately induce partial dissolution of the ASD.[95]

- **Temperature**

The relation between the solvent and antisolvent temperatures is considered as an important factor, similarly to HSM DoE. Additionally, the cooling temperature in the interaction chamber and in the heat exchanger after the IXC may influence the process. It is to be noted that in the IXC, streams are pressurized and accelerated to a high velocity in a confined space, which leads to a rising in temperature.[19,51,53] The effect of chamber cooling will be studied in an experiment around this DoE's center point.

- **Solvent/Antisolvent (S/AS) ratio and feed solids' concentration**

Both variables will be addressed in the same approach as in the HSM. In HPH, the interaction chambers enable a fine control of supersaturation if adequate ratios are selected.[6]

The variables for HPH DoE are summarized in Table 3.2 and DoE schematization is presented in Figure 3.2.

Table 3.2 – Summary of variables for HPH DoE along with their possible impact on process/product attributes. Selected factors are highlighted in bold.

Variables	Rationale
Interaction chamber type and size	May impact morphology
Pressure in HPH/Piston Pump	May impact assay and yield
Antisolvent temperature	May impact morphology, assay and yield
Chamber cooling temperature*	May impact assay and yield
Solvent/Antisolvent ratio**	May impact assay and yield
Feed solids' concentration***	May impact morphology, PS and density

***** Experiment around center point; ** Initial studies; *** Repeat DoE with different concentrations.

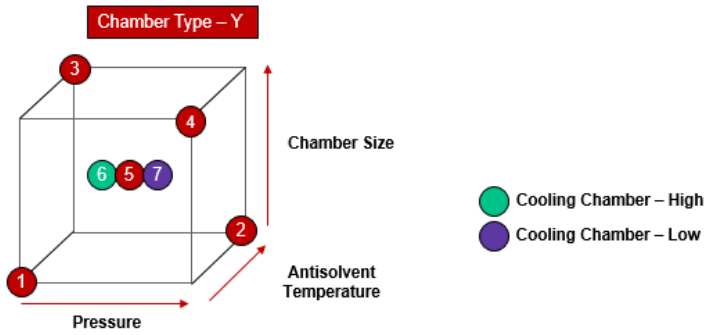

Figure 3.2 – HPH DoE Schematization – example with Y-type chamber. (Initial Experimental Plan).

3.1.2.3. Concentration and Diafiltration Step – Crossflow filtration (CFF) with hollow-fiber membranes

- **Membrane features (pore size, area of filtration)**

Membrane's pore size and filtration area have an influence on particles retention and overall, on filtration efficiency. In particular, the pore size should be adequate to retain the target product to avoid losses to the permeate stream. In addition, pore size may play a role in minimizing fouling: with smaller pores, particulate material cannot enter and block the pores.[76] A standard guideline for product concentration recommends to use UF filter with a nominal molecular weight cut-off (NMWC) that is 3x to 5x less than the molecular weight of the target product.[76] A conservative approach was to have a NMWC of 500 kD (equivalent to a range of 50 – 100 nm) to minimize any potential yield losses. Therefore, this variable will not be studied in the DoE and it will be selected based on supplier information. The available filtration area reflects on the permeate flux and it is intended to study its impact around the DoE's center point.

- **Membrane Material**

The membrane material should be selected according to the chemical compatibility to the solvent in use and operating pressure and temperature. This decision will be based on literature and on supplier information and datasheet, thus, this variable will not be studied in the DoE.

- **Pressure (TMP) and Crossflow rate**

As address in the State of the art section, TMP is the driving force in membrane processes and should be fine-tunned along with crossflow rate, to optimize the highest flux possible, while avoiding/minimizing the formation of the cake layer at membrane surface.

- **Temperature**

Temperature can influence the viscosity, increase the presence of degradation products and reduce material stability. Also higher temperatures can increase the tendency to crystallization, by residual dissolution.

- **Concentration factor (Solids' concentration)**

The concentration factor should be carefully studied since particle growth may occur, without adequate mixing.[23,76] As solvent is removed, particles are concentrated and the tendency to aggregate increases.

- **Diafiltration factor**

The diafiltration factors represents the extent to which original solvent and antisolvent mixture is replaced by antisolvent solely. The plan will be to "track" the organic solvent in retentate stream with a conductometer until ICH levels are acceptable, thus this factor is excluded from the DoE.

The variables for CFF DoE are summarized in Table 3.3 and DoE schematization is presented in Figure 3.3.

Table 3.3 – Summary of variables for CFF DoE along with their possible impact on process/product attributes. Selected factors are highlighted in bold.

Variables	Rationale
Porous size*/**Area of filtration**	May impact yield, membrane efficiency
Membrane Material*	May impact process, yield, cycle time
Pressure (TMP) and Crossflow rate	May impact yield, membrane efficiency and cycle time and process cost (replace membranes more frequently)
Temperature	May impact morphology, assay, yield and membrane efficiency
Concentration Factor (solids' concentration)	May impact membrane efficiency (gel layer) and yield (increase non-recoverable product)
Diafiltration Factor**	May impact yield (if loss of particles to permeate) and cycle time

* Selected based on supplier information and literature ** Conductivity measurements

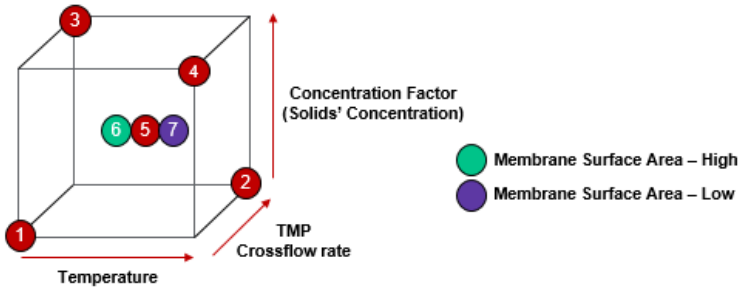

Figure 3.3 – CFF DoE Schematization (Initial Experimental Plan).

3.2. REDUCED EXPERIMENTAL PLAN

Due to the pandemic situation of COVID-19, the initially proposed experimental plan had to be readjusted. The working schedule in the laboratory facilities, the available resources and equipment had to be, forcibly, adjusted to cope with Health, Safety and Environmental (HSE) requirements, which resulted in an inevitable decrease in the number of experiments and the time to conduct them.

3.2.1. In Silico *Screening,* In Vitro *Screening and initial studies*

Only confirmatory trials from *in silico* screening results were carried out in the laboratory during *in vitro* screening. pH effect experiments remained the same. S/AS ratio studies were reduced to only 5 wt.% of feed solids' concentration.

3.2.2. *DoEs*

It was decided to perform only center point experiments in the HSM and HPH DoEs. In the concentration and diafiltration step, the DoE was also reduced to center points. The final version of the DoEs is represented bellow in Figure 3.4 to Figure 3.6.

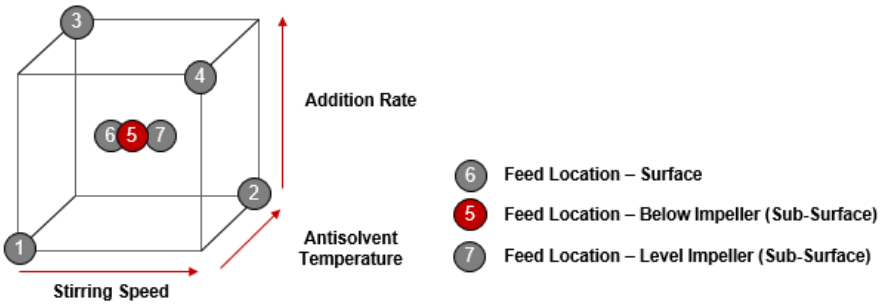

Figure 3.4 – HSM DoE Schematization (Reduced Experimental Plan).

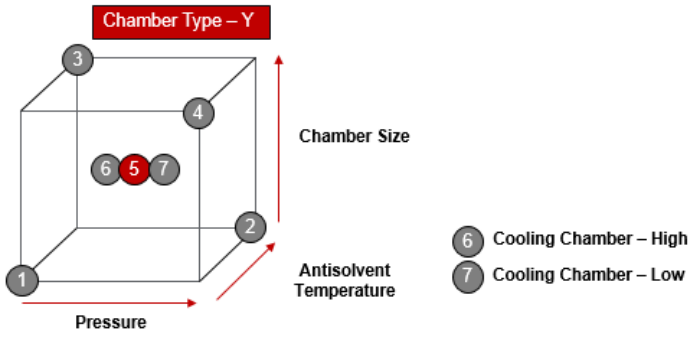

Figure 3.5 – HPH DoE Schematization (Reduced Experimental Plan).

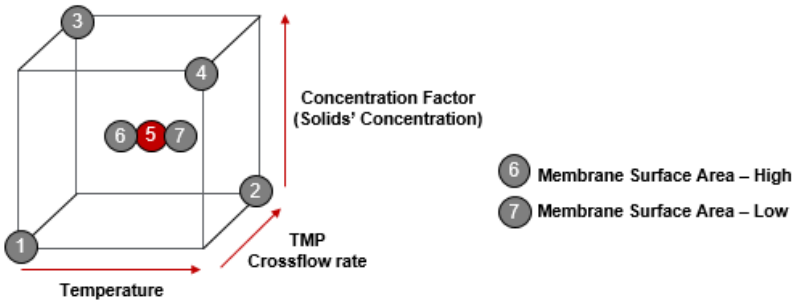

Figure 3.6 – CFF DoE Schematization (Reduced Experimental Plan).

3.3. MATERIALS

The materials used during SD benchmarks and coprecipitated prototypes production are listed in Table 3.4.

Table 3.4 – Materials used during SD benchmarks and coprecipitated prototypes production.

Material	Vendor/Manufacturer	Purity (wt.%)	C.A.S number
Furosemide (FUR)	Fagron Iberica, S.A.U.	98.5 – 101.0	54-31-9
Itraconazole (ITZ)	Fagron Iberica, S.A.U.	98,5 – 101.5	84625-61-6
Eudragit L100 (1:1methacrylic acid and methyl methacrylate co-polymer)	Evonik Röhm GmbH	Non-available	25086-15-1
HPMCAS-M (hydroxypropylmethylcellulose acetate succinate)	Shin-Etsu Chemical Co., Ltd	>95	71138-97-1
Dicloromethane (DCM)	Drogas Vigo, S.L.	100	75-09-2
Methanol (MeOH)	Drogas Vigo, S.L.	>99	67-56-1
Dimethyl sulfoxide (DMSO)	Biosolve Chimie	99.99	67-68-5
Citric Acid monohidrated	Quimidroga S.A	100	5949-29-1
Methanol gradient grade for liquid chromatography Li-Chrosolv® Reag. Ph Eur	Merck KGaA	<= 100	67-56-1
N,N-Dimethylformamide (DMF)	Sigma-Aldrich Química, S.L	<= 100	68-12-2
N,N-Dimethylacetaminde (DMA)	Sigma-Aldrich Química, S.L.	<= 100	127-19-5
N-Methyl-2-pyrrolidone (NMP)	Sigma-Aldrich Química, S.L.	<= 100	872-50-4
Acetonitrile (ACN) gradient grade for liquid chromatography LiChrosolv® Reag. Ph Eur	Merck KGaA	<= 100	75-05-8
Trifluoroacetic Acid (TFA) for spectroscopy Uvasol®	Merck KGaA	>= 80 - <= 100	76-05-1
Fasted State Simulated Intestinal Fluid (FaSSIF) powder	biorelevant.com, Ltd., United Kingdom.	70.3 - 77.7	145-42-6
Deionized water	Milli-Q® Water Purification System	Non-applicable	Non-applicable

To better understand the behavior of the molecules used as model drugs and the studied polymers, Figure 3.7 displays the chemical structures of the drugs and Table 3.5 and Table 3.6 summarize their physicochemical properties.

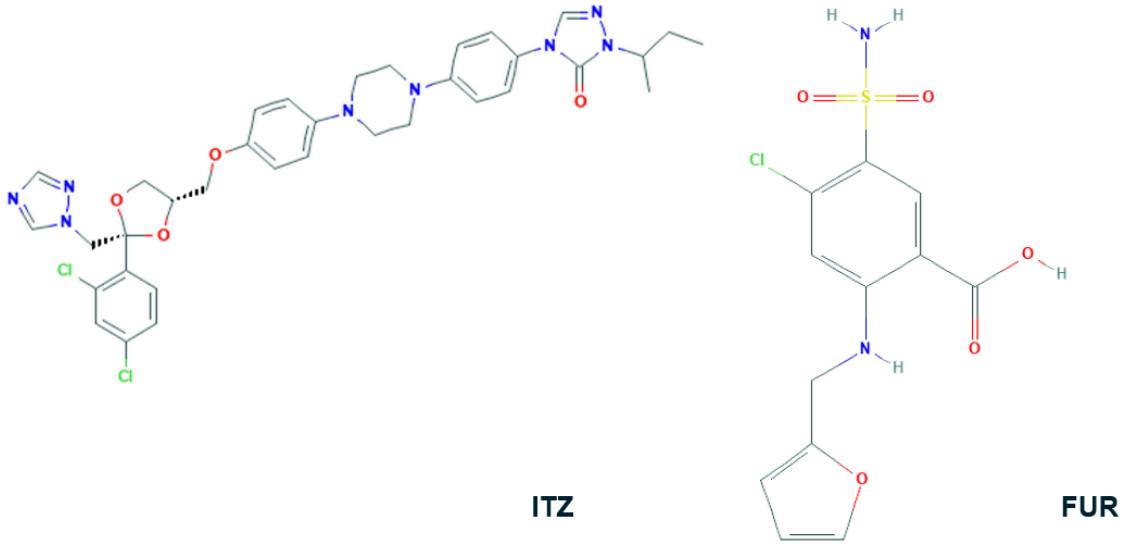

Figure 3.7 – Chemical structure of Itraconazole (ITZ) and Furosemide (FUR).

Table 3.5 – Physicochemical properties of the model drugs used in this work.

Physicochemical Characteristics	Itraconazole	Furosemide
Molecular formula	$C_{35}H_{38}Cl_2N_8O_4$	$C_{12}H_{11}ClN_2O_5S$
Molecular weight (g/mol)	705.64	330.74
LogP	6.2[a]	2.56[h]
pKa	3.7[a]	3.53, 9.90[h]
T_m (ºC)	166.2[b]	206.0[i]
T_g (ºC)	59.9[c]	61.8[j]
Aqueous solubility	Pratically insoluble[b]	73.1 mg/L (at 30ºC)[i]
In buffer at pH 1.7 (stomach) (mg/mL)	3.68[d]	0.03[d]
In buffer at pH 6.5 (jejunum/ileum) (mg/mL)	0.0003[d]	29.2[d]
Expected target dose	100 mg[f]	20, 40 or 80 mg[k]
Drug indication	Triazole antifungal agent[g]	Potent loop diuretic; hypertension and edema treatment[l]
BCS Class	II[g]	IV[l]

[a] retrieved from [26]; [b] retrieved from [96]; [c] retrieved from [97]; [d] calculated with ACD/Percepta© 2019.1.3 Build 3200; [f] retrieved from [98]; [g] retrieved from [26]; [h] retrieved from [30]; [i] retrieved from [99]; [j] retrieved from [100]; [k] retrieved from [101]; [l] retrieved from [27]

Table 3.6 – Physicochemical properties of the studied polymers.

Polymer	Chemical category	Molecular weight (g/mol)	Classification	Solubility/ Dissolution pH	T_g (ºC)	Degradation temperature (ºC)
Methocel E3[a]	Cellulose ethers	8 200	Non-ionic	Water soluble	170 – 180	190
Methocel E5[a]	Cellulose ethers	10 000	Non-ionic	Water soluble	170 – 180	190
Methocel E15[a]	Cellulose ethers	20 000	Non-ionic	Water soluble	170 – 180	190
HPMCP-HP55[a]	Cellulose ethers	80 000 – 130 000	Anionic	pH>5.0	133	185
HPMCAS-L[a,c]	Cellulose ethers	~ 18 000	Anionic	pH>5.5	120 – 135	200
HPMCAS-M[a,c]	Cellulose ethers	~ 18 000	Anionic	pH>6.0	120 – 135	200
HPMCAS-H[a,c]	Cellulose ethers	~ 18 000	Anionic	pH>6.8	120 – 135	200
Soluplus[a]	Polyvinyllactam polymers	118 000	Non-ionic	Water soluble	~ 70	250
PVP/VA 64[a]	Polyvinyllactam polymers	45 000 – 70 000	Non-ionic	Water soluble	106	230
Povidone K30[a,b]	Polyvinyllactam polymers	50 000	Non-ionic	Water soluble	168	>300
Eudragit EPO[a]	Methacrylate copolymers	47 000	Cationic	pH<5.0	~ 48	200
Eudragit L100[a]	Methacrylic acid copolymers	125 000	Anionic	pH>6.0	192	380
Eudragit L100-55[a]	Methacrylate copolymers	320 000	Anionic	pH>5.5	110	300

[a] Retrieved from [102]; [b] Retrieved from [103]; [c] Retrieved from [104]

3.4. METHODS

3.4.1. In Silico *Screening*

Hansen solubility parameters (HSP) for Itraconazole and Furosemide were determined with HSPiP software. In this methodology, the total solubility of a chemical entity is estimated by the solubility contribution of each of the molecule's functional groups – functional group contribution method. Each contribution is decomposed in 3 main solubility drivers: $\delta D\ dispersion$, $\delta P\ polar$ and $\delta D\ hydrogen\ bonding$. Chemical entities with similar molecular parameters are, in theory, miscible and the solubility distance between two components estimated as follows:

$$\boldsymbol{HPS\ distance^2 = 4(\delta D_1 - \delta D_2)^2 + (\delta P_1 - \delta P_2)^2 + (\delta H_1 - \delta H_2)^2}$$

Equation 3.1 – Hansen solubility parameters distance calculation.

Then, using the Solvent Optimizer tool within the HSPiP software, ITZ and FUR solubility parameters were benchmarked against the Hovione's solvent database values, to generate a set of promising solvent systems to be confirmed *in vitro.*

The miscibility assessment was performed using the Flory-Huggins (F-H) model (Equation 3.2):

$$\frac{\Delta G}{RT} = n_d ln\varphi_d + n_p ln\varphi_p + \chi_{dp} n_d \varphi_p$$

Equation 3.2 – Flory-Huggins equation.

where ΔG is the free energy of mixing, R is the gas constant, T is the absolute temperature, $n_{d,p}$ are the number of moles of the drug and polymer, respectively, $\varphi_{d,p}$ are the volume fractions of the drug and polymer, respectively, and χ_{dp} is the F-H interaction parameter. The Flory-Huggins model represents the Helmholtz free energy, where the interaction parameters are computed from the component's solubility parameters (obtained from HSPiP software) and Hovione's polymer database. Different drug-polymer ratios were assessed. Polymers from different chemical families were evaluated: methacrylic acid copolymers (Eudragit EPO, Eudragit L100, Eudragit L100-55), hydroxyl propyl methyl cellulose acetate succinate (HPMCAS-H, HPMCAS-L, HPMCAS-M), hydroxyl propyl methyl cellulose (HPMCP-HP55, Methocel E3, Methocel E5, Methocel E15), polyvinylpyrrolidone (Povidone K30, PVP/VA 64) and Soluplus.

3.4.2. In Vitro *Screening*

3.4.2.1. Solvent Screening

100 mg of each API were weighted into small vials to evaluate the solvent systems from the *in silico* screening outcome. The solvent/solvent systems were slowly added, under stirring, until complete dissolution of the API. When the solution turned clear, the vials were tightly sealed

and left overnight in a stirring plate. Solids' concentration was calculated and the solution visually evaluated (immediately and overnight).

9.5 g of the solvents/solvent system were added to 500 mg of each polymer, under stirring and the solution was visually evaluated.

3.4.2.2. Solvent Casting

5 g solutions with 5 wt.% solids' concentration and different API:Polymer ratio were prepared, under stirring, according to Table 3.7. When all of the material was completely dissolved, 40 µL of each solution were pipetted to DSC aluminum pans 3 times to assure approximately 5 mg of casted film. These pans were dried 24 hours in a tray oven at 40 ºC, to promote solvent evaporation and formation of casted films. After drying, the pans were sealed with pin-holed lids, placed in the DSC sample tray and analyzed with the mDSC method described latter in this section.

Table 3.7 – Solvent Casting – Studied conditions.

Test #	API (wt.%)	Polymer (wt.%)	API (mg)	Polymer (mg)
1	ITZ (100%)	N/AP	250	0
2	FUR (100%)	N/AP	250	0
3	ITZ (10%)	HPMCAS-M (90%)	25	225
4	ITZ (30%)	HPMCAS-M (70%)	75	175
5	ITZ (50%)	HPMCAS-M (50%)	125	125
6	ITZ (10%)	Eudragit L100 (90%)	25	225
7	ITZ (20%)	Eudragit L100 (80%)	50	200
8	ITZ (50%)	Eudragit L100 (50%)	125	125
9	FUR (20%)	HPMCAS-M (80%)	50	200
10	FUR (50%)	HPMCAS-M (50%)	125	125
11	FUR (80%)	HPMCAS-M (20%)	200	50
12	FUR (20%)	Eudragit L100 (80%)	50	200
13	FUR (50%)	Eudragit L100 (50%)	125	125
14	FUR (60%)	Eudragit L100 (40%)	150	100
15	N/AP	HPMCAS-M (100%)	0	250
16	N/AP	Eudragit L100 (100%)	0	250

N/AP – Non applicable

3.4.2.3. Supersaturation Studies

FaSSGF, Transition medium and FaSSIF Biorelevant medium Preparation

To prepare a 2 L FaSSFG Buffer with the concentration of 2 g NaCl/L and a pH of 1.6, 1800 mL of deionized water were transferred into a 2 L volumetric flask, followed by the addition of 3.998 g of sodium chloride (NaCl) and stirring in a stirrer plate RCT basic (IKA, Germany) until NaCl was completely dissolved. The pH was adjusted with concentrated hydrochloric acid (HCl) and the volume was completed with deionized water. Then, 1000 mL of this Buffer FaSSFG were

transferred into a 2 L flask and 0.1194 g of FaSSIF powder were added. To finalize, the remaining 1000 mL of Buffer FaSSFG were added to the 2 L flask, with continuous stirring.

To prepare a 2 L Transition Medium Buffer with a pH of 7.5, 3.950 g of sodium hydroxide (NaOH), 12.741 g of sodium phosphate monobasic anhydrous (NaH_2PO_4) and 19.500 g of NaCl were weighted and added to 1800 mL of deionized water in a 2 L volumetric flask. The Transition Medium Buffer solution was left to stir. pH was adjusted with concentrated HCl and NaOH. The volume was completed with deionized water. 1000 mL of Transition Medium Buffer were transferred to a 2 L flask and 8.195 g of FaSSIF powder was added, under stirring. The remaining 1000 mL were transferred to the 2 L flask and the Transitium Medium was then left to stir for 30 minutes.

To prepare 1 L of FaSSIF, 500 mL of FaSSFG and 500 mL of Transition Medium were transferred into a 1 L flask.

HPMCAS-M and Eudragit L100 Solutions in FaSSIF

Two concentrated solutions, one for each polymer, were prepared in FaSSIF. 90 mg of HPMCAS-M and 90 mg of Eudragit L100 were dissolved in 50 mL of FASSIF, respectively, to obtain 1.8 mg/mL solutions. Both solutions were placed in an ultrasonic bath Branson 8800 (Emerson, USA) for 20 minutes until complete dissolution. These solutions were diluted in 10 mL volumetric flasks, according to the concentrations required (see Table 3.8).

API Stock solutions

Two stock solutions, one for each API, were prepared according to 50 times the respective target dose. The target dose of ITZ in solution was set at 200 µg/mL – which corresponds to the concentration of 100 mg (dosage of Sporanox® capsules[98]) in 500 mL of intestinal fluid (FaSSIF). Similarly, the FUR solution concentration was set at 160 µg/mL – the equivalent concentration of 80 mg of FUR (maximum dosage of Lasix® tablets[101]) in 500 mL of FASSIF. Thus, the ITZ solution was prepared by dissolving 50 mg of ITZ in 5 mL of DMF and the FUR solution was prepared by dissolving 40 mg of FUR in 5 mL of DMF.

UV Absorbance used in supersaturation studies

UV absorbance was used to evaluate the polymer's ability to maintain the supersaturated state. These studies were conducted in a UV multi-well plate reader (Synergy|HTX Multi-Mode Microplate Reader, Biotek) using 24-well quartz microplates.

To generate supersaturated solutions, 30 µL of the corresponding API stock solution was spiked into 1.5 mL of FASSIF or polymer/FASSIF solutions already inside the well. Table 3.8 covers the studied conditions.

Table 3.8 – Supersaturation studies conditions.

Test #	API (wt.%)	Polymer (wt.%)	Polymer concentration in FASSIF (mg/mL)	Pipetted volume of the respective concentrated polymer solution (mL)
1	ITZ (100%)	N/AP	0	N/AP
2	FUR (100%)	N/AP	0	N/AP
3	ITZ (10%)	HPMCAS-M (90%)	1.80	N/AP
4	ITZ (30%)	HPMCAS-M (70%)	0.47	2.6
5	ITZ (50%)	HPMCAS-M (50%)	0.20	1.1
6	ITZ (10%)	Eudragit L100 (90%)	1.80	N/AP
7	ITZ (20%)	Eudragit L100 (80%)	0.80	4.4
8	ITZ (50%)	Eudragit L100 (50%)	0.20	1.1
9	FUR (20%)	HPMCAS-M (80%)	0.64	3.6
10*				
11*				
12	FUR (20%)	Eudragit L100 (80%)	0.64	3.6
13	FUR (50%)	Eudragit L100 (50%)	0.16	0.9
14	FUR (60%)	Eudragit L100 (40%)	0.11	0.6

* Tests 10 and 11 were not performed due to the results obtained from solvent casting.
N/AP – Non applicable

Samples were incubated at 37 ºC with continuous orbital shaking and analyzed at a selective wavelength for the API (300 nm for ITZ and 350 nm for FUR) and at a non-selective/absorbing wavelength for both APIs (450 nm). Data collection started immediately after spiking the corresponding API solution to the test medium. Absorbance measurements were performed each minute for 12 hours. All experiments were made in duplicate.

3.4.3. *Spray Drying*

Solutions Preparation at 5 wt.% solids' concentration

Two solutions of ITZ and FUR were prepared in DCM/MeOH (70/30 wt.%), at equal solids' concentration (5 wt.%), as presented in Table 3.9. Each API was added, followed by very slow addition of the polymer, under stirring and until complete dissolution.

Table 3.9 – SD solutions preparation.

API (wt.%)	API (g)	Polymer (wt.%)	Polymer (g)	DCM (g)	MeOH (g)
ITZ (30%)	9	HPMCAS-M (70%)	21	399	171
FUR (50%)	20	Eudragit L100 (50%)	20	532	228

Spray Drying

Spray drying was performed in a laboratory scale spray dryer (BÜCHI Mini Spray Dryer B-290, Switzerland) to dry: (1) the solutions of ITZ:HPMCAS-M and FUR:Eudragit L100 (benchmarks), and (2) the two suspensions produced by coprecipitation followed by CFF.

(1) Spray Drying – Benchmarks

The spray dryer was equipped with a two-fluid nozzle with 0.7 mm orifice and 1.5 mm cap and the unit was operated in closed-loop configuration (i.e. with recirculation of the drying nitrogen). Nitrogen was used as atomizing gas. Before initiating spray drying, the unit was stabilized first with nitrogen, and then with the process solvent system to guarantee stable inlet and outlet temperatures. The outlet temperature (T_{out}) was controlled by modulating the inlet temperature (T_{in}). The condenser temperature was set at -5 °C. After stabilization, the solutions were fed through a peristaltic pump at different flow rates (F_{feed}) (see Table 3.10) and atomized (F_{atom}) at the nozzle. The droplets formed were dried in the spray drying chamber by a co-current nitrogen stream (F_{drying} ≈ 20 kg/h). The dried particles were directed to a high-performance cyclone and lastly collect in an amber flask. A post-drying step was performed for the SD benchmark powders at 45 °C, under vacuum for 24 hours in a tray drying oven Vaciotem-TV (P Selecta, SA., Barcelona).

(2) Spray Drying – Suspensions produced by Coprecipitation followed by CFF

To dry the suspensions, the SD unit was operated in open-loop configuration (i.e. without recirculation of the drying nitrogen). The spray dryer was equipped with a two-fluid nozzle with 0.7 mm orifice and 1.5 mm cap and the condenser temperature was set at a higher temperature (5°C) to avoid water freezing. The spray dryer was stabilized with nitrogen, followed by stabilization with water. After stabilization, the suspensions were fed through a peristaltic pump and atomized at the nozzle (see Table 3.10). The droplets formed were dried in the spray drying chamber by a co-current nitrogen stream (F_{drying} ≈ 40 kg/h). The dried particles were directed to a set of two-coupled high-performance cyclones and lastly collect in amber flasks. No post-drying step was performed.

Table 3.10 – Spray Drying – Process Conditions.

System	T_{in} (°C)	T_{out} (°C)	F_{feed} (kg/h)	F_{atom} (kg/h)
ITZ:HPMCAS-M Solution	69	40	1.0	0.35
FUR:Eudragit L100 Solution	65	40	0.7	0.83
ITZ:HPMCAS-M Suspensions	157	80	0.6	0.83

3.4.4. *Coprecipitation*

3.4.4.1. Initial Studies: Solvent/Antisolvent Ratio Study & pH effect study

Six solutions were prepared in DMSO (solvent) at equal solids' feed concentration (5 wt.%), according to Table 3.11. The solutions were maintained under stirring (≈ 300 rpm) until complete visual dissolution was observed. Then, water (antisolvent) was added and suspensions were produced. After suspensions' settling, 1 mL of the supernatant was removed, using a filter syringe (Acrodisc® syringe filter membrane GHP, diam. 25 mm, pore size 0.45 µm) to minimize

the presence of suspended particles, and diluted with dissolution mixture (ACN:H_2O 50:50 vol.%) into volumetric flasks of 100, 50 and 25 mL. The samples were evaluated with HPLC with correspondent method described in Analytical Characterization.

Table 3.11 – Solvent/Antisolvent ratio study – tested conditions.

Test #	Ratio (wt.%)		Mass (g)		API (wt.%):Polymer (wt.%)	API (mg)	Polymer (mg)
	DMSO	H_2O	DMSO	H_2O			
1	1	3	10	30	ITZ (30%):HPMCAS-M (70%)	158	368
2	1	7	10	70	ITZ (30%):HPMCAS-M (70%)	158	368
3	1	12	10	120	ITZ (30%):HPMCAS-M (70%)	158	368
4	1	3	10	30	FUR (50%):Eudragit L100 (50%)	263	263
5	1	7	10	70	FUR (50%):Eudragit L100 (50%)	263	263
6	1	12	10	120	FUR (50%):Eudragit L100 (50%)	263	263

To evaluate the effect of pH in coprecipitation, three API:Polymer stock solutions with equivalent solids' feed concentration (5 wt.%) were prepared using DMSO as solvent, as summarized in Table 3.12. The solutions were maintained under stirring (≈ 300 rpm) until complete visual dissolution was observed.

Table 3.12 – Solutions preparation for pH effect study in coprecipitation.

Stock Solution	DMSO (g)	API (wt.%):Polymer (wt.%)	API (g)	Polymer (g)
1)	38	ITZ (30%):HPMCAS-M (70%)	0.6	1.4
2)	38	FUR (50%):Eudragit L100 (50%)	1.0	1.0
3)	38	FUR (20%):Eudragit L100 (80%)	0.4	1.6

Then, six experiments were performed in small flasks where 50 g of, either acidified or not, cold water were added under stirring (≈ 300 rpm) into 5 g of the solutions previously prepared (Table 3.13). The resultant suspensions were analyzed with PLM.

Table 3.13 – Conditions of the study of pH effect in coprecipitation.

Test #	Stock Solution	Solution (g)	Antisolvent	Antisolvent (g)
1	**1)**	5	Cold water	50
2	**1)**	5	Acidified cold water (pH=2)	50
3	**2)**	5	Cold water	50
4	**2)**	5	Acidified cold water (pH=2)	50
5	**3)**	5	Cold water	50
6	**3)**	5	Acidified cold water (pH=2)	50

Solutions Preparation for coprecipitation

Two solutions of ITZ and HPMCAS-M were prepared in DMSO, with equal solids' concentration (5 wt.%) and drug load (30wt.%), as presented in Table 3.14. The antisolvent was acidified water in a mass proportion of 1 solvent:12 antisolvent. The water was acidified with citric acid monohydrate to reach a pH of 2. One solution was intended for the coprecipitation with a high shear mixer and the other was used in the high-pressure homogenization coprecipitation process.

Table 3.14 – Coprecipitation solutions preparation.

Process	ITZ (g)	HPMCAS-M (g)	DMSO (g)	Acidified Water (g)	Citric Acid (g)
HSM	1.8	4.2	114	1 368	10.6
HPH	3.0	7.0	190	2 280	17.5

3.4.4.2. High Shear Mixer (HSM)

A high shear mixer (T 25 digital ULTRA-TURRAX®, IKA) was used to perform coprecipitation. The acidified water was initially introduced in the reactor, and its temperature set at 5 ºC. The speed of the HSM was set at 3 000 rpm. ITZ solution was exactly fed beneath the rotor/stator of the HSM, through a L-shaped tube (Figure 3.8). The solution flow rate (35 mL/min) was controlled with a peristaltic pump.

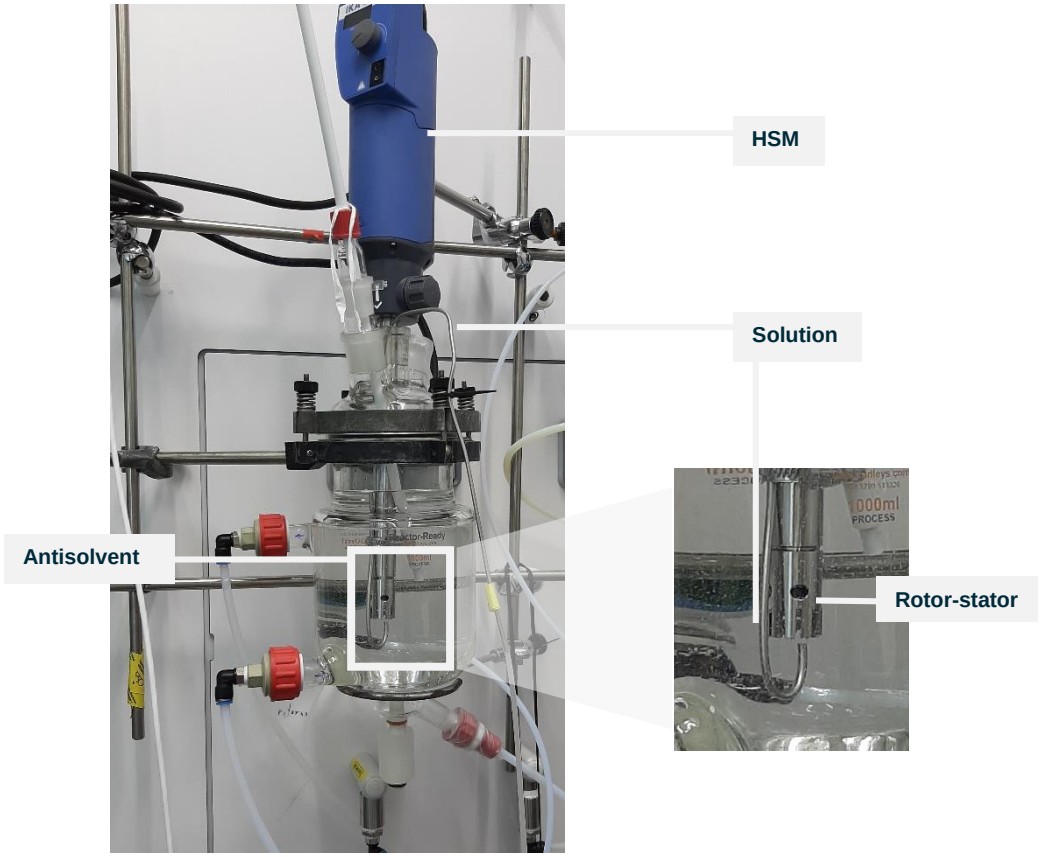

Figure 3.8 – Coprecipitation with a HSM setup.

3.4.4.3. High-Pressure Homogenization (HPH)

The other coprecipitation trial was executed with a high-pressure homogenization technique in an electric-hydraulic pilot scale homogenizer (M110EH Microfluidizer®, Microfluidics) (Figure 3.9).

To promote precipitation, the acidified water was cooled and its temperature maintained at 5 ºC. The solution was kept at room temperature, to avoid DMSO solidification. Antisolvent was gravity fed and the solution flow rate (≈ 28 mL/min) was controlled with a peristaltic pump to maintain the ratio of 1 solvent:12 antisolvent. Both streams were pressurized to, approximately, 120 bar in the intensifier pump. The combined stream passed through an Y-type interaction chamber with 75 µm diameter microchannels (F20Y), followed by Z-type chamber with 200µm diameter microchannels (H30Z). Only one passage through this setup was performed and the suspension was collected in a vessel.

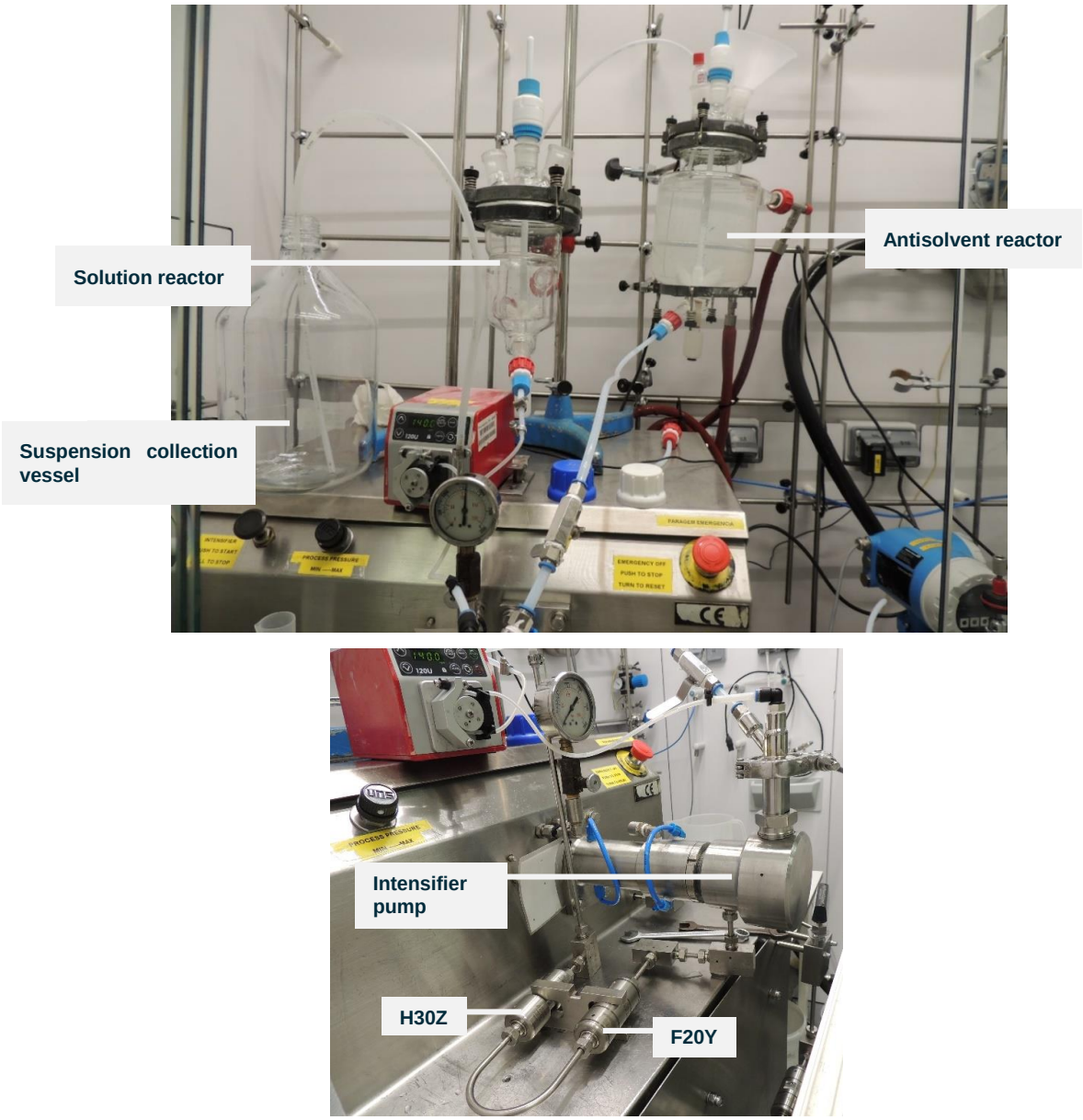

Figure 3.9 – HPH Coprecipitation setup (top) and interaction chambers and intensifier pump identification (bottom).

3.4.5. *Crossflow filtration*

Concentration and diafiltration were executed in an automated pump system – KrosFlo® KR2i Tangential Flow Filtration System (Repligen, California, USA). The system consists of a digital peristaltic pump, man/machine interface with graphical LCD display, a pump head, digital readouts of pressure values with automated shut-off controls, module stand and real-time data collection software KF Comm. The setup is shown in Figure 3.10.

Feed suspensions were kept in an ice bath to minimize residual dissolution.

3.4.5.1. Concentration and diafiltration after Coprecipitation with HSM

Concentration was carried out in two parts, where two Spectrum® Hollow fiber modules were, respectively, used: D04-E500-05-N and D06-E500-05-N.

Concerning the D04-E500-05-N module, fiber inner lumen diameter was 0.5 mm, fiber length was 41.5 cm, membrane material was modified polyethersulfone (mPES), with a total surface area of 235 cm^2. The model molecular weight cut-off (MWCO) rating was 500 kD. The material of the D06-E500-05-N module was also modified polyethersulfone (mPES), the fiber inner lumen diameter remained at 0.5 mm and MWCO rating of 500 kD. This module had a bigger fiber length (65 cm) with a higher total surface area of 370 cm^2.

In the software KF COMM, “Concentration Mode” was selected, the weight of the HSM suspension was introduced and a concentration factor of 2 defined. At “main pump section”, tubing in usage was #14, ramp rate 5 seconds, a 10 %/sec slow for valve and control shear was off. The feed flow rate was initially set at 10 mL/min and the automated backpressure valve at 0.6 bar. After all the configurations the process was initialized. Live-tracking of process variables was done, and software automatically saved data every ten seconds until de end of the trial.

In diafiltration, D06-E500-05-N module was used. Setup conditions and defined parameters did not change, except for feed flow rate which was initially set at 20 mL/min. Cold acidified water was fed to the feed reservoir through a peristaltic pump at the same permeate flow rate to keep a constant feed volume. The feed suspension was washed twice, i.e. two diafiltration volumes of acidified cold water washed through the process volume.

3.4.5.2. Concentration and diafiltration after Coprecipitation with HPH

In both concentration and diafiltration, D06-E500-05-N Spectrum® Hollow fiber module was used. To perform concentration, in the software KF COMM, “Concentration Mode” was selected, the weight of the HPH suspension was introduced and a concentration factor of 2 defined. At “main pump section”, settings remained unchanged: tubing in usage was #14, ramp rate 5 seconds, a 10%/sec slow for valve and control shear was off. The feed flow rate was initially set at 30 mL/min and the automated backpressure valve at 0.6 bar. After all the configurations the process was initialized. Live-tracking of process variables was done, and software automatically saved data every ten seconds until the end of the trial.

During diafiltration, feed flow rate was set at 18 mL/min. Setup conditions and other predefined parameters remained the same. Cold acidified water was fed to the feed reservoir through a peristaltic pump at the same permeate flow rate to keep a constant feed volume. Two diafiltration volumes of acidified cold water washed through the process volume.

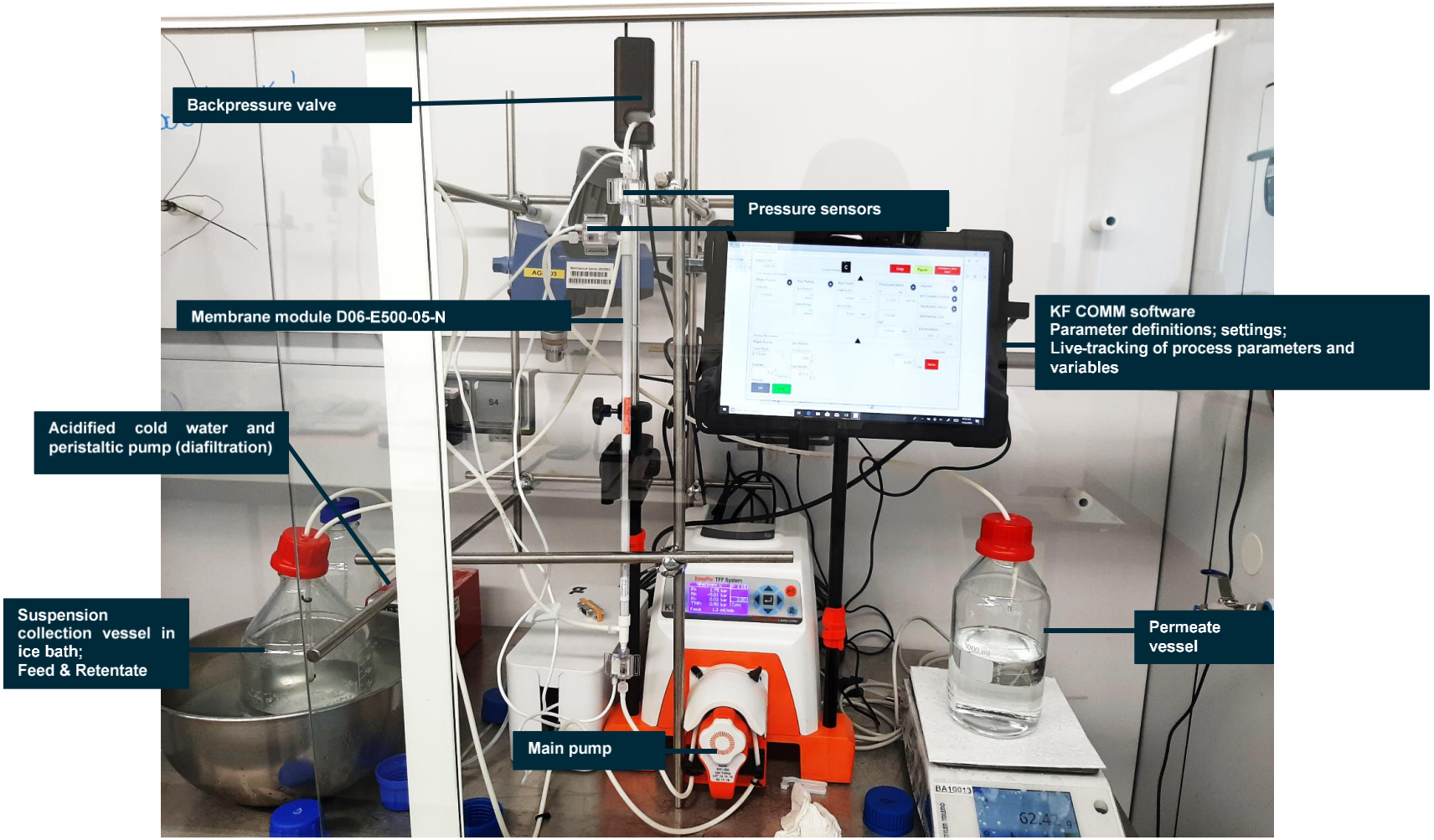

Figure 3.10 – CFF unit setup.

3.4.6. *Analytical Characterization*

mDSC and supersaturation studies were used to characterize the various samples in the screening stages, in order to identify the most promising formulation.

In the solvent/antisolvent ratio study, HPLC was used to evaluate the presence of residual API in the supernatant and PLM was used to ascertain the pH effect on coprecipitation study through birefringence evaluation.

The dried powders obtained were analytically characterized by: mDSC, XRDP, GC, TGA, HPLC, PSD, SEM, bulk density and in vitro biorelevant dissolution studies.

3.4.6.1. mDSC

Thermal analysis experiments were performed in a TA Q1000 (TA Instruments, New Castle, Delaware, USA) equipped with a refrigerated cooling system. Enthalpy response was calibrated with indium. The samples were analyzed in pin-holed DSC aluminum pans, under continuous dry nitrogen purge (50 mL/min). Samples were analyzed using a modulated heating ramp from 0 °C to 250 °C at a heating rate of 2 °C/min.

Data was analyzed and processed using the TA Universal Analysis 2000 Software (TA Instruments, New Castle, Delaware, USA). The glass transition temperature (T_g) was taken as the inflection point in the heat capacity change (ΔCp) observed in the reversible heat flow, while exothermic and endothermic peaks were identified in the non-reversible and total heat flows.

3.4.6.2. PLM

An aliquot of each suspension was added to a microscope slide and micrographs were taken in a polarized light microscope (Motic®, China).

3.4.6.3. XRPD

XRPD was performed in a D8 Advance Bruker AXS Theta-2 Theta diffractometer with a copper radiation source (Cu Kα, wavelength = 1.5406 Å), voltage 45 kV, and filament emission 40 mA. The samples were measured over a 2θ interval from 5.0076 to 39.9998° with a step size of 0.0131° and step time of 97.92 s.

3.4.6.4. GC

For SD benchmarks, 100 mg of each sample were added to 10 mL headspace GC vials. 1 mL of DMA was added into each vial. The detector was at a temperature of 270 ºC in a constant makeup mode: makeup flow – N_2 – 30 mL/min; hydrogen flow 40 mL/min; air flow 400 mL/min. The column used was DB-624, with 30 m length, 0.32 mm internal diameter and 1.8 µm of film thickness. The carrier gas was helium, and it was fed at a constant flow rate (2 mL/min). The oven conditions were as presented in Table 3.15.

For coprecipitated prototypes, 100 mg of each sample were added to 20 mL headspace GC vials. 2 mL of NMP were added into each vial. The detector was at a temperature of 250ºC in

a constant makeup mode: makeup flow – N_2 – 30 mL/min; hydrogen flow 40 mL/min; air flow 400 mL/min. The column used was DB-624, with 60 m length, 0.32 mm internal diameter and 1.8 µm of film thickness. The carrier gas was helium, and it was fed at a constant flow rate (2 mL/min). The oven conditions were as presented in Table 3.15.

Table 3.15 – GC oven conditions for SD benchmarks and coprecipitated prototypes samples.

Oven conditions	SD benchmarks samples	Coprecipitated prototypes samples
Equilibration time (min)	0.0	0.05
Initial temperature (ºC)	32	40
Initial time (min)	5.0	4.0
Rate 1 (ºC/min)	0.5	3.0
Final temperature (ºC)	37	60
Hold time 1 (min)	0.0	0.0
Rate 2 (ºC/min)	8.0	5.0
Final temperature (ºC)	85	80
Hold time 2 (min)	0.0	2.0
Rate 3 (ºC/min)	30	35
Final temperature (ºC)	220	200
Hold time 3 (min)	2.0	2.0
Rate 4 (ºC/min)	N/AP	35
Final temperature (ºC)	N/AP	220
Hold time 4 (min)	N/AP	5.0
Total run time (min)	27.5	27.67

N/AP – Non applicable

3.4.6.5. TGA

Thermogravimetric analysis experiments were performed in a TGA550 (TA Instruments, New Castle, Delaware, USA) and the data was analyzed and processed using the TA Universal Analysis 2000 Software (TA Instruments, New Castle, Delaware, USA). Samples were analyzed using a heating rate of 10 °C/min to 350 °C.

Water content was calculated from the difference between the weight loss retrieved from TGA results and GC results (where the organic solvents were quantified).

3.4.6.6. HPLC

Itraconazole and Furosemide quantification in the solid dispersions was performed using a Waters HPLC system (model 717plus Autosampler) with a dual wavelength absorbance detector (model 2487) and a binary HPLC pump (model 1525) (Waters, Milford, MA, USA).

An X-Bridge BEH Shield RP18 (4.6 mm x 150 mm x 2.5 µm) column was used and its temperature maintained at 45 ºC. The mobile phase consisted of 50:50 %vol. ACN and water and 0.1 %vol. of TFA and the isocratic flow rate was set at 1 mL/min. The dissolution mixture was

90:10 %vol. MeOH:H_2O for ITZ samples and 50:50 %vol. ACN:H_2O for FUR samples. The injection volume was 20 µL for ITZ samples and 10 µL for FUR samples. The UV absorbance was measured at λ = 270 nm and λ = 275 nm. The chromatographs were collected and the areas under the peaks integrated using Empower Version 2.0 (Waters, Milford, MA, USA).

Method assessment

To assess if the developed analytical method was suitable for its purpose, calibration curves, LoQ (limit of quantification), repeatability assay and system suitability tests were performed.

10 mg of crystalline ITZ were dissolved in 100 mL of dissolution mixture to obtain a stock solution of 100 µg/mL (target concentration). This solution was further diluted to obtain solutions with 80, 50, 20 10, 5, 1, 0.2, 0.1, 0.05 % of the target concentration, to determine ITZ linearity.

10 mg of crystalline FUR were dissolved in 100 mL of dissolution mixture to obtain a 100 µg/mL solution and then diluted to obtain a stock solution of 50 µg/mL. This solution was further diluted to obtain solutions with 80, 50, 20 10, 5, 1, 0.2, 0.1, 0.05 % of the target concentration, to determine FUR linearity.

3.4.6.7. PSD

Particle size distribution was assessed by laser diffraction technology in Sympatec dry dispersion unit (Sympatec HELOS/BR Rodos/M Aspiros Sympatec GmbH, Clausthal-Zellerfeld, Germany). Two lenses with different measuring ranges were used: R2 (0.45 - 87.5 µm) and R5 (4.5 - 875 µm). In the dispersing method, the feed velocity was set at 50 mm/s and the pressure was set at 5 bar.

3.4.6.8. SEM

Each sample was attached to carbon tapes (Ted Pella Inc., CA, USA) fixed in aluminum stubs. Excess powder was removed with a jet of pressurized air. Phenom ProX scanning electron microscope (Thermo Fisher Scientific, USA) was used to examine the morphology of the particles produced in high vacuum mode and the acceleration voltage was 10 kV.

3.4.6.9. Bulk density

Bulk density was determined by gently filling a graduated cylinder with a specific volume and registering the corresponding weight. Measurements were made in triplicate.

3.4.6.10. In vitro biorelevant dissolution studies

Calibration curves

Two calibration curves were determined to calculate the API concentration during *in vitro* dissolution study. The requirements were: prepare a concentrated standard solution for each API at its particular target concentration; and dilute it reaching a concentration of at least 40x lower than target concentration.

The ITZ standard concentrated solution (200 µg/mL) was prepared by weighting 10 mg of crystalline ITZ into a 50 mL volumetric flask. The volume was completed with MeOH. To construct the calibration curve, 8 diluted solutions were prepared from this initial standard solution with the following concentrations: 160, 120, 80, 40, 20, 10, 8, 4 µg/mL.

The FUR standard concentrated solution (160 µg/mL) was prepared by weighting 16 mg of crystalline FUR into a 100 mL volumetric flask. The volume was completed with DMF. To construct the calibration curve, 7 diluted solutions were prepared from this initial standard solution with the following concentrations: 128, 80, 40, 16, 8, 4, 1.6 µg/mL.

All standard solutions were prepared and their absorbance was read at 290 nm on the same day.

In vitro biorelevant dissolution studies were performed with an in-house developed methodology that requires less product and less FaSSGF and Transition Medium.

Target concentration of each API was determined considering the target dose (ITZ = 100 mg; FUR = 80 mg) and a total volume of 500 mL of FaSSIF, similarly to the description in Supersaturation Studies section. ITZ target concentration corresponded to 200 µg/mL, while FUR target concentration corresponded to 160 µg/mL.

The rationale of this new methodology is to have this previously determined API target concentration in a total final volume of FaSSIF of 10 mL.

FaSSFG and Transition Medium were prepared as previously described in the Supersaturation Studies Method.

FaSSFG (pH 1.6) and Transition Medium (pH 7.5) were heated to 37 ºC in an incubator shaker. The correspondent amount of ASD product was weighted, considering the target concentration for each API into small test tubes. 5 mL of FaSSFG at 37 ºC were added to each small test tube and the timer was started. Sampling timepoints were: 10, 20, 30, 40, 50, 60, 75, 90, 120, 180 and 240 min. At each timepoint, the necessary sample volume was withdrawn from the small test tube to a quartz cuvette. Sample absorbance was measured at 290 and 410 nm in an UV-spectroscopy and the sample being analyzed returned to the corresponding small test tube. After reading the absorbance of the 30 min timepoint, pH was shifted by the addition of 5 mL of Transition Medium to each small test tube, turning dissolution medium into a Fasted State Simulated Intestinal Fluid (FaSSIF). The absorbance measurements at the different timepoints proceeded as formerly described. The small test tubes were kept in the incubator shaker with orbital shaking (100 rpm) at 37 ºC, until the end of the study.

4

Results and Discussion

4.1. *IN SILICO* SCREENING

The Hansen Solubility Parameters estimated for both drugs with HSPiP software are reported in Table 4.1.

Table 4.1 – Itraconazole and Furosemide Hansen Solubility Parameters.

API	Hansen Solubility Parameters			
	δTot $(MPa)^{1/2}$	δD $(MPa)^{1/2}$	δP $(MPa)^{1/2}$	δH $(MPa)^{1/2}$
ITZ	26.0	22.8	11.2	5.7
FUR	27.8	20.4	14.0	12.8

By benchmarking these HSP against the Hovione's solvent database values, a list containing different solvents/solvent mixtures with the respective %vol. was obtained using the Solvent Optimizer tool within the HSPiP software. Table 4.2 and Table 4.3 present the solvent benchmark results for ITZ and FUR, respectively. The distances between solvent HSP and the API HSP are organized from smaller to higher distances, being this the key factors for solvent selection. A smaller distance is thermodynamically favorable, because chemical entities with similar molecular parameters are, in theory, miscible.[105]

Table 4.2 – Itraconazole Solvent Benchmark.

Solvent 1	vol.%	Solvent 2	vol.%	HSP Distance to ITZ
DMSO	**100**	**-**	**-**	**12.0**
Acetone	20	DCM	80	13.0
DCM	100	-	-	12.3
DCM	**90**	**Methanol**	**10**	**13.4**
Acetone	100	-	-	14.7
Acetone	88	Ethanol	12	15.0
Ethanol	100	-	-	19.7
Methanol	100	-	-	23.2

Table 4.3 – Furosemide Solvent Benchmark.

Solvent 1	vol.%	Solvent 2	vol.%	HSP Distance to FUR
DMSO	**77**	**Water**	**23**	**7.2**
DMSO	51	DCM	49	9.4
DMSO	56	Ethanol	44	9.5
Methanol	**36**	**DCM**	**64**	**9.8**
DMSO	65	Methanol	35	10.0
Ethanol	44	DCM	56	10.0
Acetone	73	Water	27	10.2
DCM	100	-	-	11.1
DMSO	**100**	**-**	**-**	**11.7**
Acetone	38	Ethanol	62	11.8
Acetone	53	Methanol	47	12.3
Ethanol	100	-	-	12.5
Methanol	100	-	-	14.9

Approximations were done as well as the conversion to wt.% as a more practical unit of measure during manufacturing. Based on these results, a set of solvents/solvent systems was selected as most promising to be confirmed *in vitro*:

- **For itraconazole**: **DCM/MeOH (90/10 wt.%)** as a solvent system for the spray drying process (benchmarks), since they both are volatile organic solvents, miscible and there was in-house experience with this API. Additionally, **DCM/MeOH (80/20 wt.%)** and **DCM/MeOH (70/30 wt.%)** were also considered to test API solubility *in vitro*, given the solubility limitations of some polymers with bare DCM. **DMSO** was selected as a promising solvent for the coprecipitation process, due its high theoretical capacity of solubilizing the API (the theoretical closest distance between API/solvent solubility parameters from all the results). Since CFF would be integrated, being a high boiling point solvent was not a drawback.
- **For furosemide**: **DMC/MeOH (70/30 wt.%)** as a solvent system for the spray drying process (benchmarks); **DMSO/H2O (75/25 wt.%)** for coprecipitation due

to the smaller HSP distance to FUR and miscibility between them. In addition, pure **DMSO** was considered to test API solubility *in vitro* as well.

The selected solvent systems to be confirmed *in vitro* are summarized in Table 4.4.

Table 4.4 – Selected solvent systems to be confirmed in vitro.

API	Solvent System	wt.%
ITZ	DMSO	100
	DCM/MeOH	90/10
	DCM/MeOH	80/20
	DCM/MeOH	70/30
FUR	DMSO	100
	DMSO/H2O	75/25
	DCM/MeOH	70/30

Even though this analysis was not made, for future work this author recommends to also calculate the HSP distance between solvent systems and the chosen polymers after miscibility assessment.

The *in silico* screening to identify ITZ and FUR leading formulations was based on the thermodynamics miscibility assessment from the calculated API Hansen solubility parameters and Flory-Huggins equation (Equation 3.2). Figure 4.1 and Figure 4.2 represent the miscibility assessment between both drugs and polymers considered. Results are summarized in Table 4.5.

Table 4.5 – Itraconazole and furosemide Flory-Huggins inflection point.

Polymer	Maximum API Load (wt.%) Spinodal point	
	Itraconazole	Furosemide
Methocel E3	20%	-
Methocel E5	20%	-
Methocel E15	20%	-
HPMCP-HP55	50%	-
HPMCAS-L	34%	-
HPMCAS-M	41%	-
HPMCAS-H	32%	-
Soluplus	19%	50%
PVP/VA 64	28%	-
Povidone K30	29%	-
Eudragit EPO	17%	52%
Eudragit L100	18%	49%
Eudragit L100-55	15%	42%

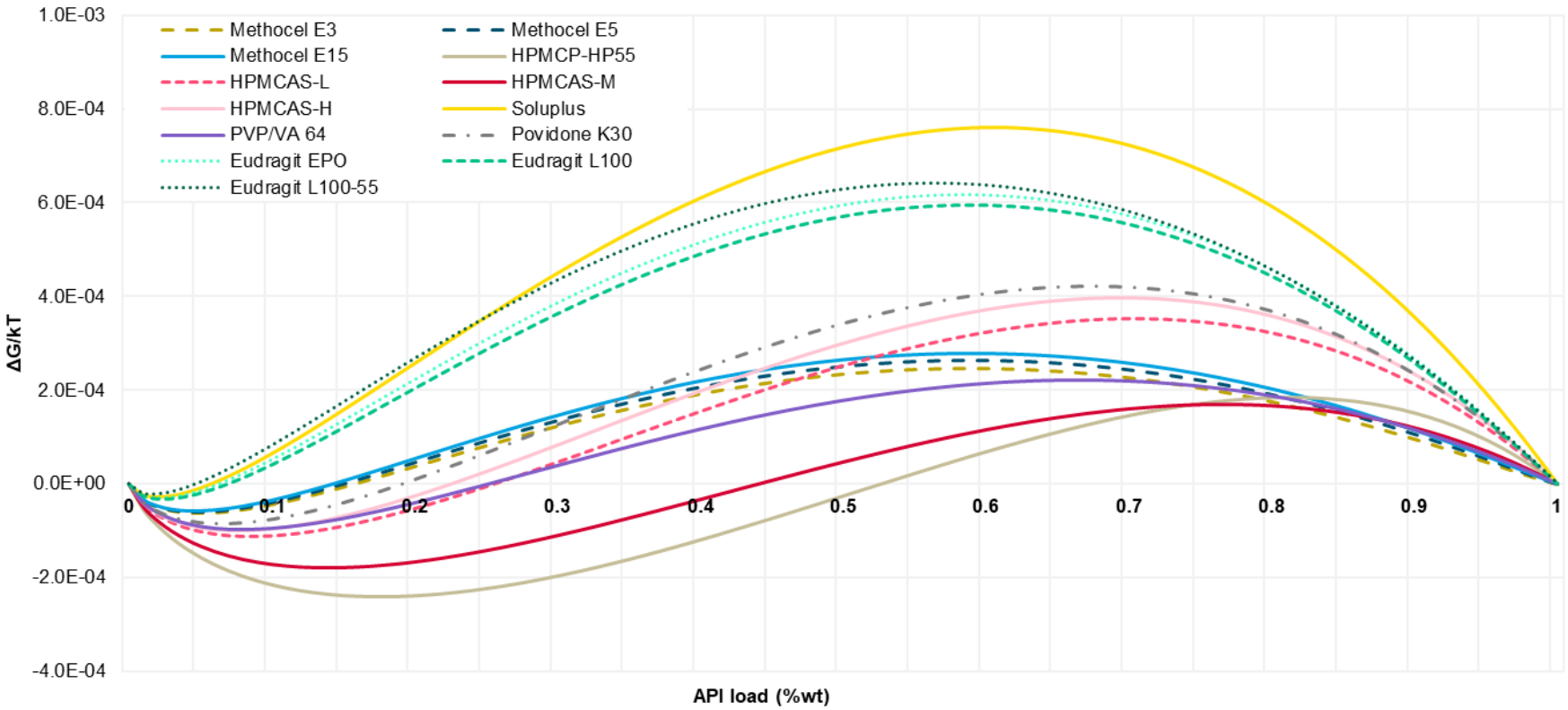

Figure 4.1 – Itraconazole/Polymer Flory-Huggins plot.

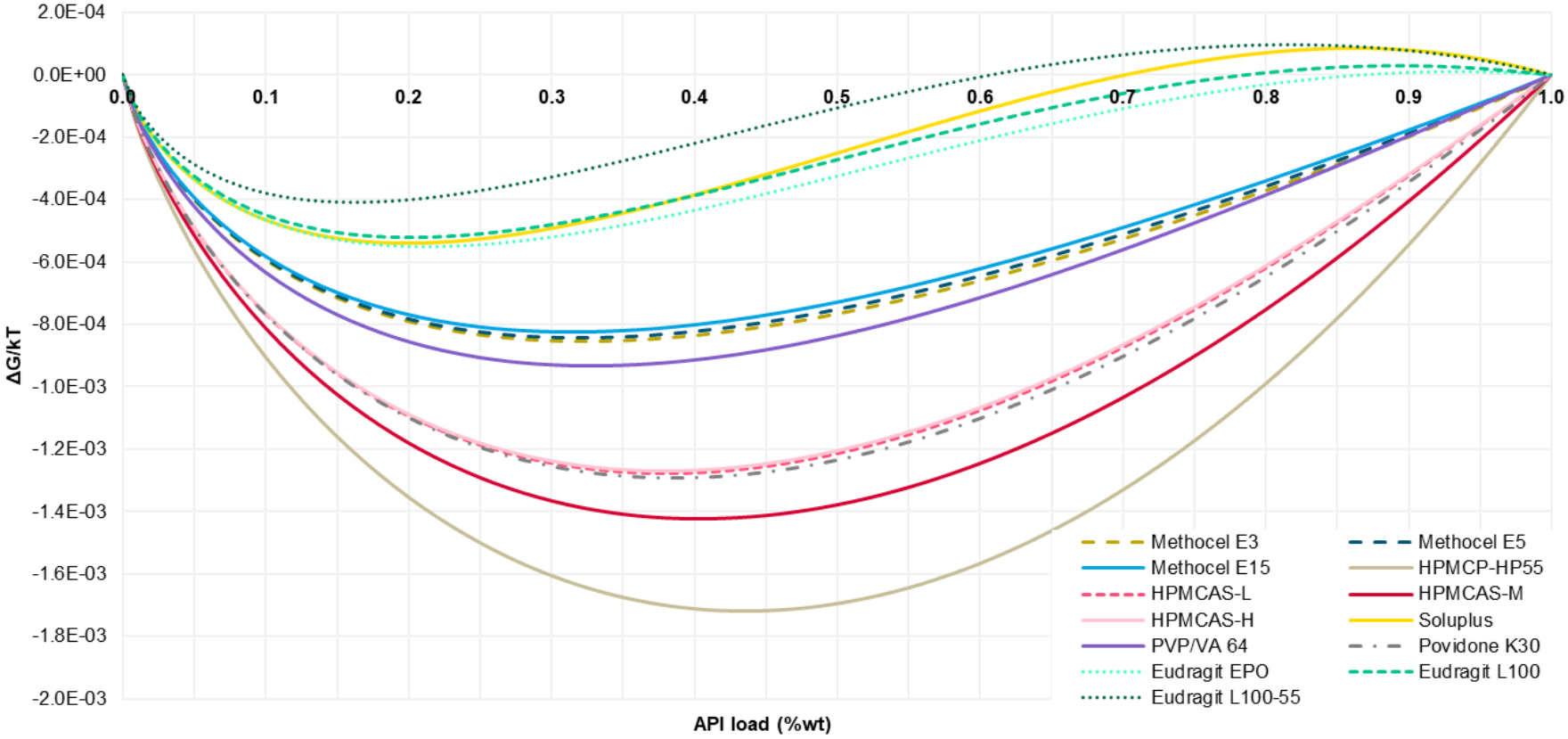

Figure 4.2 – Furosemide/Polymer Flory-Huggins plot.

It was decided to narrow down the selection to enteric polymers/anionic polymers. Enteric polymers prevent gastric degradation of drug, since they are insoluble at stomach acidic pH but soluble at intestinal neutral pH, and they can achieve higher bioavailability of weakly basic drugs, as ITZ.[106] From the above listed polymers, the anionic polymers are the following: methacrylic acid copolymers (Eudragit L100, Eudragit L100-55), hydroxyl propyl methyl cellulose acetate succinate (HPMCAS-H, HPMCAS-L, HPMCAS-M) and hydroxypropylmethylcellulose phthalate (HPMCP-HP55).

Minimum energy may traduce into a more likely thermodynamically stable formulation. On the other hand, lower spinodal points may be representative of less ideal formulations, with lower miscibility potential.

For ITZ, cellulosic polymers seemed to yield more ideal formulations, due to their higher spinodal points, particularly for cases as HPMCAS-M and HPMCP-HP55. For this reason and due to laboratory material availability, HPMCAS-M was chosen as the lead polymer for ITZ. For FUR, an overall phenomenon is noticed: for some polymers it does not exist a spinodal point. This may indicate a more promising miscibility profile. Therefore, and for comparison motives, HPMCAS-M was also selected. Nevertheless, one grade of the Eudragit polymer "family" – Eudragit L100 – was retained for further investigation. Although it does not seem as a good candidate for the ideal ITZ formulation, it appears to be promising for FUR formulations.

To proceed to *in vitro* screening experiments, three drug loads were chosen with the following criteria: one drug load correspondent to minimum energy in Flory-Huggins plot, one near or a slightly below spinodal point and a final drug load exceeding the maximum theoretical estimated miscibility, to evaluate the behavior of a high energy and "stressed" formulation and polymer performance *in vitro*. With this approach, it is intended to acquire advanced knowledge on the influence of the stabilizing polymer and drug load. To point out that for FUR:HPMCAS-M, as no inflection point was observed in Flory-Huggins plot – which may indicate more favorable formulations – three standard drug loads were selected. The proposed formulations are presented in Table 4.6.

Table 4.6 – Proposed formulations for in vitro screening.

API	Polymer	Drug Load (wt.%)
ITZ	HPMCAS-M	10, 30, 50
	Eudragit L100	10, 20, 50
FUR	HPMCAS-M	20, 50, 80
	Eudragit L100	20, 50, 60

4.2. *IN VITRO* SCREENING

4.2.1. *Solvent Screening*

The tested API/Solvent System compatibilities and calculated experimental solubilities are reported in Table 4.7.

Table 4.7 – API solubilities tests results.

API	Solvent System (wt.%)	[Solids']$_{obtained}$ (wt.%)	Solubility$_{exp}$ (mg/mL)	Immediate Results	Overnight Results
ITZ	DCM:MeOH (90/10)	19.0	291.0	Very rapid dissolution. Clear	Almost dried out. White paste
ITZ	DMSO	1.6	17.4	More slow dissolution. Clear	Completely clear
ITZ	DCM:MeOH (80/20)	23.5	357.7	Rapid dissolution. Clear	White paste, not completely dried. "Milky" effect
ITZ	DCM:MeOH (70/30)	15.8	205.7	Rapid dissolution. Clear	Completely clear
FUR	DCM:MeOH (70/30)	2.6	29.7	Rapid dissolution. Clear	Completely clear
FUR	DMSO:H2O (75/25)	4.2	46.9	Slow dissolution. Clear	Completely clear. Yellowish tone
FUR	DMSO	3.3	38.0	Slow dissolution. Clear	Completely clear. Yellowish tone

For ITZ, DMSO was the solvent with the lowest distance from the *in silico* screening. However, DCM:MeOH mixtures better promoted ITZ solubilization when tested *in vitro*. DMSO seems to be more thermodynamically favorable solvent (due to the low HSP distance), but less favorable kinetically – it took more time to yield a completely clear solution. Concerning the volatile solvent mixtures, a maximum solids (drug) load of 24 wt.% was achieved with DCM:MeOH (80/20 wt.%). When left overnight with stirring, only the solution with DCM:MeOH (70/30 wt.%) remained clear as shown in Figure 4.3, while DCM:MeOH (90/10 wt.%) and DCM:MeOH (80/20 wt.%) experiments showed complete or partial precipitation (highlighted with red) at the bottom of the vial. This may be explained by two main reasons. Solvent mixtures were added until a completely clear solution was obtained, resulting in a large and "empty" headspace volume in the vials of these experiments: very small volumes of DCM:MeOH mixtures were added and any small changes may had an influence the liquid-vapor equilibrium, affecting solubility. On the other hand, DCM:MeOH (70/30 wt.%) has a higher methanol content and MeOH has a higher boiling point (64.70 ºC) than DCM (39.75 ºC).[107,108]

For FUR, the solvent system that enabled a higher solids' load was DMSO:H_2O (75/25 wt.%) which is in agreement with *in silico* screening results. Nevertheless, the results are not far

apart from each other. All solvent systems remained completely clear after 24 hours under stirring, as observed in Figure 4.3.

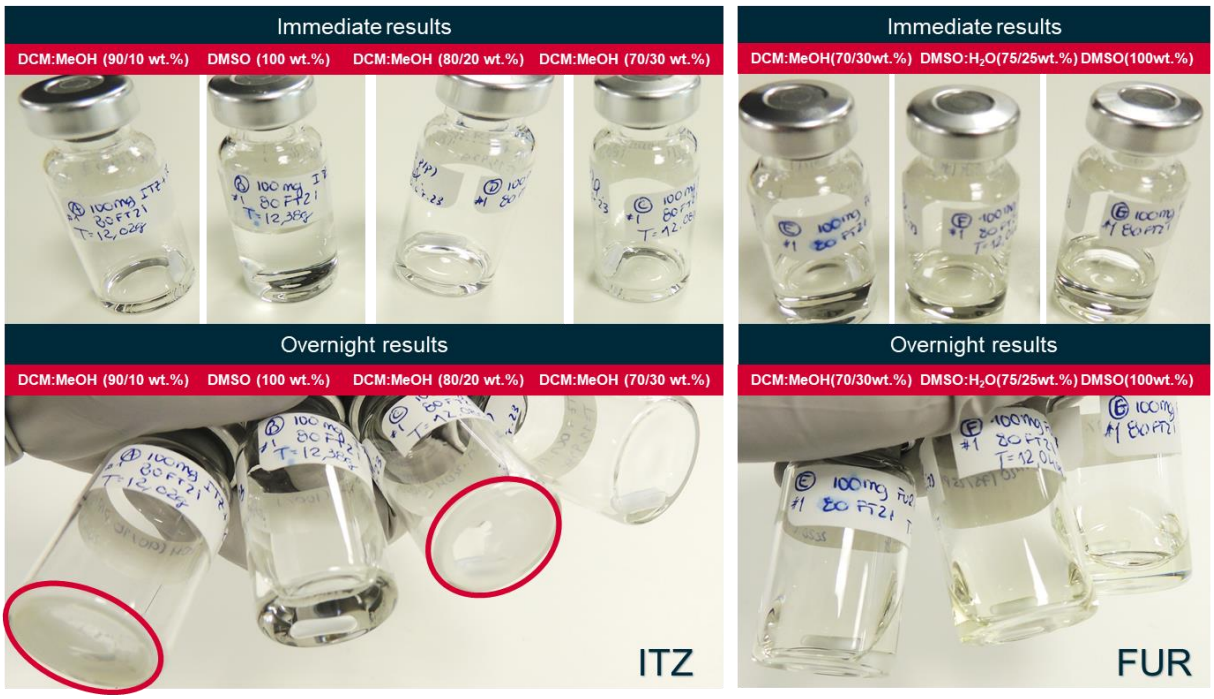

Figure 4.3 – ITZ and FUR Solvent Screening immediate and overnight results.

Polymer compatibilities with the different solvent system under evaluation were tested at 5 wt.% solids' feed concentration and the results and images are represented in Table 4.8 and Figure 4.4.

DMSO:H_2O (75/25 wt.%) was not considered as a suitable solvent system, particularly for HPMCAS-M. Therefore, this solvent system was excluded. A possible way to circumvent this, could be by heating the solution, but that assessment was not performed. Complete dissolution in DMSO was noticed for both polymers. Concerning the volatile solvent mixtures, DCM:MeOH (70/30 wt.%) was the one more promising for both polymers. A solvent system ranking for these polymers can be:

- **HPMCAS-M**: DCM:MeOH (90/10 wt.%) ≈ DCM:MeOH (70/30 wt.%) ≈ DMSO >> DMSO:H_2O (75/25 wt.%);
- **Eudragit L100**: DCM:MeOH (80/20 wt.%) ≈ DCM:MeOH (70/30 wt.%) ≈ DMSO > DMSO:H_2O (75/25 wt.%) >> DCM:MeOH (90/10 wt.%)

Table 4.8 – Solvent Screening – Polymer dissolution results.

Polymer	Solvent System (wt.%)	Results
HPMCAS-M	DCM:MeOH (90/10)	Total dissolution. Clear. Yellowish tone
HPMCAS-M	DCM:MeOH (70/30)	Total dissolution. Clear. Yellowish tone
HPMCAS-M	DMSO	Total dissolution. Clear. Yellowish tone, Bubbles at surface
HPMCAS-M	DMSO:H_2O (75/25)	Didn't dissolve. Suspension aspect
Eudragit L100	DCM:MeOH (90/10)	Didn't dissolve. Formed a gel-like ball that didn' disappeared overnight
Eudragit L100	DCM:MeOH (80/20)	Completely clear. Took a more time to dissolve
Eudragit L100	DCM:MeOH (70/30)	Completely clear. More rapid dissolution than in the previous conditions
Eudragit L100	DMSO	Completely clear
Eudragit L100	DMSO:H_2O (75/25)	Formed a gel-like ball that disappeared overnight

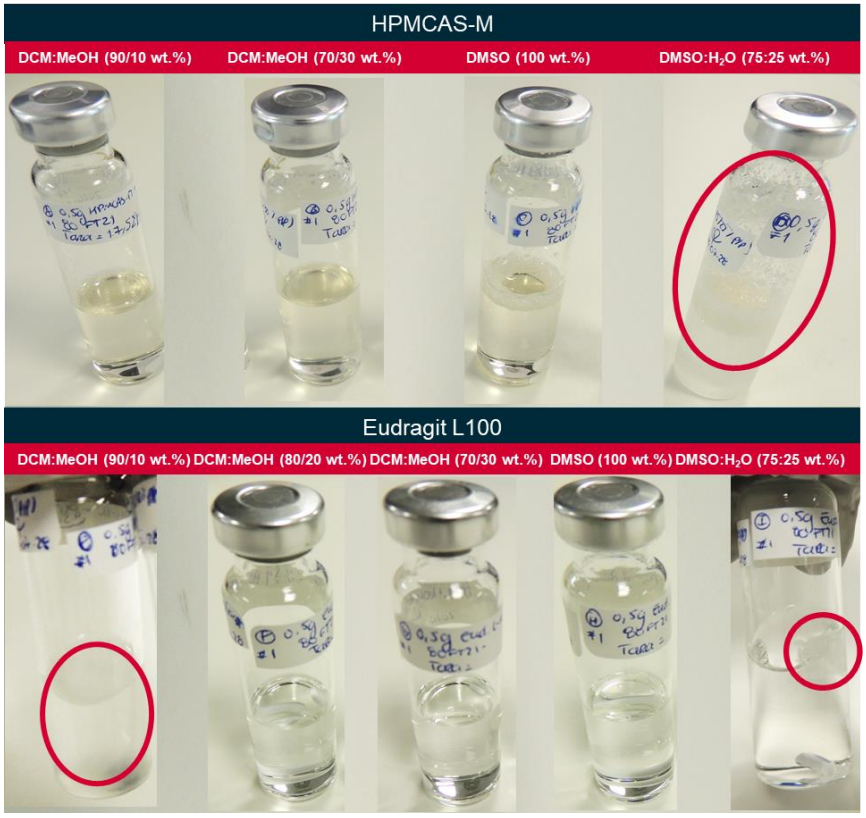

Figure 4.4 – HPMCAS-M and Eudragit L100 Solvent Screening results.

Correlating API and polymers *in vitro* screening results, two solvent systems were chosen, one for coprecipitation process and a volatile solvent mixture (mandatory criteria) for spray drying process. DCM:MeOH (70/30 wt.%) was selected for the spray drying process, since it was the volatile solvent system that showed a better performance in dissolving all compounds. On the other hand, DMSO was considered as the most suitable solvent for coprecipitation. Even though pure DMSO lead to a lower FUR concentration when comparing to DMSO:H_2O (75/25 wt.%), the

difference does not seem substantial and, by choosing bare DMSO, further challenges with polymer dissolution will be avoided. This seemed as the most efficient decision, albeit it was not required to choose the same solvent for the two APIs in each process.

4.2.2. *Solvent Casting*

Based on *in silico* screening results, solvent casting trials were conducted with two polymers – HPMCAS-M and Eudragit L100 – and different drug loadings to narrow the formulation variables. The casted films inside the pans undergo mDSC characterization. The mDSC profiles analysis was based on frequently recognized rules in the literature[8,109]:

- Single value for glass transition temperature (T_g) – between T_gs of the pure components – detected in the reversible heat flow implies that the API and polymer are homogeneously, being an amorphous solid solution;
- Two separate T_gs suggest amorphous-amorphous phase separation had occurred and drug/polymer rich phases can exist. Other thermal events – recrystallization/melting – may also be detected in this scenario.

The solvent casting results are summarized in Table 4.9 and for more detailed information (i.e. temperatures and mDSC profiles) regarding the analytical characterization of the pure compounds and the casted films see Appendix (Figure A.1 to Figure A.3). The characterization of the pure components allowed to confirm melting and glass transition temperatures reported on the literature: ITZ $T_{melting}$ = 166.3 ºC[96], FUR $T_{melting}$ = 206.3 ºC[99], HPMCAS-M T_g = 123.4 ºC and Eudragit L100 T_g = 191.2 ºC[102].

Table 4.9 – Solvent casting results.

API	Polymer	Drug load (wt.%)	Number of T_gs	T_g (ºC)	Presence of melting peaks
ITZ	HPMCAS-M	10	1	116.4	No
	HPMCAS-M	30	1	104.6	No
	HPMCAS-M	50	1	73.5	Yes
	Eudragit L100	10	1	191.5	No
	Eudragit L100	20	1	181.8	No
	Eudragit L100	50	1	135.1	Yes
FUR	HPMCAS-M	20	2	82.2 117.2	Yes
	HPMCAS-M	50	1	81.4	Yes
	HPMCAS-M	80	Inconclusive	-	Yes
	Eudragit L100	20	1	154.2	No
	Eudragit L100	50	1	141.0	Yes
	Eudragit L100	60	Inconclusive	-	Yes

ITZ formulations with HPMCAS-M and Eudragit L100 equally presented melting peaks at 50 wt.% drug load, which may indicate presence of crystalline material. At lower drug loads and for both polymers, no signs of crystallization or amorphous-amorphous phase separation were observed in the thermograms, which may indicate that these may be promising formulations.

In FUR:HPMCAS-M formulation at the lowest drug load (20 wt.%), two T_gs were detected, which may indicate from start that it is not an amorphous solid solution. Increasing drug load, other thermal events were identified in the mDSC profiles. This was the first indicator that HPMCAS-M may not be the most promising polymer for FUR formulations, even though the Flory-Huggins plot curve didn't possess a spinodal point for this polymer. Only HPMCAS-M formulation with 20 wt.% drug load was considered for further studies. Concerning Eudragit L100 formulations, they exhibited only one T_g until 50 wt.% of FUR, which may indicate that these were amorphous solid solutions. However, thermal events were also identified at 50 and 60 wt.% FUR. This does not necessarily nullify that these were amorphous solutions. In fact, at higher drug loadings is common to spot other thermal events (e.g. recrystallization, melting…), that may have been triggered by heating during the mDSC, not necessarily corresponding to the presence of crystalline material.[8]

To point out that solvent casting is a worst-case scenario as solvent drying in a tray oven is not representative of the real process, i.e. spray drying, where drying is much faster. Therefore, even if mDSC results may indicate occurrence of phase separation/crystallinity presence, that may not happen further ahead in benchmarks production. Solvent casting should be considered as a primary assessment that serves as a guidance for the experimental screening.

4.2.3. *Supersaturation studies*

To evaluate the extent of supersaturation for each drug-polymer system, supersaturation experiments were carried out by adding a concentrated drug stock solution to a solution of each polymer (at different loads) dissolved in FaSSIF. To have a standard reference, an additional experiment was performed by adding the drug solution to FASSiF medium, without any polymer dissolved. With his methodology, polymer performance is evaluated in terms of its capacity of inhibit crystallization and maintain API supersaturation in solution. An extended API supersaturation profile may lead in an *in vivo* setting to improved exposure in the gastrointestinal tract.

Overall, the results obtained demonstrate that the ability of amorphous drug-polymer mixtures to generate and maintain supersaturation is dependent on both the type of carrier polymers and the drug loadings.

The average results for the ITZ supersaturation trials are reported in Figure 4.5. HPMCAS-M exhibited an outstanding supersaturation performance, since it maintained ITZ supersaturation over the 12 hours of the test, even at the highest drug load being studied (50 wt.%). Eudragit L100 revealed the higher supersaturation levels during the first 5 hours for the 90:10 wt.% polymer:API formulation, but API crystallization overcame this initial advantage. Eudragit L100 performance weakened at higher drug loads, especially at 50 wt.% drug load, where polymer performance was even poorer than bare API behavior in FASSiF (red data in Figure 4.5).

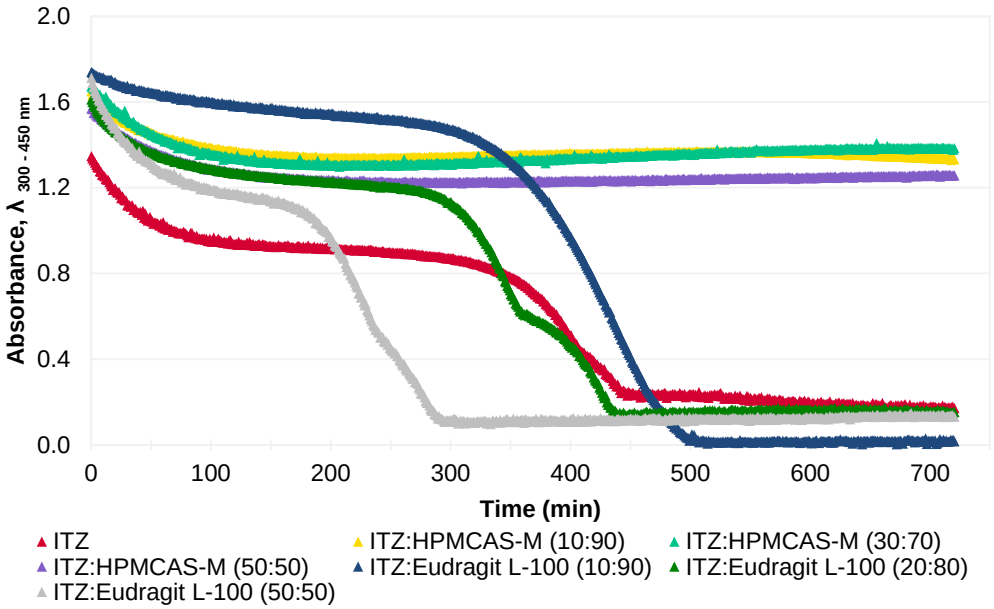

Figure 4.5 – ITZ supersaturation studies results.

On the other hand, in FUR trials, no abrupt decline of supersaturation was noticed and the average results from different trials are not far apart, as represented in Figure 4.6. Nevertheless, the only FUR/HPMCAS-M formulation under analysis exhibits the lowest supersaturation values, with a slight decay being noticed. At the same drug load (20 wt.%), Eudragit L100 revealed a better performance than HPMCAS-M (Figure 4.7, left). At 50 wt.% drug load, Eudragit L100 still sustains supersaturation and a slight decline starting after the 8th hour for formulation with 60 wt.% drug load was detected (Figure 4.7, right).

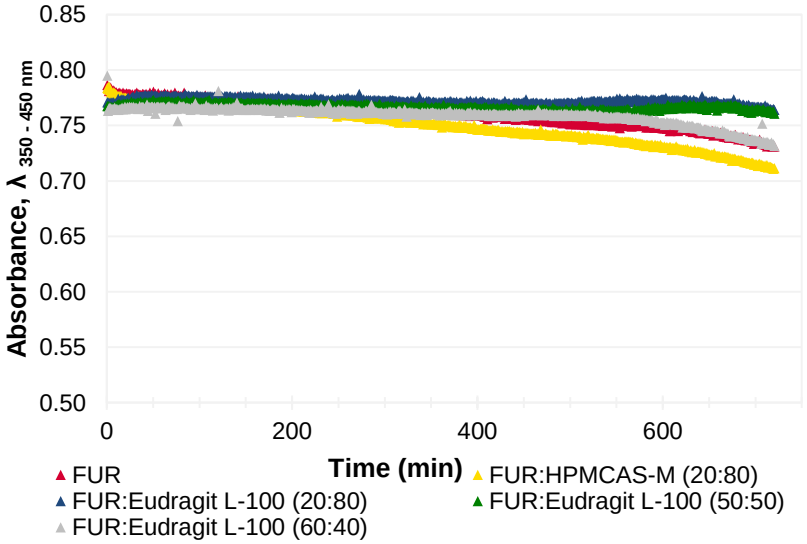

Figure 4.6 – FUR supersaturation studies results.

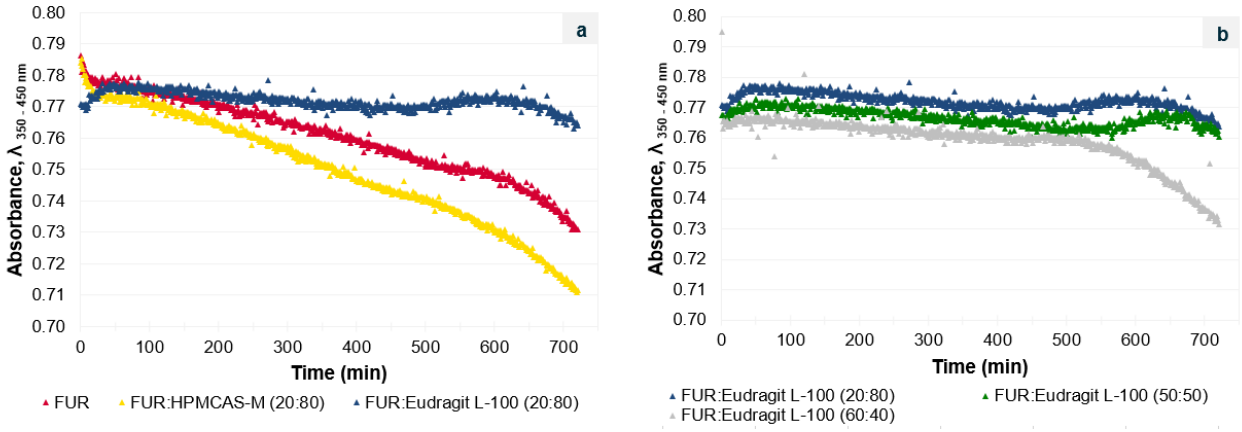

Figure 4.7 – FUR supersaturation studies results: Polymer evaluation (a) at same drug load; drug load impact on FUR:Eudragit L100 formulations (b).

Table 4.10 summarizes main results from *in vitro* screening and Figure 4.8 schematizes a qualitative evaluation of the different formulations in solvent casting and supersaturation studies.

Based on the entire set of generated *in silico* and *in vitro* results, moving forward for lab-scale SD benchmarks and coprecipitated prototypes manufacturing, the final lead formulation proposal was:

- ITZ (30 wt.%):HPMCAS-M (70 wt.%)
- FUR (50 wt.%):Eudragit L100 (50 wt.%)

The formulations presented are the best compromise between the assessed physical stability variables (high single T_gs by DSC) and supersaturation performance. HPMCAS-M seemed to result as a more promising ITZ formulation, especially in supersaturation studies, and Eudragit L100 was the best ranking candidate for FUR formulations, in both studies. Formulation with HPMCAS-M and 30 wt.% ITZ exhibited a great supersaturation performance and no indication of phase separation by DSC results. Even though other thermal events visible in mDSC for 50 wt.% FUR, that does not necessarily correspond to crystalline material presence; furthermore, it is relevant to try having the higher drug loading possible, since it avoids further larger volumes of final dosage forms (e.g. tablets).

Table 4.10 – Summarizing results of in vitro screening.

API	Polymer	Solvent Casting Results	Supersaturation Studies Results	Solvent System (wt.%)
ITZ	HPMCAS-M	Physical stability up to 30 wt.% ITZ	Better performance at any API:Polymer ratios; Maintains supersaturation	DCM:MeOH (70/30)
	Eudragit L100	High physical stability	Eudragit L100 does not sustain supersaturation for more than 350 minutes, even at the lowest drug load	
FUR	HPMCAS-M	HPMCAS-M does not ensure physical stability	Weaker performance when comparing with Eudragit L100 at the same API:Polymer ratio;	DCM:MeOH (70/30)
	Eudragit L100	Higher physical stability, but endo-thermic peaks at 50 wt.% FUR	Eudragit L100 seems to preserve supersaturation up to 50 wt.% FUR	

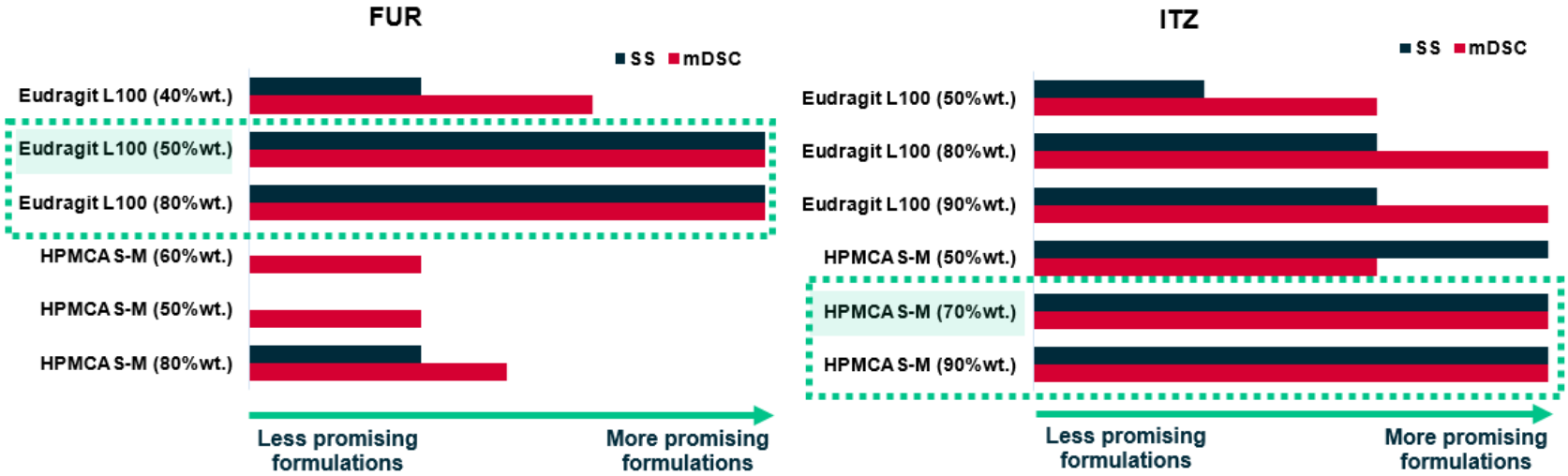

Figure 4.8 – Qualitative evaluation of the different formulations in solvent casting (mDSC) and supersaturation studies (SS).

4.3. SPRAY DRYING BENCHMARKS

All spray drying experiments ran smoothly. Some product accumulation of spray drying occurred at the bottom of the drying chamber, connecting parts to the cyclone and inside the cyclone itself, especially during ITZ solution drying, as shown in Figure 4.9. This corroborates with the higher yield obtained of FUR:Eudragit L100 solution drying. Main process data and yield are summarized in Table 4.11.

Figure 4.9 – Product accumulation during spray drying. FUR solution drying (a) ITZ solution drying (b).

Table 4.11 – SD main process data and yield.

	FUR SD benchmark	ITZ SD benchmark
Feed solution parameters		
Formulation	FUR:Eudragit L100	ITZ:HPMCAS-M
Drug/Polymer (wt.%)	50:50	30:70
Feed solids' concentration (wt.%)	5	5
T_{feed} (ºC)	Room temperature	Room temperature
Spray drying parameters		
Nozzle (orifice/core) (mm)	0.7 / 1.5	0.7 / 1.5
F_{drying} (kg/h)	20	20
F_{atom} (kg/h)	0.83	0.35
Tout (ºC)	40	40
Ffeed (kg/h)	0.7	1.0
Spray drying yield		
Drying time (min)	73	35
Yield (dry basis) (wt.%)	90.6	68.0

4.4. SOLVENT/ANTISOLVENT RATIO STUDY

Results from S/AS ratio study are displayed in Figure 4.10. For both API, the acquired data were adjusted with exponential trend lines, since a decrease in API supernatant concentration at increasing rates is noticeable – supernatant concentration resembles to an exponential decay while increasing antisolvent content. Only three experiments were made and the coefficient of determination, R^2, obtained may have been impacted by the small amounts and minor changes during sample preparation, for example, which may have affected the results. However, the tendency of supernatant concentration variation with antisolvent ratio was, in fact, captured.

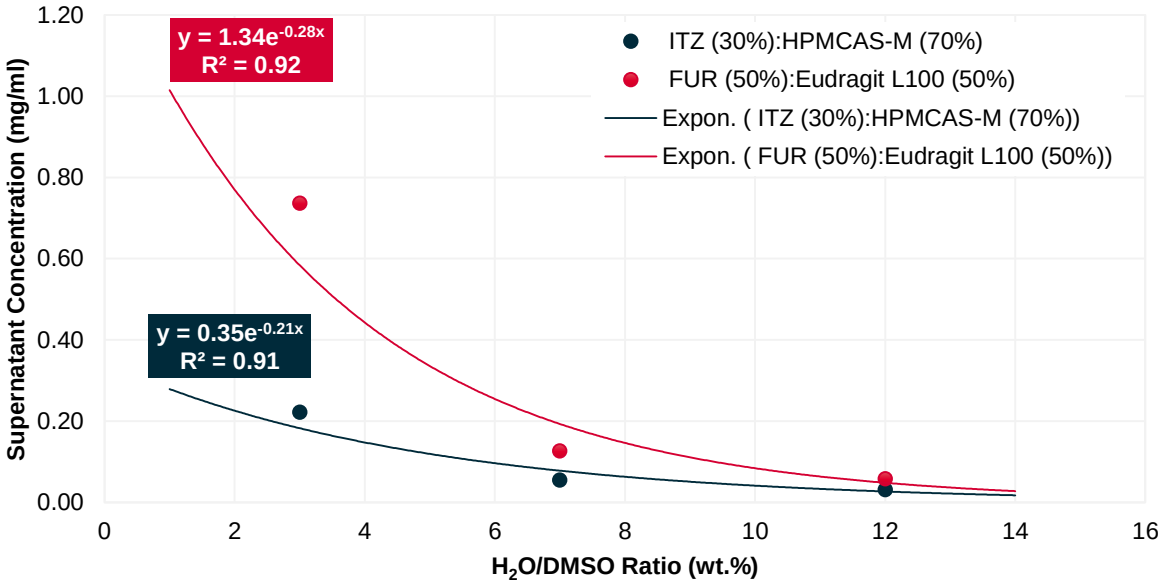

Figure 4.10 – Supernatant concentration of ITZ and FUR as a function of H_2O/DMSO ratio (wt.%).

Furthermore, API concentration in the supernatant relative to initial API concentration was calculated and the results to each trial are summarized in Table 4.12. This is a simple metric to assess how much of the initially loaded API did not precipitate. Precipitation at lower S/AS ratios (1 DMSO: 3 H_2O (wt.%)) was more complete for ITZ:HPMCAS-M: only 5.5 wt.% of initial ITZ did not precipitate, while for FUR the result was, approximately, 11 wt.%. However, the adjusted trendlines appear to reach similar values for higher S/AS ratios. As a matter of fact, it is not likely to have a complete (100 wt.%) precipitation, and it would involve higher amounts of antisolvent with a major cost-benefit ratio to the processing costs.

Table 4.12 – S/AS ratio studies results.

API (wt.%):Polymer (wt.%)	Ratio (wt.%)		$[API]_{Initial}$	$\frac{[API\ Supernatant]_{exp.}}{[API]_{Initial}}$ (%)
	DMSO	H_2O	(mg/mL)	
ITZ (30%):HPMCAS-M (70%)	1	3	4.04	5.5%
	1	7	2.00	2.8%
	1	12	1.22	2.6%
FUR(50%):Eudragit L100 (50%)	1	3	6.73	10.9%
	1	7	2.00	6.4%
	1	12	2.04	2.9%

Although a S/AS ratio of 1:10 (wt.%) could have been an appropriate choice, it was decided to adopt on a more conservative S/AS ratio of 1:12 (wt.%) for both drug formulations.

4.5. pH EFFECT ON COPRECIPITATION STUDY

A polarized-light microscope (PLM) enables a fast feedback on the crystallinity presence, by examining a qualitative indicator – birefringence. Some amorphous polymers may also exhibit residual birefringence.

To investigate the pH effect, small amounts of suspensions were produced and analyzed through PLM, as shown in Figure 4.11. Birefringence effect is visible through the brightness in the analyzed samples. When using acidified cold water as antisolvent, the abundance of brightness spots – visible in dots or needle shaped – is lowered when comparing to the samples where only cold water was used as antisolvent. ITZ (30 wt.%):HPMCAS-M (70 wt.%) is the formulation exhibiting the presence of less crystalline material. The use of acidic cold water is particularly noticeable in FUR (50 wt.%):Eudragit L100 (50 wt.%) formulation – the amount of bright material is diminished at lower pH. Nevertheless, coprecipitation with acidic cold water still reveals visible nuclei that can result in further crystallization, by a seeding effect. An additional test was performed, lowering the drug load to 20 wt.% FUR. The reduction of crystalline presence was clearly perceptible.

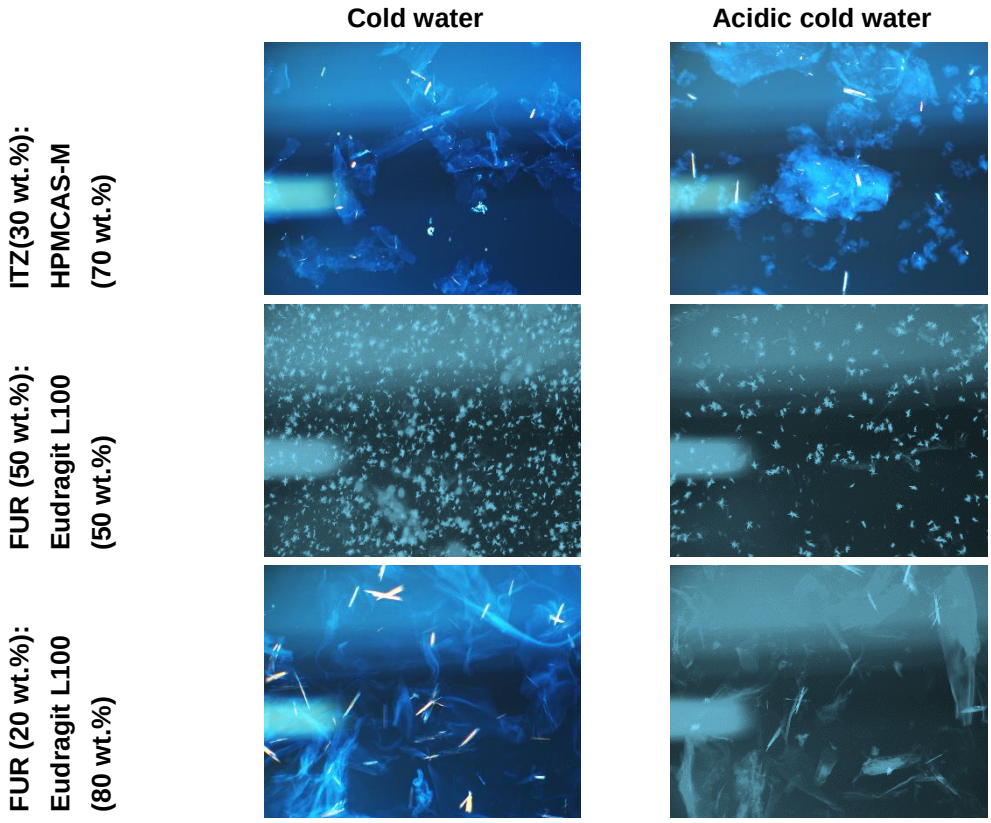

Figure 4.11 – Polarized light micrographs (x10).

Owning to the significant amount of crystallinity with FUR formulations and, as a result of the reduced experimental time in the laboratory, it was decided to move forward with ITZ formulation, exclusively, for further production of coprecipitated prototypes.

It is relevant to highlight that FUR is a relative small molecule, with a molecular weight below 500 g/mol – this property can preclude the production of an amorphous product.[44] Contrariwise, larger molecules are more prone to amorphous state conversion, since they can establish more complex conformations, delaying nucleation and crystal growth.[44] Moreover, FUR has a Log P of 2.56 (< 3), which may lead to a higher affinity to water (antisolvent), inducing phase-separation.[44] More key physicochemical properties of the API suggested in the literature for coprecipitation process are mentioned in Table A.3 in Appendix.

4.6. COPRECIPITATION OBSERVATIONS

Coprecipitation was only performed with ITZ (30 wt.%):HPMCAS-M (70 wt.%) formulation. Two solutions of drug and polymer dissolved in DMSO were prepared and coprecipitation was carried out through two techniques: HSM and HPH.

Coprecipitation with HSM was apparently uneventful, yielding a white suspension (with 0.4 wt.% ITZ:HPMCAS-M solids' load), as showed in Figure 4.12.This trial was completed in four minutes.

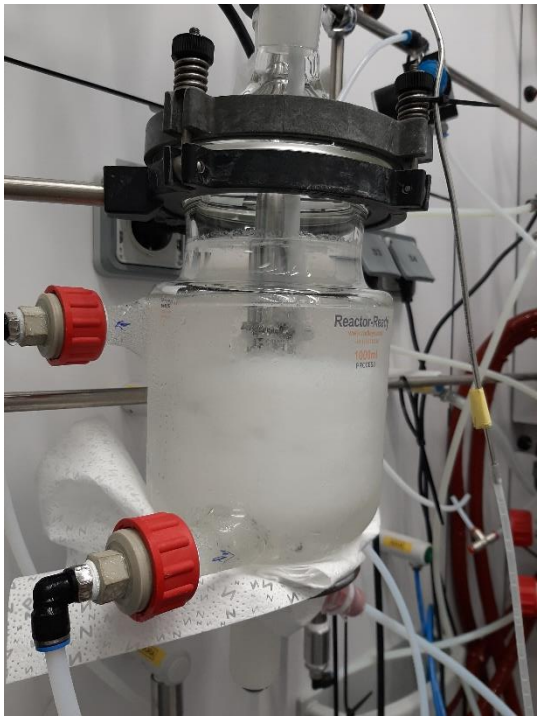

Figure 4.12 – Result from ITZ HSM suspension.

Coprecipitation with HPH ran seemingly smoothly. However, near the end of the trial, product losses (~ 50 mL) occurred inside the intensifier pump as showed in Figure 4.13. HPH duration was ten minutes, yielding a white suspension as well.

Figure 4.13 – Product losses inside the intensifier pump.

Both suspensions were left two settle, prior crossflow filtration, and particles accumulated at the bottom of the flasks.

4.7. CFF WITH HOLLOW FIBER MEMBRANES

4.7.1. *Concentration and diafiltration of HSM ITZ suspension*

Concentration of ITZ suspension from HSM started using the D04-E500-05-N membrane module with 235 cm^2. This membrane, which was washed and integrity tested, was previously used in the placebo proof-of-concept. The integrity test indicated that the membrane was proper for further use.

As soon as the unit was initiated and filtration started, an abrupt increase in inlet pressure was noticed. Inlet pressure readings kept increasing until the maximum allowable pressure, of 2 bar, was reached. Automatically the unit would shut down and filtration had to be manually re-started. This reoccurred throughout almost 350 minutes (over five hours) and feed flow rate and pressure on the valve were readjusted several times, trying to avoid high inlet pressures. Also, between restarts, additional attempts to unclog the membrane module were performed (washings with water and backflushing, according to supplier's recommendations). Near the end of the trial, the maximum operational flowrate was 1 mL/min, which was completely counter-productive. The increases in inlet pressure could be associated with two main causes: membrane integrity may had been compromised even though it was integrity tested before; or clogging may have occurred most likely due to agglomerates blocking the inner lumen of the hollow fibers. An adequate membrane selection, namely with a higher inner fiber diameter, would minimize these blockage challenges when concentrating suspensions. Due the process difficulties, data collection had considerable fluctuations, and, thus, is not presented in this section.

To conclude concentration of this suspension, the membrane was changed to a different module (D06-E500-05-N), new and with a higher surface area – 370 cm^2. Even though it is recommended, agitation of the feed suspension was not performed (in all trials). This was mainly associated with equipment constraints that precluded a safe operation, due to size of the flask containing the suspension volume. Also the feed tubing was placed in a less concentrated layer of the suspension to avoid further blockage of the membrane. However, this decision could have led to particle growth or the increase of the tendency to form aggregates.

Filtration started by setting feed flow rate at 10 mL/min, resulting in a permeate flux of approximately 16 $Lm^{-2}h^{-1}$, as presented in Figure 4.14. As the process stabilized, a higher feed flow rate (20 mL/min) was introduced in the software, resulting in a permeate flux of approximately 33 $Lm^{-2}h^{-1}$. Concentration was finally completed within 10 minutes. TMP suffered a small increment, paired up with the increase in the permeate flux. Permeate was visually clear of particles as showed in Figure 4.15. Therefore, product losses to the permeate were mitigated.

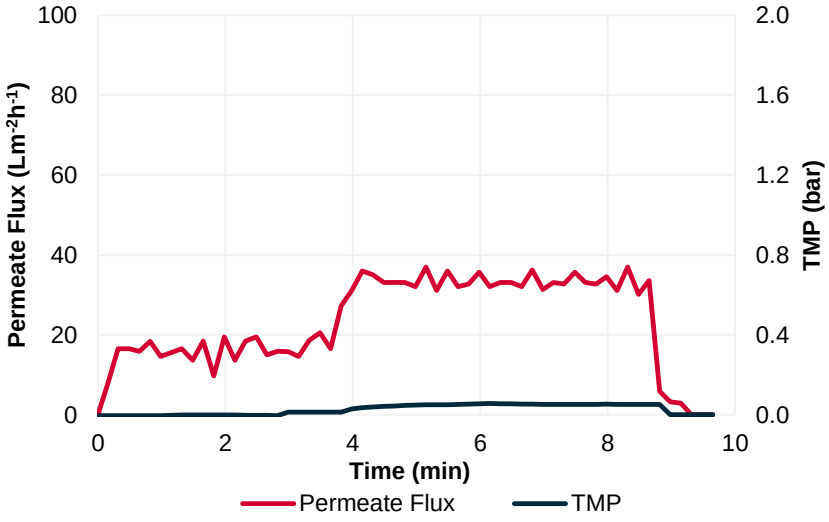

Figure 4.14 – Permeate flux rate and TMP during concentration (ending) of ITZ HSM suspension.

Figure 4.15 – Permeate during ITZ HSM suspension concentration.

During ITZ HSM suspension diafiltration, DMSO was washed twice with acidic water. To execute diafiltration, “concentration mode” was selected in the software and an external peristaltic pump fed acidic water to the feed reservoir. The acidic water flow rate was adjusted to the same permeate flow rate, to guarantee a constant feed volume.

Diafiltration took around 80 minutes, which corresponds to a total of two washes, and the permeate flux and TMP fluctuations over time are represented in Figure 4.16. During the initial 10 minutes of operation, oscillations are noticed, mostly due to automated controls of the unit software. After these 10 minutes, permeate flux stabilized at, approximately, 30 $Lm^{-2}h^{-1}$. The abrupt decrease at minute 40 is associated with pausing the system, that was necessary to drain out the permeate recipient. The weighting scale had a limiting weight and the permeate flask itself had a maximum capacity.

TMP followed the same tendency as permeate flux, with the initial fluctuations. However, it suffered a slight increase after pausing the unit, from 0.11 bar to 0.19 bar, which was most likely due to some particle accumulation at membrane's surface or adjustment/tare of the TMP in the software.

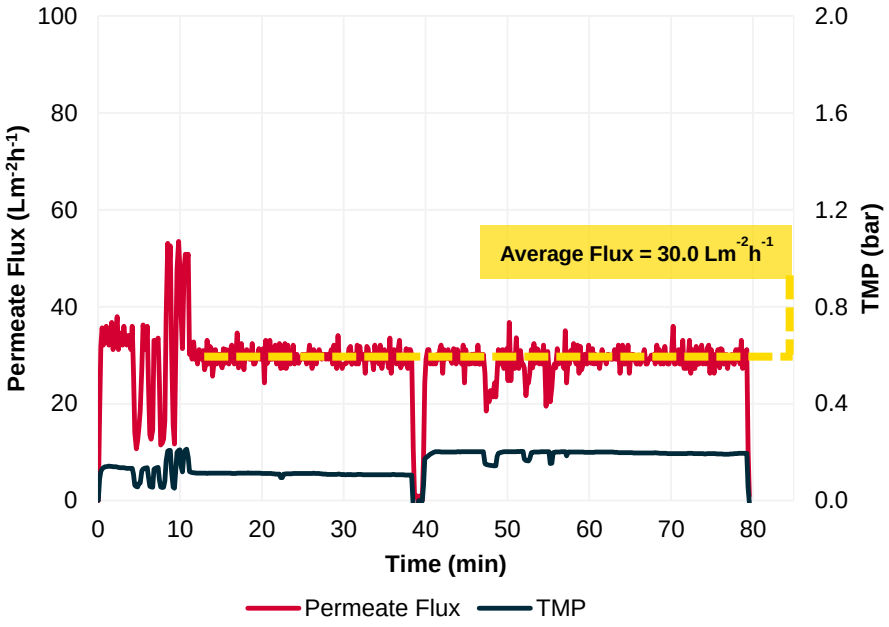

Figure 4.16 – Permeate flux rate and TMP during diafiltration of ITZ HSM suspension.

4.7.2. *Concentration and diafiltration of HPH ITZ suspension*

Concentration of ITZ HPH suspension occurred uneventfully, with a total duration of 60 minutes. However, oscillations in the pressure readings were detected, particularly in inlet pressure, as highlighted in Figure 4.17. Even though the filtration unit didn't stop, sometimes it would automatically lower the pre-defined set points. The initial estimations for the TMP setpoint were, in hindsight, conservative and the system would adjust flowrate automatically to meet said setpoint. Therefore, during concentration, feed flow rate and pressure on the valve had to be readjusted.

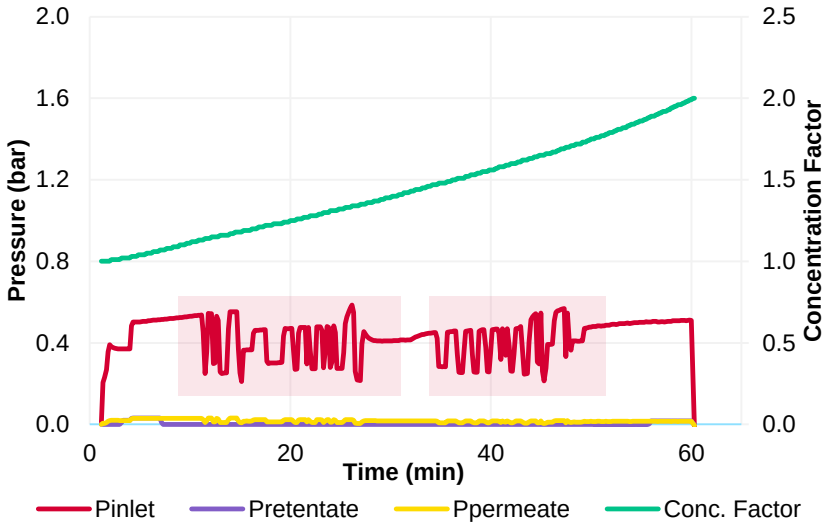

Figure 4.17 – Pressures and concentration factor variation over time during concentration of ITZ HPH suspension.

The permeate flux and TMP variation over concentration time is presented in Figure 4.18. As expected, biggest fluctuations in both TMP and permeate flux coincide with the same fluctuations addressed in the previous paragraph. Moreover, permeate flux appears to present a slightly decreasing tendency. This could be a result of particle accumulation – fouling – on the hollow fibers, restraining their filtration efficiency. During concentration, no particles were observed in the permeate flask.

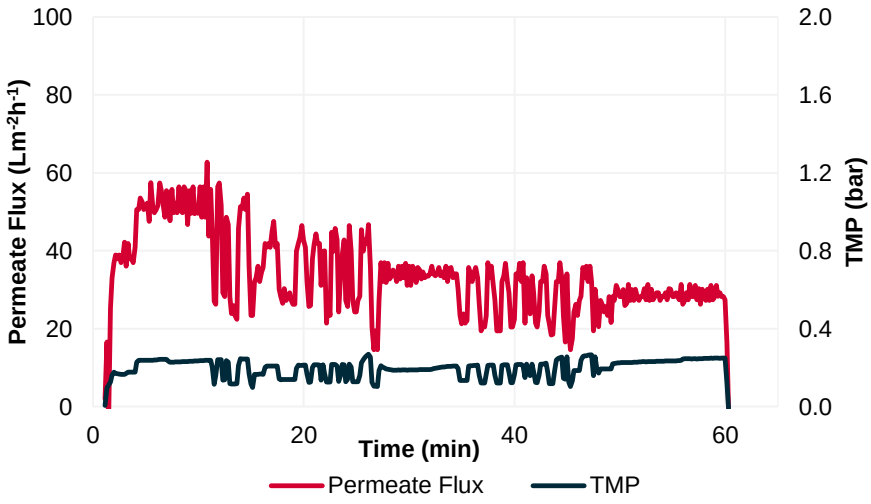

Figure 4.18 – Permeate flux rate and TMP during concentration of ITZ HPH suspension.

Diafiltration of ITZ HPH suspension was carried out as previously described – an external peristaltic pump fed the acidic water at the same rate the permeate was being removed, to guarantee a constant feed volume. Diafiltration consisted in two process volume washes and lasted for, approximately, 112 minutes. Permeate flux and TMP variations during diafiltration are displayed in Figure 4.19. The decreases observed in both variables are associated with system

pausing, to drain out the permeate recipient. The average permeate flux was 29.5 $Lm^{-2}h^{-1}$, similar to the permeate flux registered during ITZ HSM suspension diafiltration. TMP had an increase tendency, reaching 0.5 bar at the end of the experiment which, most likely, is associated with particle accumulation.

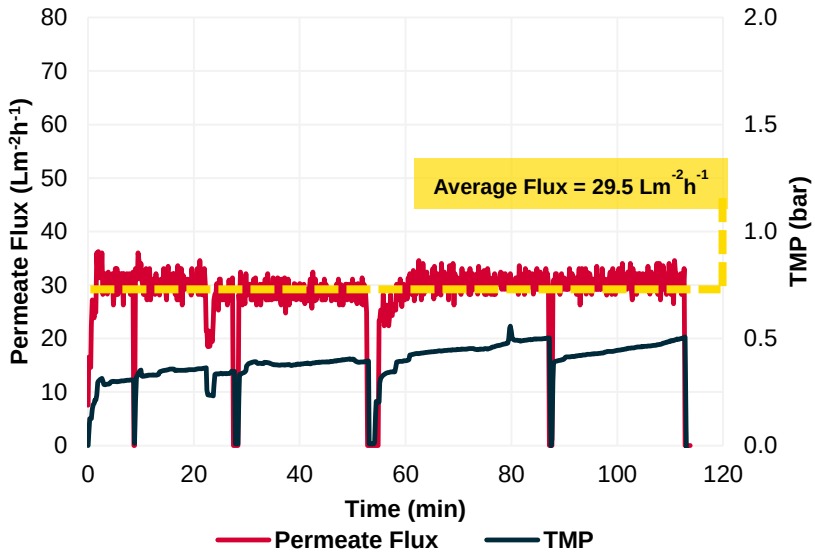

Figure 4.19 – Permeate flux rate and TMP during diafiltration of ITZ HPH suspension.

4.8. ISOLATION OF COPRECIPITATED PROTOTYPES THROUGH SPRAY DRYING

All the coprecipitated materials were isolated by spray drying, after diafiltration. A two-fluid nozzle was used, as characteristic of suspension drying, to minimize clogging. Nevertheless, clogging did occur on few instances, but it was easily solved by purging nitrogen through the nozzle. The main challenge with isolation was, in fact, related with product losses in the chamber and in the cyclone as showed in Figure 4.20.

Figure 4.20 – Product accumulation during spray drying. a) first cyclone during ITZ HSM suspension isolation; b) drying chamber and cyclone during ITZ HPH suspension isolation.

The product accumulated in the cyclone's walls appeared to be crystalline in nature, particularly at the top connection. In all likelihood, the presence of citric acid impacted isolation to some extent and was incorporated in the final formulation/product. As the product accumulated, cyclone's performance diminished, not being able to collect the dried product, which resulted in reduced yields (HPH prototype ≈ 20 wt.%; HSM prototype ≈ 30% wt.). Furthermore, the second cyclone was clear, with no product coverage on its walls. So, it did not improve dried product recovery, which could indicate that finer material was not being collected and escaped to the HEPA filter.

To prevent further impact during isolation, and still maintain the acidic pH needed for suspension stability, another choice for the acid should be studied. Moreover, a last diafiltration step with just deionized water could be another strategy to minimize impact of acid content during isolation.

4.9. ANALYTICAL CHARACTERIZATION OF SPRAY-DRIED BENCHMARKS AND COPRECIPITATED PROTOTYPES

This subchapter will solely cover the analytical characterization of the ITZ formulations, i.e. ITZ SD benchmark and ITZ HPH and HSM coprecipitated prototypes. As addressed in pH EFFECT ON COPRECIPITATION STUDY, the FUR formulation did not proceed to coprecipitation prototypes production. Nevertheless, analytical characterization of FUR SD benchmark is presented in Appendix.

4.9.1. *Morphology and Particle Size Distribution*

The SEM results for ITZ SD benchmark and coprecipitated prototypes are displayed in Figure 4.21 to Figure 4.22.

A shriveled or buckled particle morphology was observed for SD benchmark. This is aligned with a slower drying kinetics during spray drying (F_{Feed} = 1.0 kg/h). Particle agglomerations were not ubiquitous for ITZ SD benchmark.

Concerning ITZ HPH prototype, particles seemed very porous and bigger than SD benchmarks. Moreover, some bigger particles appear to be, in fact, agglomerates, presenting smaller particles adhered to the surface – this may be attributed to the higher electrostatic attraction of smaller particles. Two structures with well-defined edges were identified (highlighted with red in Figure 4.21) which can indicate the presence of crystalline material, to be confirmed by XRPD analysis.

ITZ HSM prototype presented agglomerates that were visible during sample preparation, and later confirmed with SEM images. It seems that sphere particles were produced during coprecipitation but, somehow, they apparently aggregated or even fused with each other – resulting in structures exceeding 100µm (see Figure 4.22).

Another point that can have contributed to the agglomeration observed in both coprecipitation prototypes was the incorporation of citric acid into the final product.

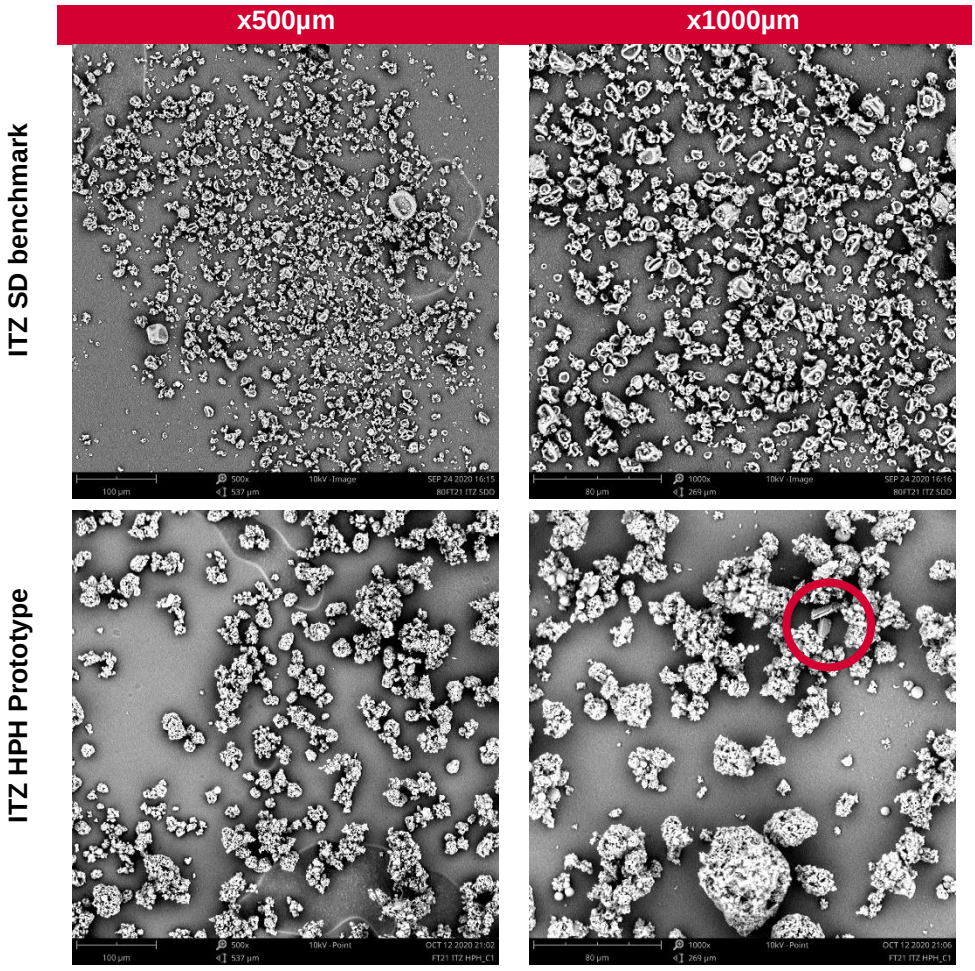

Figure 4.21 – SEM micrographs of ITZ SD benchmark and ITZ HPH Prototype at 500 and 1000x magnification.

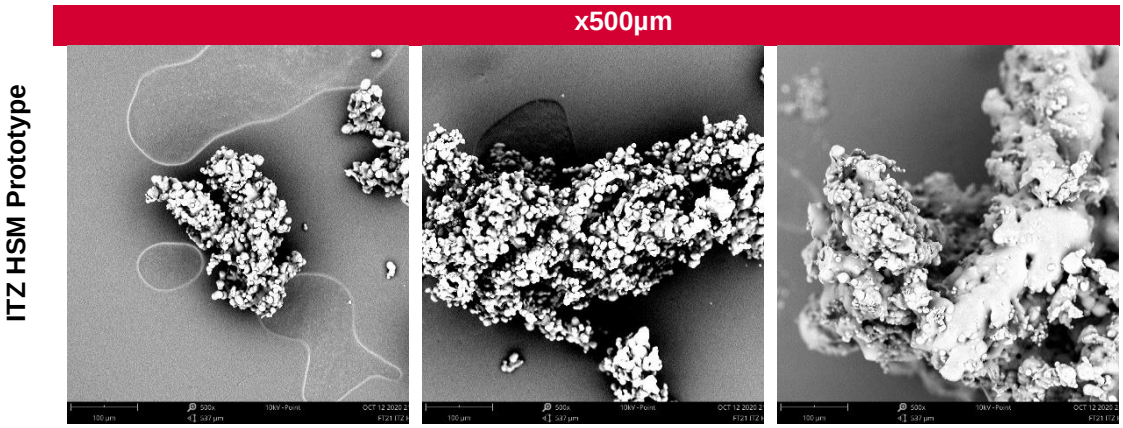

Figure 4.22 – SEM micrographs of ITZ HSM Prototype at 500x magnification.

SEM results were also relevant as a first assessment of particle size. Each Sympatec lens has a specific range to measure PSD so its selection should be adequate. Based on this, the R2 lens with a range of 0.45 – 87.5 µm was selected to analyze the SD benchmark. For the

coprecipitation prototypes, due to the presence of bigger particles and agglomerates, R5, a lens with a wider range of 4.5 – 875 µm was more appropriate.

PSD results are presented in Figure 4.23 and Figure 4.24. 90 % of the ITZ SD particles (D_v90) is under 20 µm, which may be explained by the difference in F_{Feed} and F_{Atom} ($F_{Feed,\ ITZ\ SD}$ = 1.0 kg/h; $F_{Atom,\ ITZ\ SD}$ = 0.35 kg/h).

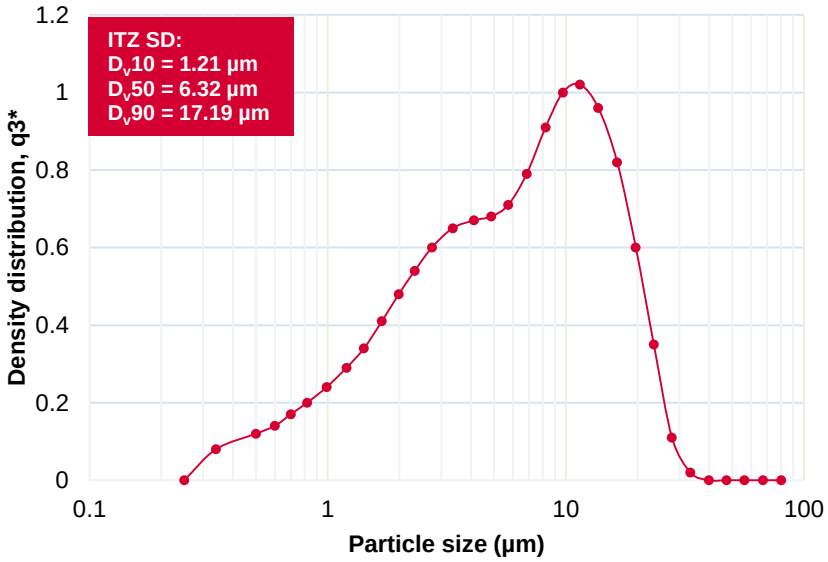

Figure 4.23 – PSD of ITZ SD Benchmark.

PSD profiles of coprecipitated prototypes are clearly distinct, but both exhibit two separated populations. Concerning ITZ HSM, large agglomerates were expected, after SEM imaging. PSD confirmed it, with a well-defined population above 100 µm. For the ITZ HPH sample, smaller particles are represented in the first population, with 50 % of the material being bellow 57 µm, approximately. The second population (> 100 µm) corresponds to the agglomerates formed by particle aggregation and deposition of smaller particles at the surface. Regarding the use of the R5 lens, a drawback is that any submicron population, typical for coprecipitated ASD, may not be captured in the PSD profile.

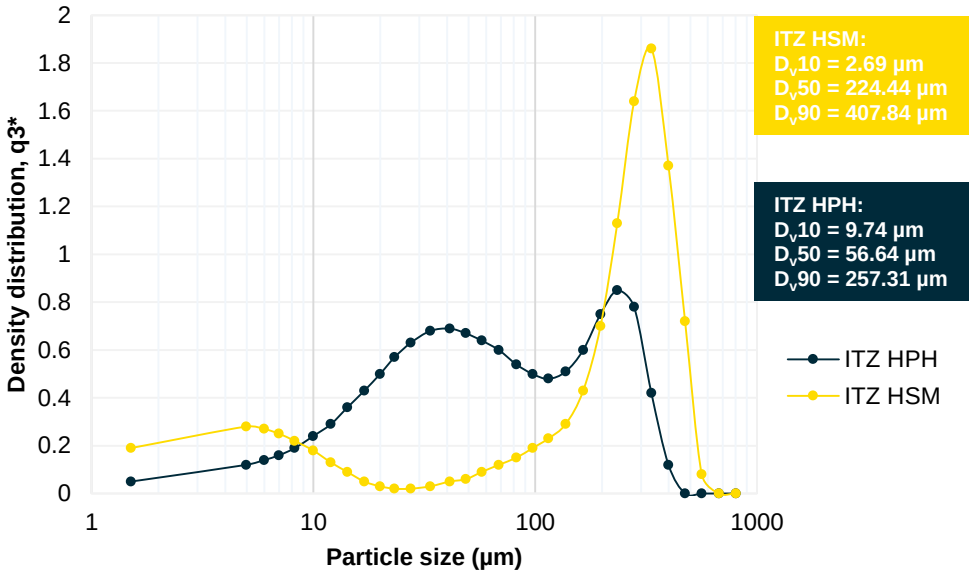

Figure 4.24 – PSD of ITZ HPH and ITZ HSM Coprecipitated prototypes.

4.9.2. *Drug's solid-state and molecular arrangement*

XRPD revealed a halo characteristic of amorphous form and lack of X-ray diffraction peaks corresponding to the crystalline drug in ITZ SD benchmark (Figure 4.25).

For the ITZ HPH prototype, although XRPD displays a halo-like layout, meaning that some amount of the drug was converted to amorphous form, it clearly exhibits distinctive peaks of the crystalline API (Figure 4.26), indicating that this was not a completely amorphous powder and crystalline material correspondent to ITZ was present. Crystals were observed with SEM (highlighted in Figure 4.21), but the majority of the particles did not reveal typical crystalline shapes (e.g. well-defined structures, edges, symmetric conformations). In addition, a sample of crystalline citric acid was also analyzed with XRPD (see Figure A.9 in Appendix), but no corresponding peaks were identified in the ITZ HPH prototype.

Due the thick consistency of the ITZ HSM coprecipitated agglomerates, most likely due to the presence of citric acid, it was not possible to prepare its XRPD sample. Therefore, no XRPD result was acquired for this prototype.

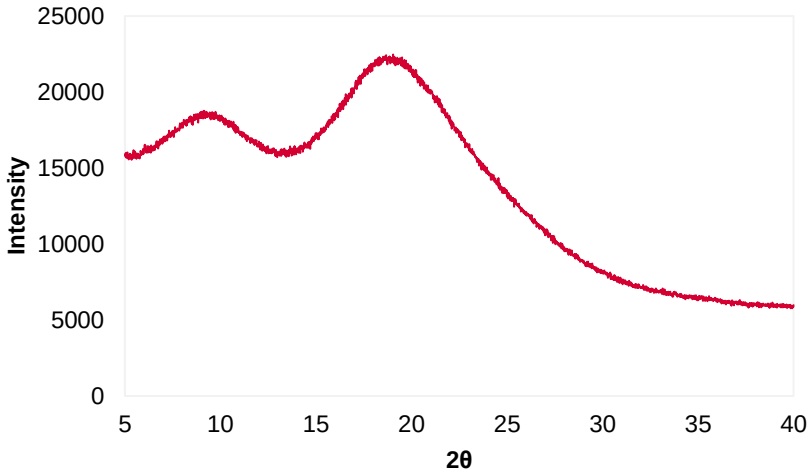

Figure 4.25 – Powder diffractogram of ITZ SD benchmark.

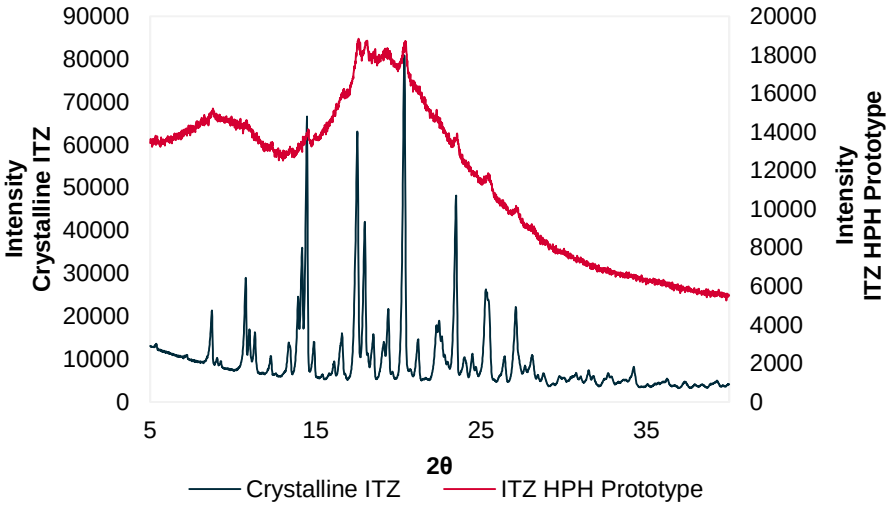

Figure 4.26 – Powder diffractogram of ITZ HPH Prototype overlaid with crystalline ITZ diffractogram.

Concerning mDSC of SD benchmark and coprecipitated prototypes, the main results are presented in Table 4.13 and the analyzed thermographs are available in Figure A.4 in Appendix for more information.

For ITZ SD benchmark, only one T_g was identified at 91 ºC, between T_gs of the pure components, and no melting peaks were observed. Along with the results from XRPD, it is concluded that the product was an ASD.

ITZ HPH prototype presented two T_gs and melting endotherm, which indicates phase separation and crystallinity presence. This result is aligned with crystallinity detection in XRPD.

For ITZ HSM prototype the results were not perceptive, but a melting endotherm was identified near melting temperature of crystalline ITZ, which may also indicate crystallinity presence. XRPD information is needed to clarify this result.

Table 4.13 – Thermal analysis of SD benchmark and coprecipitated prototypes.

Product	Number of T_gs	T_g (ºC)	Presence of melting peaks
ITZ SD	1	91.4	No
ITZ HPH	2	116.2 125.8	Yes
ITZ HSM	Inconclusive	-	Yes

The obtained results for bulk density, residual solvents, water content and assay of SD benchmark and coprecipitation prototypes are summarized in Table 4.14.

Table 4.14 – Summary of SD benchmark and coprecipitated prototypes analytical characterization.

Analytical Characterization			ITZ SD benchmark	ITZ HPH prototype	ITZ HSM prototype
GC	DCM	(ppm)	110	N/AP	N/AP
	MeOH	(ppm)	20	N/AP	N/AP
	DMSO	(ppm)	N/AP	37 425	77 159
TGA	Water	(wt.%)	0.16	11.16	26.74
Bulk density		(g/cm^3)	0.23	0.18	0.17
HPLC	Assay		101.5%	137.0%	97.1%
XRPD			Amorphous	Crystallinity	N/D
PSD	D_v10	(µm)	1.21	9.74	2.69
	D_v50	(µm)	6.32	56.64	224.44
	D_v90	(µm)	17.19	257.31	407.84

N/A – not applicable; N/D – not determined

4.9.3. *Bulk Density*

Bulk density of ITZ benchmark and prototypes is between 0.1 – 0.3 g/cm^3. This is a typical range for bulk density of spray dried and coprecipitated powers.[44,110]

4.9.4. *Assay*

API assay in each powder was calculated using HPLC and presented considering label claim. According to WHO, the generally accepted limit for API content in a drug product is ± 5 % of the label claim (i.e. 95.0 – 105.0 %).[111] For products in development stages, the range for assay is typically 90.0 – 110.0 %.

SD benchmark presented an assay aligned with expectation, as well as HSM prototype. However, in the HPH coprecipitated prototype the result is higher than expected.

By adding citric acid to lower the water's pH, the citric acid was incorporated into the coprecipitated particles during the isolation stage in both coprecipitated prototypes. Hence, for assay calculations, it was assumed a total incorporation of the citric acid amount (present in the antisolvent), which consequently, lowered the initial drug load. The estimated drug load for both prototypes was now 16 wt.%. When analyzing ITZ HPH assay above 100 wt.%, this would imply that the final drug load was above the former estimated 16 wt.% and that the citric acid uptake was not total, while for HSM prototype the estimation may indicate a total uptake of citric acid. Therefore, the drug loads of coprecipitated materials may differ.

However, the higher assay value for ITZ HPH may also be a consequence of a matrix effect caused by the different behavior of the prototype in the HPLC analytical method. Matrix effects are often caused by the alteration of the behavior of target analytes, i.e. the API, in the presence of co-eluting compounds, in this case citric acid, in the same matrix.[112] Matrix effects can lead to an increase or decrease of the peak area and this possible event was not considered during the HPLC method's assessment: no accuracy was performed during the analytical method's assessment, therefore, the possibility of a matrix effect could not be confirmed. Based on the described above, no conclusions can be retrieved from the assay results for the coprecipitated prototypes.

4.9.5. *Residual Solvents and Water content*

ICH guideline recommends the acceptable amounts for residual solvents in pharmaceutical products.[45] The ICH limits for the employed solvents are: DCM = 600 ppm, MeOH = 3 000 ppm and DSMO = 5 000 ppm.[45]

GC results for ITZ SD benchmark are bellow ICH limits, indicating that secondary drying was adequate. On the other hand, DMSO quantification is above ICH limit in both coprecipitated prototypes. In HSM prototype, DMSO content is approximate the concentration in the initial suspension, meaning that this compound was practically not removed during diafiltration. In ITZ HPH prototype, DMSO was reduced to almost a half of its initial content. The number of diafiltration operations was not enough to reduce the organic solvent bellow ICH limits. Moreover, the inefficient mixing due to lack of agitation in the retentate reservoir had a severe impact on DMSO removal.

It is important to assess water content, since its presence can lower the T_g of an amorphous product.[44] As expected, water content was residual in SD benchmark, since no water was employed during production. But, for coprecipitated prototypes is significantly higher, which can compromise physical stability of the drug product, by triggering even more phase separation, increasing molecular mobility. The water content in coprecipitated prototypes is related with the extent of DMSO removal – higher in HSM prototype, where DMSO removal was lower. This is associated to the fact that DMSO and water are miscible solvents, thus, to reduce water content in coprecipitated formulations, diafiltration should be primarily optimized and/or conductivity

tracked by measurements in retentate. If even after diafiltration optimization the water content is significantly high, T_{out} during SD isolation can be increased, as long as not above T_g of the amorphous material. For detailed information, TGA thermographs are available in Appendix.

4.9.6. *In vitro biorelevant dissolution studies*

In vitro biorelevant dissolution studies were performed with the aim of testing the supersaturation extent following acid-to-neutral pH transition. pH-shift dissolution helps in correlating with *in vivo* absorption – mimicking the transition from acidic gastric conditions to intestine. The dissolution results for crystalline ITZ, ITZ SD benchmark and ITZ HPH are displayed in Figure 4.27. As expected, both SD benchmark and HPH coprecipitated prototype exhibited faster dissolutions rates and higher solubility than crystalline ITZ. The increase in API concentration for ITZ HPH prototype and ITZ SD benchmark happened after 30 minutes, coinciding with the pH shift timepoint. This was expected, as the two formulations included HPMCAS-M, an enteric polymer with a dissolution pH above 6.

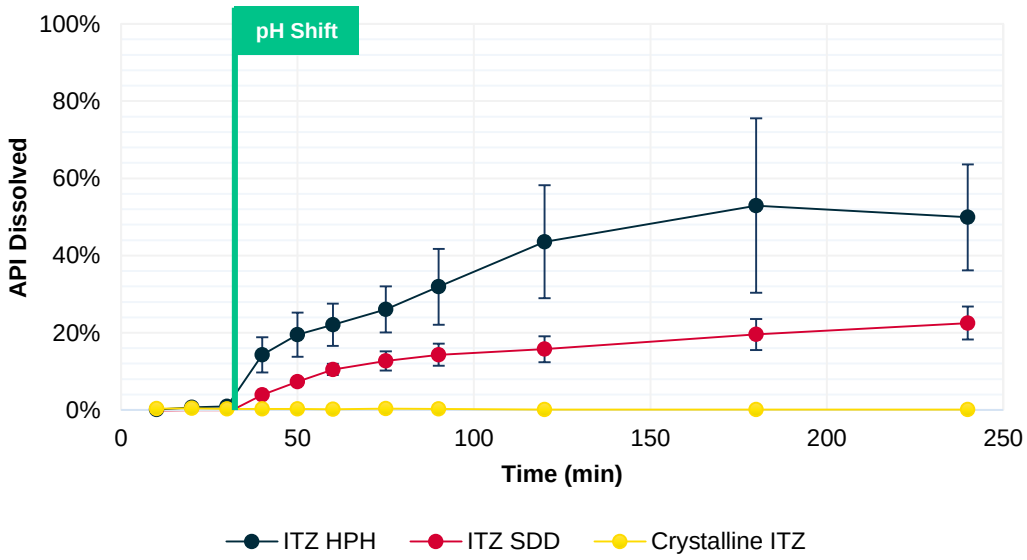

Figure 4.27 – In vitro biorelevant dissolution studies results of crystalline ITZ, ITZ SD benchmark and ITZ HPH prototype.

Crystalline ITZ exhibited the lowest area under the dissolution curve (AUC_d = 0.12 mg.min/mL), during the 240 minutes of the study.

ITZ SD benchmark was capable of maintaining supersaturation until the end of the test, with an AUC_d of 6.74 mg.min/mL. Hovione's experience suggests that AUC_d of ITZ SD should be higher.

An increased area under the curve was achieve by the ITZ HPH prototype (AUC_d = 31.83 mg.min/mL), which can be attributed to the high superficial area observed in the porous particles (Figure 4.21) and lower density, which can facilitate fluidization and justify a higher bioavailability for this prototype. For the dissolution result of this prototype there was a significant standard

deviation between both repetitions. This high variability, which precludes an assured conclusion concerning the dissolution profiles, may be related with the small number of repetitions (n=2), along with the wide span of PSD (Figure 4.24) and fluidization of the material owing to the bulk density.

Concerning the experiments conducted with ITZ HSM prototype, the powder settled at the bottom of the small test tube, hindering dissolution, thus, the dissolution profile it is not presented.

Due to lack of an agitation parts inside the small test tubes, this method may be hindering bigger particles dissolution. Bigger particles may have deposited in the bottom of the test tube or even the powder itself may not have been completely dispersed within the dissolution medium. Another drawback of this method is the possibility of particle loss during sample preparation, since small amounts of medium are withdrawn from the small test tube to the quartz cuvette and, after absorbance measurements, are returned to the small test tube. This methodology employed for *in vitro* biorelevant dissolution studies is currently under development and these may be topics of improvement.

5

Conclusions and Future Work

The work described in this Thesis was focused on the production of ASDs by coprecipitation coupled with crossflow filtration, demonstrating the feasibility of this methodology. The materials produced by this new methodology were compared with SD benchmarks to demonstrate equivalency in the *in vitro* biorelevant dissolution profiles.

The production of an ASD product with Furosemide was conceivable with spray drying. However, coprecipitation with FUR was not carried out, since during the pH effect studies severe crystallinity presence was observed by birefringence in PLM. According to the API key physicochemical properties recommended for coprecipitation process in the literature, FUR may not be a suitable candidate for this technique.[44] An outcome from this work is that a more detailed and structured study of API properties is paramount for a successful coprecipitation process.

Both ITZ HPH coprecipitated prototype and SD benchmarks were analytically characterized through DSC, XRPD, GC, TGA, HPLC, PSD, SEM, bulk density and *in vitro* biorelevant dissolution studies. Due to the presence of atypical agglomeration, it was not possible to analytically characterize the ITZ HSM coprecipitated prototype completely. ITZ HPH coprecipitated prototype seemed to exhibit a better dissolution performance than SD benchmark, which may be attributed to the porous particles and lower density. Nevertheless, the *in vitro* biorelevant dissolution methodology employed may need optimization when evaluating coprecipitated materials.

The results of this Thesis indicate that the implementation of CFF with hollow fiber membranes in the ASDs production through coprecipitation is feasible and a promising approach. CFF extends the production of ASDs by coprecipitation of “brick-dust” compounds that cannot be manufactured by typical SD or HME. By concentrating the high-volume suspensions resultant from coprecipitation, the hollow fiber membranes allow for a scale independent process. With

diafiltration, it was possible to wash the non-volatile organic solvent, DMSO, even though in this particular study further washing would be required to be below ICH limit.

Overall, the process still requires optimization, which would have been done in the context of this Thesis, had it not been for the current pandemic constrictions. Coprecipitation with HSM is one of points where improvement is warranted, particularly how the coprecipitation occurs in the mixing zone of the rotor-stator. CFF with hollow fiber membranes apparatus also needs enhancement to accomplish the desired DMSO washing and achieve results below ICH limit. Suggestions on improvements and future work in each process stage are further indicated to optimize the production of amorphous solid dispersions by the proposed methodology.

Coprecipitation process

In vitro Screening

The employed solvent casting methodology is a satisfactory technique to help delineate drug load/polymer selection. Solvent casting mimicked a slow evaporation of the volatile organic solvent mixture further selected for SD. However, this methodology, in future work, should be enhanced to mimic coprecipitation process. A high throughput miniaturized coprecipitation screening (MiCoS) was reported in the literature by *Hu et al*.[58,113] MiCoS consists of five main steps:

1. Preparation of drug and polymer stock solutions in water miscible solvents, e.g. DMA, DMSO;
2. Mixing of drug and polymer stock solutions, with a typical drug load range between 10 – 60 wt.% and 10 wt.% solids' feed concentration;
3. Coprecipitation occurs in 1 mL glass vials (96-well format) with acidified cold (5 ºC) water used as antisolvent. Solutions are added dropwise with a pipet to the antisolvent, under magnetic stirring;
4. Filtration and washing using two 96-well filter plates;
5. Filtrate is characterized with ULPC (Ultra-Performance Liquid Chromatography). Drug concentration in the filtrate is determined and with this result it is possible to calculate the drug amount in the dried powder.
6. The material in one of the 96-well plates will be further used for solid-state characterization (XRPD, Raman, PLM…) and the other plate is for kinetic solubility profile assessment using FaSSIF.

A schematization of MiCoS is represented in Figure 5.1.

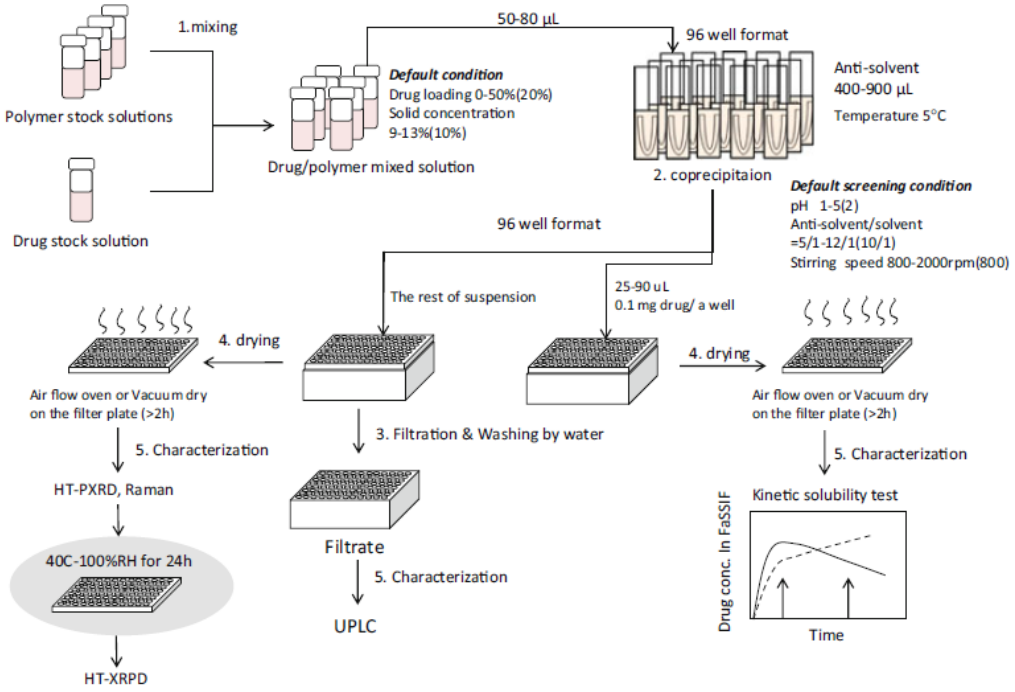

Figure 5.1 – Schematic representation of MiCoS. [Adapted from [58]]

Coprecipitation with HSM

Coprecipitation was carried out through two different technologies: HSM and HPH. In this study, HPH was the more adequate technology, even though this prototype exhibited some crystallinity. This crystallinity presence may be attributed to potential residual dissolution of the drug and stability of the amorphous product and not the HPH process itself. Therefore, a more conservative drug loading should be considered in future coprecipitation processes (e.g. 20 wt.% ITZ).

HSM needs further improvement to produce particles with desired morphology and particle size distribution, and, to avoid the formation of large agglomerates (as happened in this work). To summarize, the critical parameters of coprecipitation with a HSM are:

- **S/AS Ratio**

As a conservative S/AS ratio of 1:12 was employed, it is not considered that the main challenges of the HSM were associated with this parameter.

- **Temperature**

The temperature increases when the drug stock solution is added to the antisolvent. Moreover, the high shear mixing may also contribute to adding additional energy to the medium. If the heat is not dissipated, incomplete conversion to amorphous state can occur.[44] This also translates into the presence of remaining crystalline seeds of the API, which may induce crystallization.[44] For this reason, the temperature of the antisolvent in the reactor was set at 5 ºC, since research has shown the best temperature range is from 2 to 8 ºC.[44] Also, heating could be

applied during stock solution preparation, to avoid the presence of undissolved drug and crystalline seeds.[44]

- **Shear rate and mixing time**

Higher shear rates and longer mixing times are reported as detrimental to amorphous material production.[44] Hence, the lowest possible shear rate of the HSM was selected (3000 rpm) and the mixing time corresponded to the duration of stock solution addition (~ 4 min). To promote a rapidly contact with the antisolvent and the stock solution, a L-shaped tube fed the solution to the reactor. But, as the exit of this tubing was near the rotor-stator of the HSM, it may had submitted the solution to higher temperatures, precluding the production of amorphous particles. Therefore, solution-antisolvent mixing require optimization on both addition rate of the drug stock solution and feed localization. Currently, a high shear mixing apparatus, addressing these issues, is being designed to be implemented on the production of ASDs through coprecipitation. This design is based on the work described by *Suda et.al*, where it was reported that the design enabled fast "*mixing* [of] *two different liquids, thus achieving the highest degree of supersaturation within the shortest time and completing a uniform nucleation reaction without initiating particle growth or aggregation*".[114]

Moreover, in future work, it is essential to assess chemical and physical stability of both ITZ and FUR, with HPLC and XRPD, for example, since in the coprecipitation process (either with HSM or HPH) the particles stay in suspension while concentration, diafiltration and isolation occur. Additionally, suspension stability should be studied to support process development.

Other important factor in coprecipitation, in both HSM and HPH processes, was the addition of the citric acid. High amounts of citric acid were required to lower water's pH, to be used as antisolvent. Additionally, during diafiltration this compound was not removed, due to the use of acidic water to wash DMSO. This impacted yield during isolation through spray drying. For future work, it is advised to use other acid, preferably in liquid state, whose amounts do not impact formulation during drying. Some suggestions include the usage of acetic acid or ascorbic acid. To point out that HCl was also reported in the literature to acidify water as antisolvent in coprecipitation.[19,115] Other alternative to minimize the acid amount prior to spray drying isolation, is to perform the last diafiltration step with deionized water (non-acididfied).

CFF with hollow fiber membranes

The presence of large aggregates, particularly in the ITZ HSM suspension, impacted the crossflow filtration process. This fact was more evident with the membrane previously used in placebos trials. A few agglomerates exceeding 500 µm in ITZ HSM suspension may have been present, which could have potentially caused the fiber's blockage (0.5 mm of inner diameter). The membrane inner fiber diameter selection was conservative and a membrane with a bigger inner

fiber diameter could have been chosen to allow higher flowrates during concentration and diafiltration. This also applies to pore size. The adequate membrane selection would avoid these challenges.

Also, in future work, agitation in the retentate flask is recommended to a better homogenization, especially during diafiltration. To do so with a safe approach, the CFF setup needs equipment adjustments. Another setup improvement suggestion is the implementation of a conductometer probe in line, to track solvent mixture conductivity in retentate. In fact, the supplier provides that solution with KONDUiT. KONDUiT is an add-on module that connects to the KF Comm software from KR2i, enabling conductivity control and monitoring during diafiltration.

Scale-up strategy – Guidelines

One advantage of the incorporation of crossflow filtration with membrane modules is that it turns coprecipitation into a scale independent approach to produce amorphous solid dispersions. CFF reduces the higher volumes obtained from coprecipitation, by concentrating the suspension, and circumvents the need for secondary drying, by removing the organic solvent during diafiltration. Therefore, a strategy for the scale-up of CFF membrane process should be considered and some guidelines are presented next.

Scaling up a process involves increasing the filter area, in order to handle larger volumes of starting material without significantly changing process conditions.[76]

- After identifying the most suitable membrane module for the desired separation, it is important to maintain its characteristics, namely pore size, selectivity, materials and lumen diameter.[76,116]
- Then, optimization of TMP and crossflow rate trials can be conducted, to determine the optimal permeate flux (Figure 2.16) which increases membrane life, while minimizing cycle time and potential yield losses, before proceeding to scale-up.[117,118]
- After this, TMP, crossflow rate, feed concentration and overall process steps and time should remain constant, from small tests at lab scale to full scale production.[76,116,118,119]
- The simplest scaling strategy is linear scale-up, where system scaling is based on consistent capacity (L/m^2) from small to large scale.[120] Permeate, washing solvent/buffer and retentate volume also scale linearly with feed volume.[120] An area-time term can be calculated as the ratio of the manufacturing scale permeate volume over the average permeate flux, according to:

$$Average\ permeate\ flux = \frac{Experimental\ total\ volume\ permeated\ (L)}{device\ area\ (m^2) \times\ processing\ time\ (h)}$$

Equation 5.1 – Determination of area-time term for scale-up.

Considering the total processing time, the required area is determined, and this area can be divided into several modules with smaller areas connected to each other. Additionally,

it is recommended that an area safety factor is considered to allow some process variations.[118] 20% safety factor is recommended as a rule of thumb; however, many membrane modules are, in fact, oversized (from 20 to 200%) to compensate the flux decay phenomenon, as a consequence of membrane fouling.[118] Typically, this is achieved through a compromise between cycle time, throughput and economic viability.

- Lastly, the goal of membrane scale-up is to design a process that will have batch-to-batch reproducibility while extending membrane service life.[116] Hence, pilot scale tryouts are conducted, in order to identify the influence of feed batch-to-batch variability and to assure separation performance even after several cycles of operation followed by membrane cleaning.[116]

6

References

1. Duarte, Í. Doctoral Thesis: Development of new screening methodologies and preparation methods with application in amorphous solid dispersions and pharmaceutical cocrystals. (Universidade de Lisboa, Faculdade de Farmácia, 2016).
2. Zhong, H., Chan, G., Hu, Y., Hu, H. & Ouyang, D. A comprehensive map of FDA-approved pharmaceutical products. *Pharmaceutics* **10**, 1–19 (2018). doi:10.3390/pharmaceutics10040263
3. Bosselmann, S. & Williams, R. O. Route-Specific Challenges in the Delivery of Poorly Water-Soluble Drugs. in *Formulating Poorly Water Soluble Drugs. AAPS Advances in the Pharmaceutical Sciences Series, vol. 3* (eds. Williams III, R. O., Watts, A. B. & Miller, D. A.) 1–26 (Springer, New York, NY, 2012). doi:10.1007/978-1-4614-1144-4_1.
4. Viswanathan, P., Muralidaran, Y. & Ragavan, G. Challenges in oral drug delivery: A nano-based strategy to overcome. in *Nanostructures for Oral Medicine* (eds. Andronescu, E. & Grumezescu, A. M.) 173–201 (Elsevier Inc., 2017). doi:10.1016/B978-0-323-47720-8.00008-0.
5. Jermain, S. V., Brough, C. & Williams, R. O. Amorphous solid dispersions and nanocrystal technologies for poorly water-soluble drug delivery – An update. *Int. J. Pharm.* **535**, 379–392 (2018). doi:10.1016/j.ijpharm.2017.10.051
6. Thorat, A. A. & Dalvi, S. V. Liquid antisolvent precipitation and stabilization of nanoparticles of poorly water soluble drugs in aqueous suspensions: Recent developments and future perspective. *Chem. Eng. J.* **181**–**182**, 1–34 (2012). doi:10.1016/j.cej.2011.12.044
7. Lonare, A. A. & Patel, S. R. Antisolvent Crystallization of Poorly Water Soluble Drugs. *Int. J. Chem. Eng. Appl.* **4**, 337–341 (2013). doi:10.7763/ijcea.2013.v4.321
8. Duarte, Í., Santos, J. L., Pinto, J. F. & Temtem, M. Screening methodologies for the development of spray-dried amorphous solid dispersions. *Pharm. Res.* **32**, 222–237 (2015). doi:10.1007/s11095-014-1457-5
9. Ghadi, R. & Dand, N. BCS class IV drugs: Highly notorious candidates for formulation development. *J. Control. Release* **248**, 71–95 (2017). doi:10.1016/j.jconrel.2017.01.014
10. Hughey, J. R. & Williams, R. O. Solid-State Techniques for Improving Solubility. in *Formulating Poorly Water Soluble Drugs. AAPS Advances in the Pharmaceutical Sciences Series, vol. 3* (eds. Williams III, R. O., Watts, A. B. & Miller, D. A.) 95–131

(Springer, New York, NY, 2012). doi:10.1007/978-1-4614-1144-4_3.

11. Mendonsa, N. *et al.* Manufacturing strategies to develop amorphous solid dispersions: An overview. *J. Drug Deliv. Sci. Technol.* **55**, 101459 (2020). doi:10.1016/j.jddst.2019.101459

12. BASF. Strategies for Working with Poorly Water-Soluble APIs. *PharmTech Spons. eBooks* Sponsored, 1–29 (2020).

13. Wang, G. *et al.* Active Transportation of Liposome Enhances Tumor Accumulation, Penetration, and Therapeutic Efficacy. *Small* **16**, 1–14 (2020). doi:10.1002/smll.202004172

14. Lino, P. & Henriques, J. Amorphous Solid Dispersions: Increasing Solubility From API to Tablets. *Drug Dev. Deliv.* **19**, 32–37 (2019).

15. Dobry, D. E. *et al.* A model-based methodology for spray-drying process development. *J. Pharm. Innov.* **4**, 133–142 (2009). doi:10.1007/s12247-009-9064-4

16. Schittny, A., Philipp-Bauer, S., Detampel, P., Huwyler, J. & Puchkov, M. Mechanistic insights into effect of surfactants on oral bioavailability of amorphous solid dispersions. *J. Control. Release* **320**, 214–225 (2020). doi:10.1016/j.jconrel.2020.01.031

17. Baghel, S., Cathcart, H. & O'Reilly, N. J. Polymeric Amorphous Solid Dispersions: A Review of Amorphization, Crystallization, Stabilization, Solid-State Characterization, and Aqueous Solubilization of Biopharmaceutical Classification System Class II Drugs. *J. Pharm. Sci.* **105**, 2527–2544 (2016). doi:10.1016/j.xphs.2015.10.008

18. Williams, H. D. *et al.* Strategies to address low drug solubility in discovery and development. *Pharmacol. Rev.* **65**, 315–499 (2013). doi:10.1124/pr.112.005660

19. Duarte, Í. *et al.* Production of nano-solid dispersions using a novel solvent-controlled precipitation process — Benchmarking their in vivo performance with an amorphous micro-sized solid dispersion produced by spray drying. *Eur. J. Pharm. Sci.* **93**, 203–214 (2016). doi:10.1016/j.ejps.2016.08.011

20. Sandhu, H., Shah, N., Chokshi, H. & Malick, A. W. Overview of Amorphous Solid Dispersion Technologies. in *Amorphous Solid Dispersions. Advances in Delivery Science and Technology* (eds. Shah, N., Sandhu, H., Choi, D. S., Chokshi, H. & Malick, A. W.) 91–119 (Springer, New York, NY, 2014). doi:10.1007/978-1-4939-1598-9.

21. Shah, N. *et al.* Structured Development Approach for Amorphous Systems. in *Formulating Poorly Water Soluble Drugs. AAPS Advances in the Pharmaceutical Sciences Series, vol. 3* (eds. Williams III, R. O., Watts, A. B. & Miller, D. A.) 267–310 (Springer, New York, NY, 2012). doi:10.1007/978-1-4614-1144-4_8.

22. Vasconcelos, T., Marques, S., das Neves, J. & Sarmento, B. Amorphous solid dispersions: Rational selection of a manufacturing process. *Adv. Drug Deliv. Rev.* **100**, 85–101 (2016). doi:10.1016/j.addr.2016.01.012

23. Rowe, J. M. & Johnston, K. P. Precipitation Technologies for Nanoparticle Production. in *Formulating Poorly Water Soluble Drugs. AAPS Advances in the Pharmaceutical Sciences Series, vol. 3* (eds. Williams III, R. O., Watts, A. B. & Miller, D. A.) 501–568 (Springer, New York, NY, 2012). doi:10.1007/978-1-4614-1144-4_12.

24. Jog, R. & Burgess, D. J. Pharmaceutical Amorphous Nanoparticles. *J. Pharm. Sci.* **106**, 39–65 (2017). doi:10.1016/j.xphs.2016.09.014

25. Shah, N. *et al.* Improved Human Bioavailability of Vemurafenib, a Practically Insoluble Drug , Using an Amorphous Polymer-Stabilized Solid Dispersion Prepared by a Solvent-Controlled Coprecipitation Process. *J. Pharm. Sci.* **102**, 967–982 (2013). doi:10.1002/jps

26. L, S., B, H., Kumar T, V. V., Rao B, N. M. & Teja B, B. Studies on Solubility and Dissolution Enhancement of Itraconazole by Complexation with Sulfo-Butyl7 Ether β Cyclodextrin. *Asian J. Biomed. Pharm. Sci.* **4**, 06–16 (2014). doi:10.15272/ajbps.v4i38.592

27. Shariare, M. H. *et al.* In vitro dissolution and bioavailability study of furosemide

nanosuspension prepared using design of experiment (DoE). *Saudi Pharm. J.* **27**, 96–105 (2019). doi:10.1016/j.jsps.2018.09.002

28. Nielsen, L. H., Rades, T. & Müllertz, A. Stabilisation of amorphous furosemide increases the oral drug bioavailability in rats. *Int. J. Pharm.* **490**, 334–340 (2015). doi:10.1016/j.ijpharm.2015.05.063

29. De Caro, V. *et al.* Development and characterization of an amorphous solid dispersion of furosemide in the form of a sublingual bioadhesive film to enhance bioavailability. *Pharmaceutics* **9**, 1–16 (2017). doi:10.3390/pharmaceutics9030022

30. Takács-Novák, K. *et al.* Biorelevant solubility of poorly soluble drugs: Rivaroxaban, furosemide, papaverine and niflumic acid. *J. Pharm. Biomed. Anal.* **83**, 279–285 (2013). doi:10.1016/j.jpba.2013.05.011

31. Vankelecom, I. F. J., Gevers, L. E. M., Schäfer, T. & Crespo, J. G. Membrane Processes. in *Green Separation Processes* (eds. Afonso, C. A. M. & Crespo, J. G.) 251–289 (Wiley-VCH Verlag GmbH & Co. KGaA, 2006). doi:10.1002/3527606602.ch3f.

32. FDA. *Advancing Health through Innovation: New Drug Approvals 2019*. https://www.fda.gov/media/134493/download (2020). Accessed at 9th April 2020.

33. Johanson, G. Modeling of Disposition. in *Comprehensive Toxicology* (ed. Charlene A. McQueen) vols 1–14 153–177 (Elsevier, 2010). doi:10.1016/B978-0-08-046884-6.00108-1

34. Price, G. . & Patel, D. Drug Bioavailability. *In: StatPearls [Internet]. Treasure Island (FL): StatPearls Publishing* https://www.ncbi.nlm.nih.gov/books/NBK557852/ (2020). Accessed at 26th November 2020.

35. Chavda, H. V., Patel, C. N. & Anand, I. S. Biopharmaceutics classification system. *Syst. Rev. Pharm.* **1**, 62–69 (2010). doi:10.4103/0975-8453.59514

36. Dahan, A. & Miller, J. M. The solubility-permeability interplay and its implications in formulation design and development for poorly soluble drugs. *AAPS J.* **14**, 244–251 (2012). doi:10.1208/s12248-012-9337-6

37. Noyes, A. A. . & Whitney, W. R. The rate of solution of solid substances in their own solutions. *J. Am. Chem. Soc.* **19**, 930–934 (1897). doi:10.1021/ja02086a003

38. Dokoumetzidis, A. & Macheras, P. A century of dissolution research: From Noyes and Whitney to the Biopharmaceutics Classification System. *Int. J. Pharm.* **321**, 1–11 (2006). doi:10.1016/j.ijpharm.2006.07.011

39. Tran, P. *et al.* Overview of the manufacturing methods of solid dispersion technology for improving the solubility of poorly water-soluble drugs and application to anticancer drugs. *Pharmaceutics* **11**, 1–26 (2019). doi:10.3390/pharmaceutics11030132

40. Huang, S. & Williams III, R. O. Effects of the Preparation Process on the Properties of Amorphous Solid Dispersions. *AAPS PharmSciTech* **19**, 1971–1984 (2018). doi:10.1208/s12249-017-0861-7

41. Laitinen, R. . *et al.* Theoretical Considerations in Developing Amorphous Solid Dispersions. in *Amorphous Solid Dispersions. Advances in Delivery Science and Technology* (eds. Shah, N., Sandhu, H., Choi, D. S., Chokshi, H. & Waseem Malick, A.) 35–90 (Springer, New York, NY, 2014). doi:https://doi.org/10.1007/978-1-4939-1598-9_2.

42. Patil, H., Tiwari, R. V. & Repka, M. A. Hot-Melt Extrusion: from Theory to Application in Pharmaceutical Formulation. *AAPS PharmSciTech* **17**, 20–42 (2016). doi:10.1208/s12249-015-0360-7

43. Singh, A. & Van den Mooter, G. Spray drying formulation of amorphous solid dispersions. *Adv. Drug Deliv. Rev.* **100**, 27–50 (2016). doi:10.1016/j.addr.2015.12.010

44. Shah, N. *et al.* MBP Technology: Composition and Design Considerations. in *Amorphous Solid Dispersions. Advances in Delivery Science and Technology* (eds. Shah, N., Sandhu,

H., Choi, D. S., Chokshi, H. & Waseem Malick, A.) 323–350 (Springer, New York, NY, 2014). doi:10.1007/978-1-4939-1598-9_10.

45. European Medicines Agency. *ICH guideline Q3C (R6) on impurities: Guideline for Residual Solvents*. *International Conference on Harmonization of Technical Requirements for Registration of Pharmaceuticals for Human Use* (2019).

46. Santos, D. *et al.* Spray Drying: An Overview. in *Biomaterials - Physics and Chemistry - New Edition* (ed. Pignatello, R.) 9–31 (IntechOpen, 2017). doi:10.5772/intechopen.72247.

47. Miller, D. A. & Gil, M. Spray-Drying Technology. in *Formulating Poorly Water Soluble Drugs. AAPS Advances in the Pharmaceutical Sciences Series, vol. 3* (eds. Williams III, R. O., Watts, A. B. & Miller, D. A.) 363–442 (Springer, New York, NY, 2012). doi:10.1007/978-1-4614-1144-4_10.

48. Hou, H. H. *et al.* Impact of Method of Preparation of Amorphous Solid Dispersions on Mechanical Properties: Comparison of Coprecipitation and Spray Drying. *J. Pharm. Sci.* **108**, 870–879 (2019). doi:10.1016/j.xphs.2018.09.008

49. Rao, Q. *et al.* Enhancement of the apparent solubility and bioavailability of Tadalafil nanoparticles via antisolvent precipitation. *Eur. J. Pharm. Sci.* **128**, 222–231 (2019). doi:10.1016/j.ejps.2018.12.005

50. Shah, N. *et al.* Development of novel microprecipitated bulk powder (MBP) technology for manufacturing stable amorphous formulations of poorly soluble drugs. *Int. J. Pharm.* **438**, 53–60 (2012). doi:10.1016/j.ijpharm.2012.08.031

51. Panagiotou, T., Mesite, S. V. & Fisher, R. J. Production of norfloxacin nanosuspensions using microfluidics reaction technology through solvent/antisolvent crystallization. *Ind. Eng. Chem. Res.* **48**, 1761–1771 (2009). doi:10.1021/ie800955t

52. Morales, J. O., Watts, A. B. & McConville, J. T. Mechanical Particle-Size Reduction Techniques. in *Formulating Poorly Water Soluble Drugs. AAPS Advances in the Pharmaceutical Sciences Series, vol. 3* (eds. Williams III, R. O., Watts, A. B. & Miller, D. A.) 133–170 (Springer, New York, NY, 2012). doi:10.1007/978-1-4614-1144-4_4.

53. Villalobos-Castillejos, F. *et al.* Fabrication of Nanoemulsions by Microfluidization. in *Nanoemulsions: Formulation, Applications, and Characterization* (eds. Jafari, S. M. & McClements, D. J.) 207–232 (Academic Press, 2018). doi:https://doi.org/10.1016/B978-0-12-811838-2.00008-4.

54. Panagiotou, T. & Fisher, R. Improving Product Quality with Entrapped Stable Emulsions: From Theory to Industrial Application. *Challenges* **3**, 84–113 (2012). doi:10.3390/challe3020084

55. Riewe, J. *et al.* Antisolvent precipitation of lipid nanoparticles in microfluidic systems – A comparative study. *Int. J. Pharm.* **579**, 119167 (2020). doi:10.1016/j.ijpharm.2020.119167

56. Su, Y. & Mesite, S. Production of Nanoemulsion Adjuvants using High Shear Fluid Processing. in *Morden Vaccine Adjuvants & Delivery Systems* (2015).

57. Zhao, H., Wang, J. X., Wang, Q. A., Chen, J. F. & Yun, J. Controlled liquid antisolvent precipitation of hydrophobic pharmaceutical nanoparticles in a MicroChannel reactor. *Ind. Eng. Chem. Res.* **46**, 8229–8235 (2007). doi:10.1021/ie070498e

58. Hu, Q., Wyttenbach, N., Shiraki, K. & Choi, D. S. Miniaturized Screening Tools for Polymer and Process Evaluation. in *Amorphous Solid Dispersions. Advances in Delivery Science and Technology* (eds. Shah, N., Sandhu, H., Choi, D. S., Chokshi, H. & Waseem Malick, A.) 165–195 (Springer, New York, NY, 2014). doi:10.1007/978-1-4939-1598-9_5.

59. Wyttenbach, N. *et al.* Miniaturized screening of polymers for amorphous drug stabilization (SPADS): Rapid assessment of solid dispersion systems. *Eur. J. Pharm. Biopharm.* **84**, 583–598 (2013). doi:10.1016/j.ejpb.2013.01.009

60. Paudel, A., Meeus, J. & Mooter, G. Van den. Structural Characterization of Amorphous Solid Dispersions. in *Amorphous Solid Dispersions. Advances in Delivery Science and*

Technology (eds. Shah, N., Sandhu, H., Choi, D. S., Chokshi, H. & Waseem Malick, A.) 421–485 (Springer, New York, NY, 2014). doi:10.1007/978-1-4939-1598-9_14.

61. Kaushik, R., Budhwar, V. & Kaushik, D. An Overview on Recent Patents and Technologies on Solid Dispersion. *Recent Pat. Drug Deliv. Formul.* **14**, (2020). doi:10.2174/1872211314666200117094406

62. Liu, X., Feng, X., Williams, R. O. & Zhang, F. Characterization of amorphous solid dispersions. *J. Pharm. Investig.* **48**, 19–41 (2018). doi:10.1007/s40005-017-0361-5

63. Yin, Z., Ma, Y., Tanis-Kanbur, B. & Chew, J. W. Fouling behavior of colloidal particles in organic solvent ultrafiltration. *J. Memb. Sci.* **599**, 117836 (2020). doi:10.1016/j.memsci.2020.117836

64. Buonomenna, M. G. & Bae, J. Organic solvent nanofiltration in pharmaceutical industry. *Sep. Purif. Rev.* **44**, 157–182 (2015). doi:10.1080/15422119.2014.918884

65. Chen, D., Sirkar, K., Jin, C., Singh, D. & Pfeffer, R. Membrane-based Technologies in the Pharmaceutical Industry and Continuous Production of Polymer-coated Crystals/Particles. *Curr. Pharm. Des.* **23**, 242–249 (2017). doi:10.2174/1381612822666161025145229

66. Cui, Y. & Chung, T. Pharmaceutical concentration using organic solvent forward osmosis for solvent recovery. *Nat. Commun.* **9**, 1–9 (2018). doi:10.1038/s41467-018-03612-2

67. Mulder, M. Introduction. in *Basic Principles of Membrane Technology* 1–21 (Kluwer Academic Publishers, Dordrecht, 1996). doi:10.1007/978-94-009-1766-8.

68. Mulder, M. Membrane Processes. in *Basic Principles of Membrane Technology* 280–415 (Kluwer Academic Publishers, Dordrecht, 1996). doi:10.1007/978-94-009-1766-8.

69. Musumeci, T., Leonardi, A., Bonaccorso, A., Pignatello, R. & Puglisi, G. Tangential Flow Filtration Technique: an Overview on Nanomedicine Applications. *Pharm. Nanotechnol.* **06**, 48–60 (2018). doi:10.2174/2211738506666180306160921

70. Shah, N. K., Ivone, R., Shen, J. & Meenach, S. A. A comparison of centrifugation and tangential flow filtration for nanoparticle purification: A case study on acetalated dextran nanoparticles. *Particuology* **50**, 189–196 (2020). doi:10.1016/j.partic.2019.06.004

71. Mulder, M. Module and Process Design. in *Basic Principles of Membrane Technology* 465–520 (Kluwer Academic Publishers, Dordrecht, 1996). doi:10.1007/978-94-009-1766-8.

72. Ottoboni, S. *et al.* Development of a Novel Continuous Filtration Unit for Pharmaceutical Process Development and Manufacturing. *J. Pharm. Sci.* **108**, 372–381 (2019). doi:10.1016/j.xphs.2018.07.005

73. Wankat, P. C. Introduction to Membrane Separation Processes. in *Separation Process Engineering Includes Mass Transfer Analysis* (ed. Goodwin, B.) (Prentice Hall, 2012).

74. Narkevich, I. A., Semin, A. A., Kartashova, N. S. & Teslev, A. A. Pilot and industrial absorption-chromatographic and membrane technologies for isolation and purification of plant- and animal-based active pharmaceutical ingredients. *Pharm. Chem. J.* **50**, 698–703 (2017). doi:10.1007/s11094-017-1515-5

75. Paipuri, M. Numerical Modelling of Membrane filtration using Lattice Boltzmann and Finite Volume Methods. (Swansea University, 2014). doi:10.13140/RG.2.2.26191.79524.

76. GE Healthcare Life Sciences. *Cross Flow Filtration Method Handbook*. (General Electric Company, 2014).

77. Synder Filtration. Types of Filtration. *Pressure-Driven Membrane Filtration Processes* https://synderfiltration.com/learning-center/articles/introduction-to-membranes/pressure-driven-membrane-filtration-processes/. Accessed at 2nd June 2020

78. Sheth, J. P., Qin, Y., Sirkar, K. K. & Baltzis, B. C. Nanofiltration-based diafiltration process for solvent exchange in pharmaceutical manufacturing. *J. Memb. Sci.* **211**, 251–261

(2003). doi:10.1016/S0376-7388(02)00423-4

79. Doran, P. M. Unit Operations. in *Bioprocess Engineering Principles* (ed. Doran, P.) 445–595 (Academic Press, 2013). doi:10.1016/B978-0-12-220851-5.00011-3.

80. Filtration Solutions Inc. Hollow Fiber Membrane Filter, High Packing Density Membrane | Filtsol. https://filtsol.com/main/index.php/technical-info/hollow-fiber-membranes. Accessed at 19th June 2020.

81. Balster, J. Spiral Wound Membrane Module. in *Encyclopedia of Membranes* (eds. Drioli, E. & Giorno, L.) (Springer Berlin Heidelberg, 2015). doi:10.1007/978-3-642-40872-4.

82. Berk, Z. Membrane processes. in *Food Science and Technology* (ed. Berk, Z.) 233–257 (Academic Press, San Diego, 2009). doi:https://doi.org/10.1016/B978-0-12-373660-4.00010-7.

83. Mohammad, A. W. *et al.* Nanofiltration membranes review: Recent advances and future prospects. *Desalination* **356**, 226–254 (2015). doi:10.1016/j.desal.2014.10.043

84. Marchetti, P., Jimenez Solomon, M. F., Szekely, G. & Livingston, A. G. Molecular Separation with Organic Solvent Nanofiltration: A Critical Review. *Chem. Rev.* **114**, 10735–10806 (2014). doi:10.1021/cr500006j

85. Livingston, A. G., Peeva, L. G. & Silva, P. Organic Solvent Nanofiltration. in *Membrane Technology* (eds. Pereira Nunes, S. & Peinemann, K.) 203–228 (Wiley-VCH Verlag GmbH & Co. KGaA, 2006). doi:10.1002/3527608788.ch11.

86. Chen, D., Singh, D., Sirkar, K. K. & Pfeffer, R. Porous hollow fiber membrane-based continuous technique of polymer coating on submicron and nanoparticles via antisolvent crystallization. *Ind. Eng. Chem. Res.* **54**, 5237–5245 (2015). doi:10.1021/acs.iecr.5b00155

87. Chen, D., Singh, D., Sirkar, K. K. & Pfeffer, R. Continuous synthesis of polymer-coated drug particles by porous hollow fiber membrane-based antisolvent crystallization. *Langmuir* **31**, 432–441 (2015). doi:10.1021/la503179t

88. Chen, D., Singh, D., Sirkar, K. K. & Pfeffer, R. Continuous preparation of polymer coated drug crystals by solid hollow fiber membrane-based cooling crystallization. *Int. J. Pharm.* **499**, 395–402 (2016). doi:10.1016/j.ijpharm.2016.01.008

89. Tuo, L. *et al.* Separations: Materials, Devices and Processes: A Novel Hollow Fiber Membrane-Assisted Antisolvent Crystallization for Enhanced Mass Transfer Process Control. *AIChe J.* **65**, 734–744 (2019). doi:10.1002/aic.16438

90. Fukuda, I. M., Pinto, C. F. F., Moreira, C. D. S., Saviano, A. M. & Lourenço, F. R. Design of Experiments (DoE) applied to Pharmaceutical and Analytical Quality by Design (QbD). *Brazilian J. Pharm. Sci.* **54**, 1–16 (2018). doi:10.1080/03639045.2017.1291672

91. Politis, S. N., Colombo, P., Colombo, G. & Rekkas, D. M. Design of experiments (DoE) in pharmaceutical development. *Drug Dev. Ind. Pharm.* **43**, 889–901 (2017). doi:10.1080/03639045.2017.1291672

92. Juran, J. M. *Juran on Quality by Design. The New Steps for planning Quality into Goods and Services*. (The Free Press, 1992).

93. Yu, L. X. *et al.* Understanding pharmaceutical quality by design. *AAPS J.* **16**, 771–783 (2014). doi:10.1208/s12248-014-9598-3

94. Umetrics AB. *Design of Experiments - Principles and Applications*. (2000).

95. Pis Yong, A., Aminul Islam, M. & Hasan, N. A Review: Effect of Pressure on Homogenization. *Nat Sci* **35**, 1–22 (2017).

96. National Center for Biotechnology Information. PubChem Annotation Record for Itraconazole. *Hazardous Substances Data Bank (HSDB)* https://pubchem.ncbi.nlm.nih.gov/source/hsdb/7839 (2020). Accessed at 27th November

2020.

97. Six, K. . *et al.* Characterization of Solid Dispersions of Itraconazole and Hydroxypropylmethylcellulose Prepared by Melt Extrusion, Part II. *Pharm. Res.* **20**, 1047–1054 (2003). doi:10.1023/A:1024414423779

98. INFARMED. Folheto Informativo - Sporanox 100 mg cápsulas Itraconazol. 1–8 (2011).

99. National Center for Biotechnology Information. PubChem Annotation Record for Furosemide. *Hazardous Substances Data Bank (HSDB)* https://pubchem.ncbi.nlm.nih.gov/source/hsdb/3086#section=Odor. (2020). Accessed at 27th November 2020.

100. Hagner, L. *et al.* Preparation of an amorphous sodium furosemide salt improves solubility and dissolution rate and leads to a faster T max after oral dosing to rats. *Eur. J. Pharm. Biopharm.* **85**, 942–951 (2013). doi:10.1016/j.ejpb.2013.09.002

101. Sanofi-Aventis U.S. *LASIX® (furosemide) Tablets 20, 40, and 80 mg*. https://www.accessdata.fda.gov/drugsatfda_docs/label/2012/016273s066lbl.pdf (2011).

102. Vaka, S. R. K. *et al.* Excipients for Amorphous Solid Dispersions. in *Amorphous Solid Dispersions. Advances in Delivery Science and Technology* (eds. Shah, N., Sandhu, H., Choi, D. S., Chokshi, H. & Waseem Malick, A.) 123–161 (Springer, New York, NY, 2014). doi:10.1007/978-1-4939-1598-9_4.

103. Ousset, A. *et al.* Prediction of phase behavior of spray-dried amorphous solid dispersions: Assessment of thermodynamic models, standard screening methods and a novel atomization screening device with regard to prediction accuracy. *Pharmaceutics* **10**, (2018). doi:10.3390/pharmaceutics10010029

104. Shin-Etsu. Shin-Etsu AQOAT® Product Information. *Pharmaceutical excipients* 3 https://www.setylose.com/fileadmin/download_pfmd/49.pdf (2019).

105. Abbott, S., Hansen, C. M. & Yamamoto, H. *Hansen Solubility Parameters in Practice*. (Hansen-Solubility.com, 2015).

106. Yoshida, T., Lai, T. C., Kwon, G. S. & Sako, K. pH- and ion-sensitive polymers for drug delivery. *Expert Opin. Drug Deliv.* **10**, 1497–1513 (2013). doi:10.1517/17425247.2013.821978

107. National Center for Biotechnology Information. PubChem Annotation Record for Methanol. *Hazardous Substances Data Bank (HSDB)* https://pubchem.ncbi.nlm.nih.gov/source/hsdb/93 (2020). Accessed at 27th November 2020.

108. National Center for Biotechnology Information. PubChem Annotation Record for DICHLOROMETHANE. *Hazardous Substances Data Bank (HSDB)* https://pubchem.ncbi.nlm.nih.gov/source/hsdb/66 (2020). Accessed at 27th November 2020.

109. Baird, J. A. & Taylor, L. S. Evaluation of amorphous solid dispersion properties using thermal analysis techniques. *Adv. Drug Deliv. Rev.* **64**, 396–421 (2012). doi:10.1016/j.addr.2011.07.009

110. Gaspar, F., Vicente, J., Neves, F. & Authelin, J.-R. Spray Drying: Scale-Up and Manufacturing. in *Amorphous Solid Dispersions. Advances in Delivery Science and Technology* (eds. Shah, N., Sandhu, H., Choi, D. S., Chokshi, H. & Waseem Malick, A.) 261–302 (Springer, New York, NY, 2014). doi:10.1007/978-1-4939-1598-9_8.

111. World Health Organisation Expert Committee on Specifications for Pharmaceutical Preparations. Annex 6: Guidelines on submission of documentation for a multisource (generic) finished pharmaceutical product : quality part. *WHO Technical Report Series* 317–387 (2014).

112. Zhou, W., Yang, S. & Wang, P. G. Matrix effects and application of matrix effect factor. *Bioanalysis* **9**, 1839–1844 (2017). doi:10.4155/bio-2017-0214

113. Hu, Q., Choi, D. S., Chokshi, H., Shah, N. & Sandhu, H. Highly efficient miniaturized coprecipitation screening (MiCoS) for amorphous solid dispersion formulation development. *Int. J. Pharm.* **450**, 53–62 (2013). doi:10.1016/j.ijpharm.2013.04.040

114. Suda, A. *et al.* Continuous Fabrication of Monodisperse Ceria–Zirconia–Yttria Composite Oxide Nanoparticles Using a Novel High-Shear Agitation Reactor. *ACS Omega* **3**, 6560–6565 (2018). doi:10.1021/acsomega.8b00730

115. Sim, T. *et al.* Characterization and pharmacokinetic study of itraconazole solid dispersions prepared by solvent-controlled precipitation and spray-dry methods. *J. Pharm. Pharmacol.* **69**, 1707–1715 (2017). doi:10.1111/jphp.12805

116. Hildebrandt, J. R. Scale-Up and Optimization of Membrane Processes. in *Chromatographic and Membrane Processes in Biotechnology* (eds. Costa, C. A. . & Cabral, J. S.) 415–428 (Springer, Dordrecht, 1991). doi:10.1007/978-94-011-3470-5_23.

117. Raghunath, B., Bin, W., Pattnaik, P. & Janssens, J. Best Practices for Optimization and Scale-Up of Microfiltration TFF Processes. *Bioprocess. J.* **11**, 30–40 (2012). doi:10.12665/j111.raghunath

118. Tutunjian, R. S. Scale-Up Considerations for Membrane Processes. *Bio/Technology* **3**, 615–626 (1985). doi:10.1038/nbt0785-615

119. Ball, P. Scale-up and scale-down of membrane-based separation processes. *Membr. Technol.* **2000**, 10–13 (2000). doi:10.1016/S0958-2118(00)86634-3

120. Lutz, H.; Raghunath, B. Ultrafiltration Process Design and Implementation. in *Process Scale Bioseparations for the Biopharmaceutical Industry* (eds. Shukla, A. A., Etzel, M. R. & Gadam, S.) 298–330 (CRC Press, Boca Raton, FL, 2006). doi:10.1201/9781420016024.

121. Conductivity Measurement in high purity water samples below 10 µSiemens/cm. *IC Controls application Notes* (2012).

Appendix

Table A.1 – Examples of drugs according to the BCS. [Adapted from [35]]

CLASS I	CLASS II	CLASS III	CLASS IV
Chloroquine	Carbamazepine	Acyclovir	Coenzyme Q_{10}
Diltiazem	Danazol	Atenolol	Cyclosporin A
Metoprolol	Glibenclamide	Captopril	Ellagic acid
Paracetamol	Ketoconazole	Cimetidine	Furosemide
Propanolol	Nifedipine	Metformin	Ritonavir
Theophylline	Phenytoin	Neomycin B	Saquinavir
Verapamil	Troglitazone	Ranitidine	Taxol

Table A.2 – Different Kinds of Y-Type and Z-Type Chambers and Their Minimum Internal Dimensions.[53]

Y-TYPE CHAMBER		Z-TYPE CHAMBER	
Style of Chamber	**Microchannel Dimensions (μm)**	**Style of Chamber**	**Microchannel Dimensions (μm)**
F12Y	75	G10z	87
F20Y	75	H10z	100
J20Y	125	L10z	150
J30Y	125	H210z	200
		H30z	200
		L21z	250
		H30z	300

Table A.3 – Important physicochemical API properties for coprecipitation process. [Adapted from[44]]

Critical properties	Criteria
Ionization constant	pKa of the drug should not be higher than 5 to ensure complete precipitation during initial coprecipitation and to minimize dissolution during subsequent rinsing and washing cycles. pH of the anti-solvent should not exceed drug's pka (ideal precipitation conditions are two units below the pKa)
Functional group	Potential of interaction and reactivity with polymer estimated
Chemical stability	Chemically stable in extreme pH ranges where coprecipitation occurs
	Chemically stable in organic solvent for at least 24 h
H bonding acceptors and donors	H acceptor>7
Crystallinity	API should not form solvate(s) with the solvent(s) Low crystallization tendency
Molecular Weight	MW>500
Lipophilicity	log P>3
Miscibility estimate	Negative free energy of mixing estimated by solubility parameter

Solvent Casting

APIs	Polymers

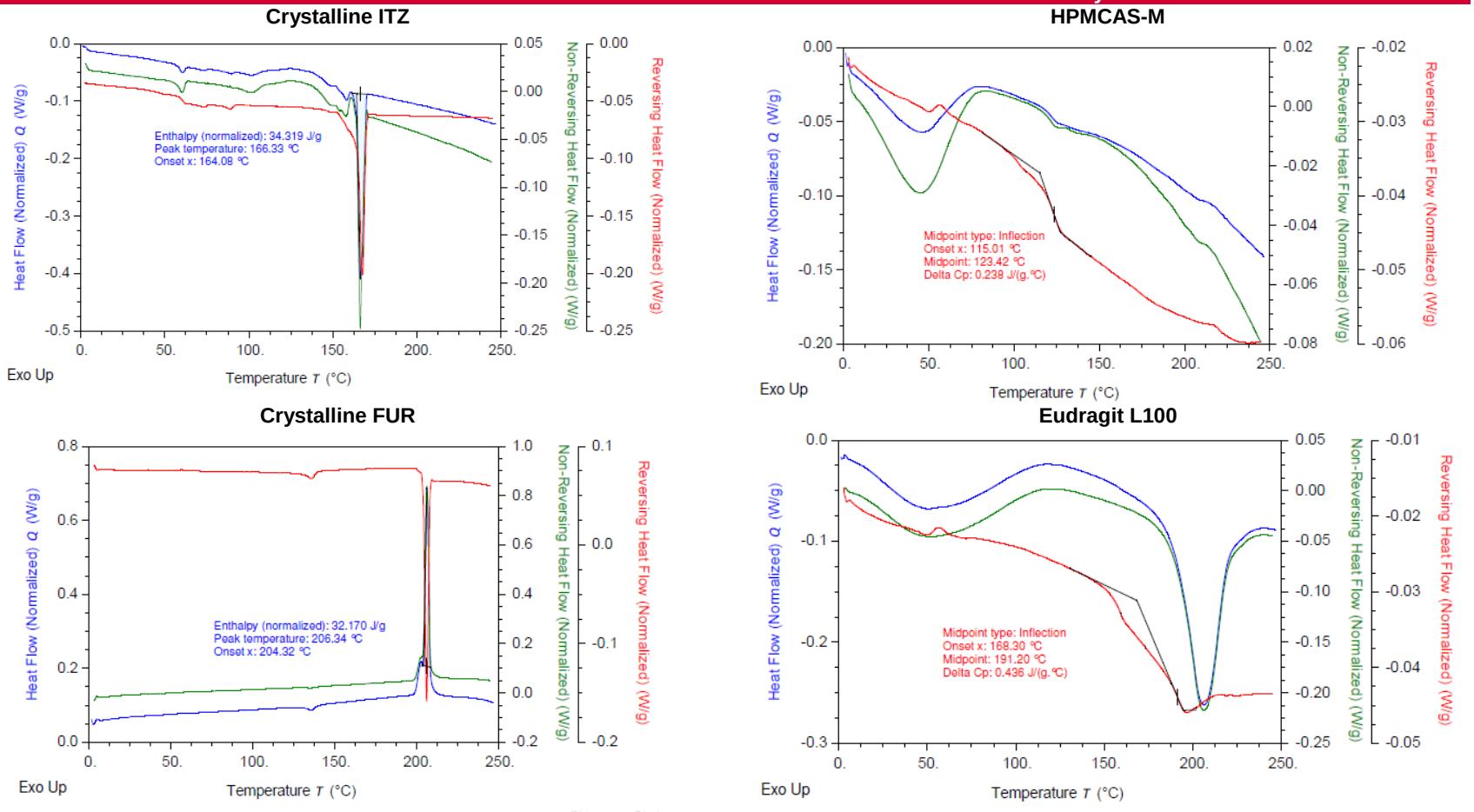

Figure A.1 – Crystalline ITZ, crystalline FUR, HPMCAS-M and Eudragit L100 mDSC profiles.

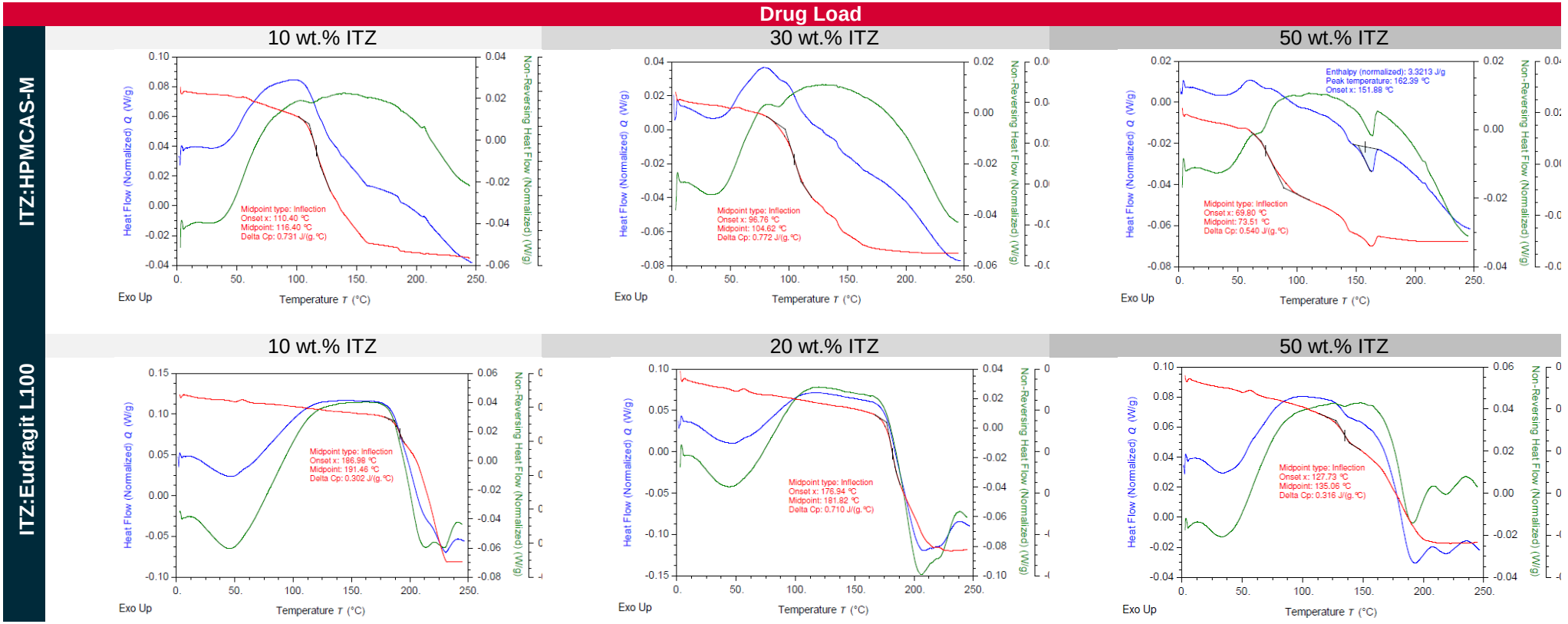

Figure A.2 – Solvent casting: ITZ:HPMCAS-M and ITZ:Eudragit L100 formulations mDSC profiles.

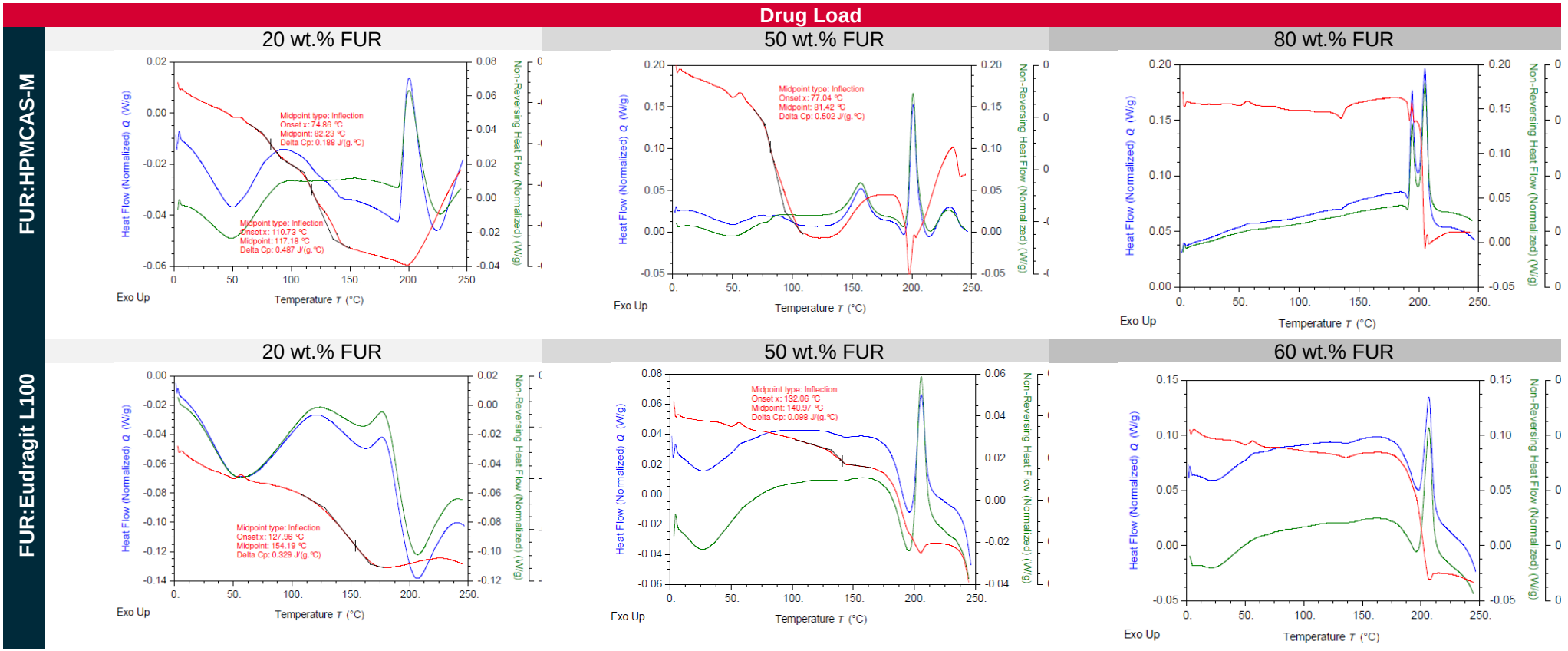

Figure A.3 – Solvent casting: FUR:HPMCAS-M and FUR:Eudragit L100 formulations mDSC profiles.

mDSC Characterization of SD benchmarks and coprecipitated prototypes

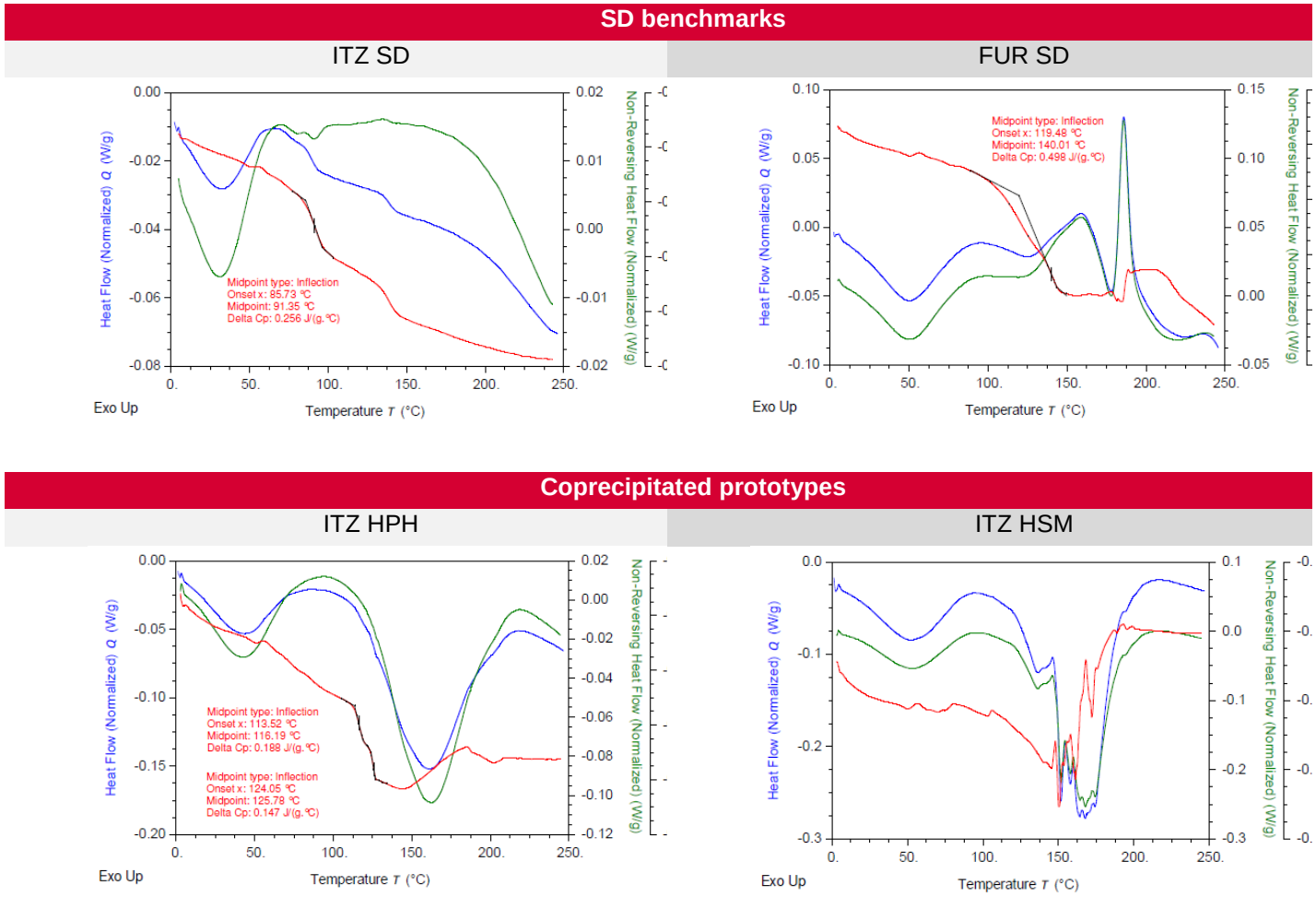

Figure A.4 – mDSC profile for SD benchmarks and coprecipitated prototypes.

TGA Characterization of SD benchmarks and coprecipitated prototypes

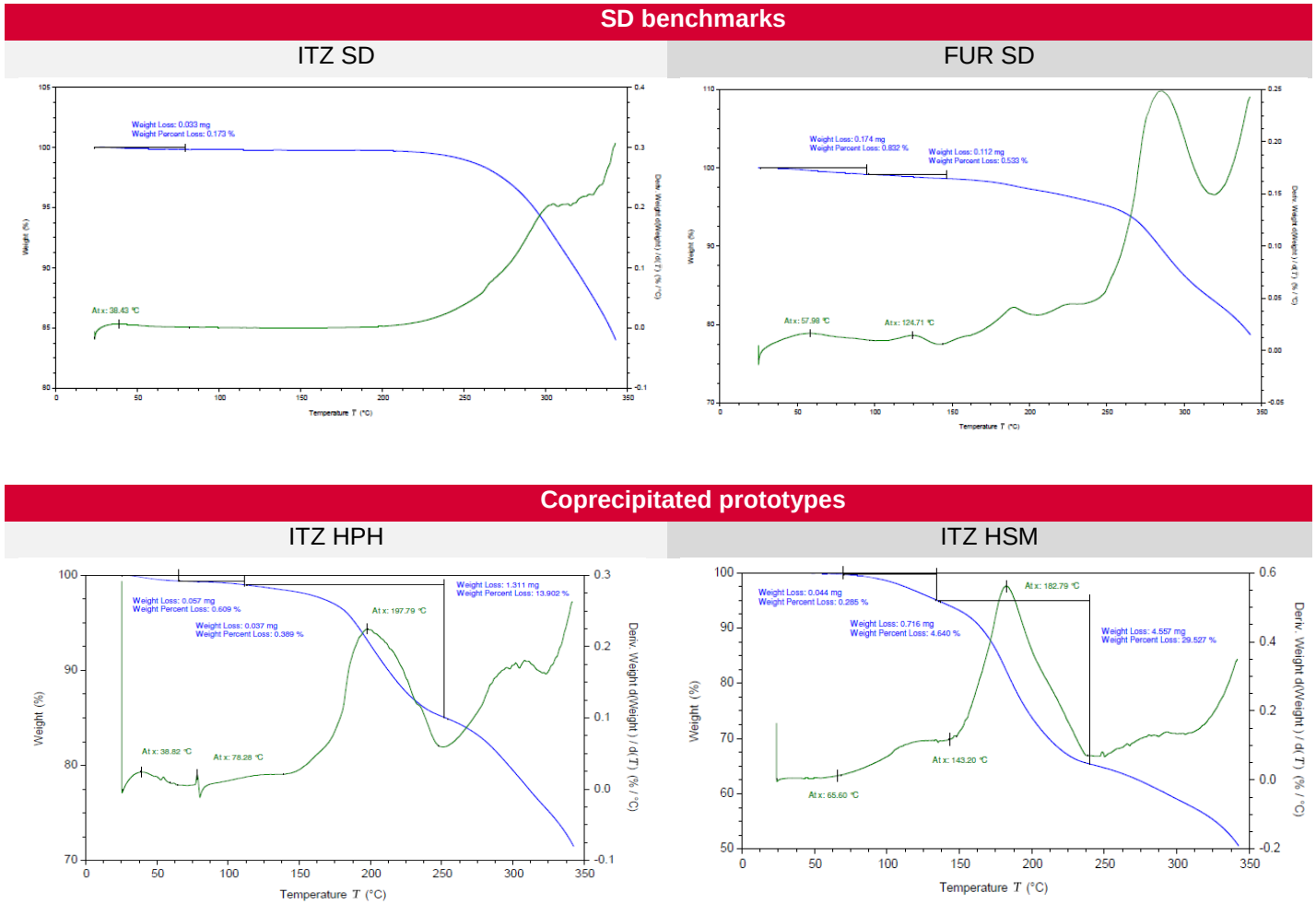

Figure A.5 – TGA profile for SD benchmarks and coprecipitated prototypes.

Analytical Characterization of FUR SD benchmark

A shriveled or buckled particle morphology was observed (Figure A.6) for FUR SD benchmark, which Is aligned with a slower drying kinetics during spray drying (F_{Feed} = 0.7 kg/h).

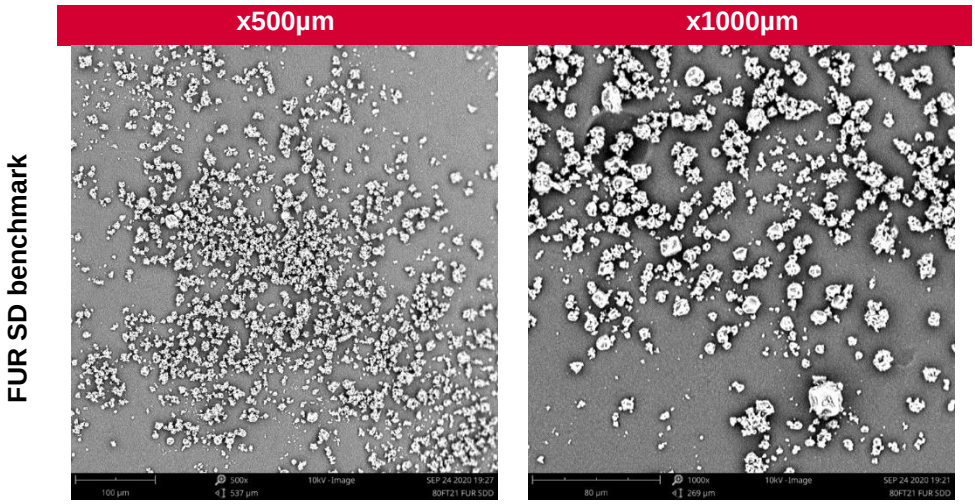

Figure A.6 – SEM micrographs of FUR SD benchmark at 500 and 1000x magnification.

PSD was assessed with Sympatec R2 lens (range 0.45 – 87.5 µm). 90 % of the particles (D_v90) is under 20 µm (Figure A.7).

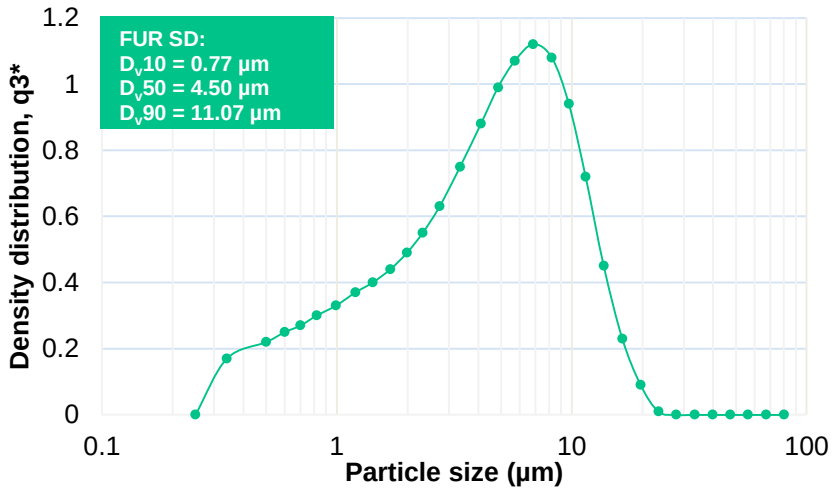

Figure A.7 – PSD of FUR SD Benchmark.

XRPD (Figure A.8) revealed a halo characteristic of amorphous form and lack of X-ray diffraction peaks corresponding to the crystalline FUR.

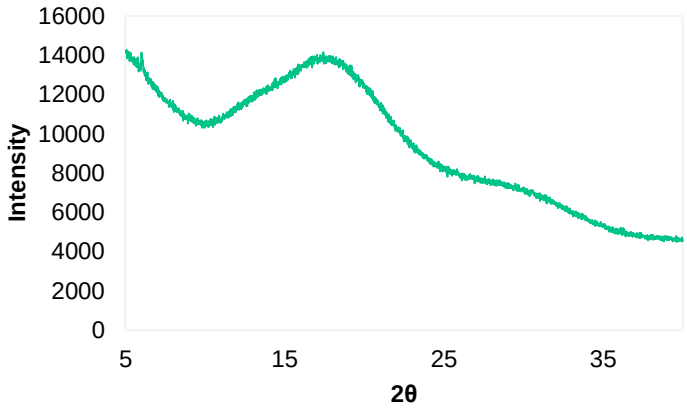

Figure A.8 – Powder diffractogram of FUR SD benchmark.

Table A.4 – Summary of FUR SD benchmark analytical characterization.

Analytical Characterization			FUR SD benchmark
GC	DCM	(ppm)	4 855
	MeOH	(ppm)	927
	DMSO	(ppm)	N/AP
TGA	Water	(wt.%)	0.79
Bulk density		(g/cm^3)	0.29
HPLC	Assay		98.3%
DSC	T_g	(ºC)	140.0
XRPD			Amorphous
PSD	D_v10	(µm)	0.77
	D_v50	(µm)	4.5
	D_v90	(µm)	11.07

N/A – not applicable

FUR SD benchmark exhibited a high glass transition temperature of approximately 140 ºC and the presence of a melting peak. As addressed before, the occurrence of other thermal events is usual at higher drug loadings and may have been caused by heating during DSC.[8] XRPD indicated that the material was amorphous, confirming that the thermal events were not attributed to crystallinity presence.

Concerning residual solvents quantification, DCM is above ICH limit. For FUR SD product, either vacuum was not sufficient, due to the fact that the available laboratory tray oven did not allow drying with nitrogen sweep, which is the more likely scenario; or this particular formulation requires a secondary drying duration of more than 24 hours. As DCM was not removed from FUR SD to acceptable values, it can negatively impact the physical stability of this amorphous product, by lowering the T_g or triggering API dissolution in certain domains.[44] Ultimately, this may lead to recrystallization, compromising product's shelf life and the overall bioavailability enhancement strategy of the ASD product.

TGA, bulk density and assay results are as expected.

Powder diffractogram of Citric Acid

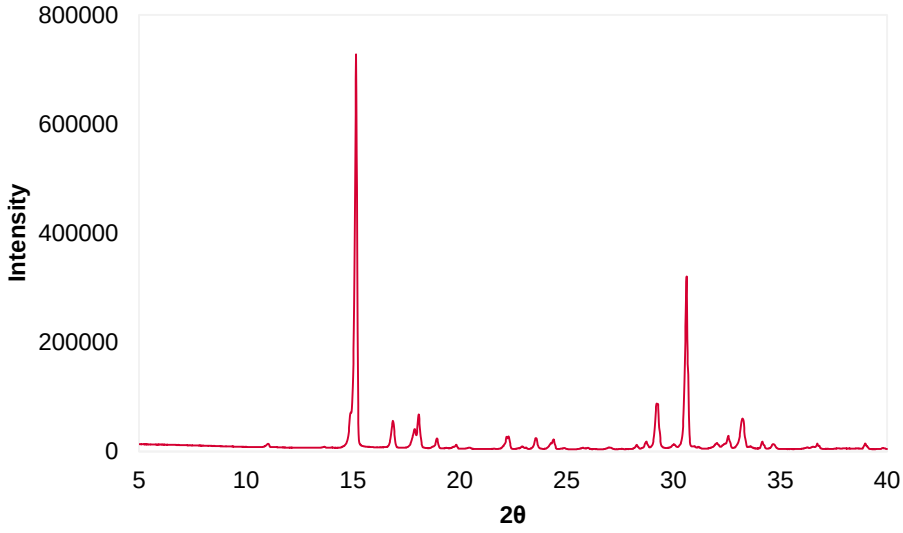

Figure A.9 – Powder diffractogram of Citric Acid.

Conductivity Curve

To understand the extent to which organic solvent and antisolvent mixture is being replaced by water, a conductivity curve was plotted prior to diafiltration. The conductivity curve consisted in the execution of a limited number of measurements to evaluate conductivity variation with the solvent mass fraction. Solvent mixtures with different DMSO/water (solvent/antisolvent) ratios were prepared (see Table A.5) and 3 conductivity measurements were made. The conductivity of water and DMSO was also measured individually. Conductivity was measured with a Mettler Toledo SG3 conductometer.

The plan was to measure in-line conductivity during diafiltration, “tracking” the organic solvent content in retentate stream with the conductometer until ICH levels were acceptable.

Table A.5 – Conductivity curve: experimental results.

Ratio (wt.)		$Conductivity_{average}$
DMSO	H_2O	(µS/cm)
N/AP	1	1.24
1	N/AP	0.00
1	1	0.19
1	3	0.63
1	7	0.93
1	12	1.07
1	20	1.08
1	50	1.19

N/A – not applicable

Conductivity curve is plotted in Figure A.10. A clear tendency was perceived. However, conductivity measurements of deionized water present an off-set from values reported in literature (0.055µS/cm).[121] This may be due to the equipment limitations and sensibility, and for this reason conductivity curve was not employed in this manuscript.

Nevertheless, this type of inline measurement is recommended to track the efficiency of the diafiltration steps in real time.

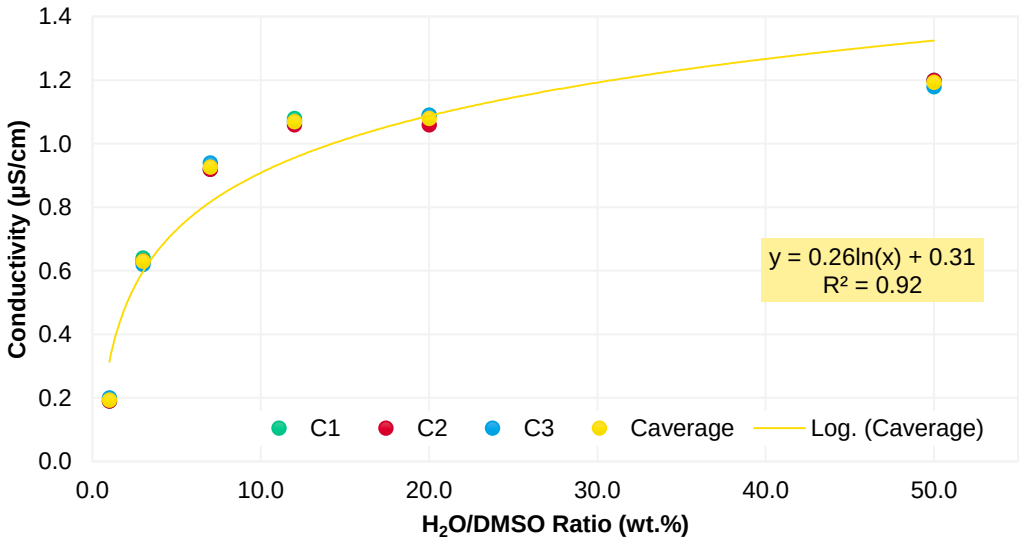

Figure A.10 – Conductivity Curve.